INVESTIGATION OF MEASURING SYSTEM REQUIREMENTS FOR INSTRUMENT LOW VISIBILITY APPROACH

DUNSTAN GRAHAM

WARREN F. CLEMENT

LEE GREGOR HOFMANN

Distribution of this document is unlimited.

FOREWORD

The research reported here was accomplished for the United States Air Force by Systems Technology, Inc., Hawthorne, California, under Contract No. F33615-69-C-1904. The program was sponsored by the Air Force Flight Dynamics Laboratory, Air Force Systems Command, Wright-Patterson Air Force Base, Ohio.

This research was initiated in support of the Air Force Flight Dynamics Laboratory Tactical Instrument Landing Program (TACLAND). Although the TACLAND program has been completed, the results of this investigation apply to the new Advanced Landing System Program of the Air Force.

The Air Force project engineer was Captain James D. Dillow. Dunstan Graham served as the contractor's technical director and project engineer.

The research was performed during the period from July 1969 to June 1970. The manuscript was released by the authors for publication in June 1970.

This technical report has been reviewed and is approved.

C. B. WESTBROOK
Chief, Control Criteria Branch
Aeronautical Systems Division
Air Force Flight Dynamics Laboratory

ABSTRACT

A practical method of determining measuring system requirements for instrument low visibility approach is presented. The method is made to depend on system analysis of the airplane, its control system, and the guidance system, as well as on atmospheric turbulence inputs and radio guidance system fluctuation noise. Requirements on the system are set in terms of a low value of the accident exposure multiplier which is related to the probability of a missed approach in the assumed environment.

The application of the method is demonstrated in connection with two examples: manual-flight director approach in the A-7D attack airplane, and automatically coupled approach with an advanced "windproof" flight control system in the DC-8 transport aircraft. The results, including particularly the implied requirements on scan rate for a scanning beam instrument low visibility approach system, demonstrate the interconnections between scanning rate, flight control, and overall system performance.

CONTENTS

Page

Page

LIST OF FIGURES (cont'd)

LIST OF TABLES

Page

Page

LIST OF TABLES (cont'd)

SYMBOLS

a	Half-power frequency bandwidth of a stochastic input $i(t)$; polynomial coefficient
$a(s)$	A polynomial function of s
a_y	Lateral acceleration at the center of gravity
a_y', $a_y^{(1)}$	Lateral acceleration at a distance ℓ_x, ℓ_z from the c.g., $a_y' = a_y + \ell_x \dot{r} - \ell_z \dot{p}$
a_z	Normal acceleration at the center of gravity
a_z'	Normal acceleration at a distance ℓ_x from the c.g., $a_z' = a_z - \ell_x \dot{q}$
b	Wing span; polynomial coefficient
$b(s)$	A polynomial function of s
c	Mean aerodynamic chord; a polynomial coefficient
$c(s)$	A polynomial function of s
c.g.	Center of gravity
C	Crosswind velocity; an array involving the coefficients of $c(s)$
C_D	Drag coefficient, $D/\frac{1}{2}\rho U_o^2 S$
C_{D_α}	Drag coefficient variation with angle of attack, $\partial C_D/\partial \alpha$
C_{D_u}	Non-dimensional variation of C_D with speed; $U_o \partial C_D/2 \partial U_o$
C_ℓ	Rolling moment coefficient, $\text{Roll Moment}/\frac{1}{2}\rho V_{T_o}^2 Sb$
C_{ℓ_β}	Dihedral parameter, variation of rolling moment coefficient with sideslip, $\partial C_\ell/\partial \beta$
$C_{\ell_{\delta_a}}$	Aileron rolling effectiveness, $\partial C_\ell/\partial \delta_a$
$C_{\ell_{\delta_r}}$	Rudder rolling effectiveness, $\partial C_\ell/\partial \delta_r$
C_{ℓ_p}	Roll damping coefficient $\partial C_\ell/\partial \left(\frac{pb}{2V_{T_o}}\right)$

SYMBOLS (cont'd)

C_{ℓ_r} Roll coefficient due to yawing velocity, $\partial C_\ell / \partial (\frac{rb}{2V_{T_o}})$

C_L Lift coefficient, $nW/\frac{1}{2}\rho U_o^2 S$

C_{L_α} Lift-curve slope, $\partial C_L / \partial \alpha$

$C_{L_{\dot\alpha}}$ $\partial C_L / \partial (\dot\alpha c / 2U_o)$; unsteady lift coefficient due to rate of change of angle of attack

C_{L_δ} Control-surface lift effectiveness, $\partial C_L / \partial \delta$

C_{L_q} $\partial C_L / \partial (qC/2U_o)$; lift coefficient due to pitching velocity

C_{L_u} Non-dimensional variation of C_L with speed, $U_o \partial C_L / 2\partial U_o$

C_M Pitching moment coefficient, Pitching Moment$/\frac{1}{2}\rho U_o^2 Sc$

C_{M_α} $\partial C_M / \partial \alpha$

$C_{M_{\dot\alpha}}$ $\partial C_M / \partial (\frac{\dot\alpha c}{2U_o})$; $U_o C_{M_{\dot w}}$

C_{M_δ} Control-surface pitch effectiveness, $\partial C_M / \partial \delta$

C_{M_q} Pitch damping coefficient, $\partial C_M / \partial (\frac{qc}{2U_o})$

C_{M_u} $U_o \partial C_M / 2\partial U_o$

C_n Yawing moment coefficient, Yawing Moment$/\frac{1}{2}\rho V_{T_o}^2 Sb$

C_{n_β} Static directional stability, $\partial C_n / \partial \beta$

$C_{n_{\delta_a}}$ Aileron yawing effectiveness, $\partial C_n / \partial \delta_a$

$C_{n_{\delta_r}}$ Rudder yawing effectiveness, $\partial C_n / \partial \delta_r$

C_{n_p} $\partial C_n / \partial (\frac{pb}{2V_{T_o}})$

SYMBOLS (cont'd)

C_{n_r} $\partial C_n / \partial (\frac{rb}{2V_{T_o}})$

C_y Lateral force coefficient, Lateral Force$/\frac{1}{2}\rho V_{T_o}^2 S$

C_{y_β} Variation of C_y with sideslip angle, $\partial C_y / \partial \beta$

$C_{y_{\delta_r}}$ Rudder side-force effectiveness, $\partial C_y / \partial \delta_r$

C_{y_p} $\partial C_y / \partial (\frac{pb}{2V_{T_o}})$; side force coefficient due to rolling velocity

C_{y_r} $\partial C_y / \partial (\frac{rb}{2V_{T_o}})$; side force coefficient due to yawing velocity

d A polynomial coefficient; displacement normal to the glide slope in a vertical plane containing the glide slope

$d(s)$ A polynomial function of s

dt Time differential

D Drag; with a double subscript, an element of $D(T)$; an array involving the coefficients of $d(s)$

$D(T)$ Covariance matrix

e Naperian base 2.71828 ...

f_s Pilot's scanning frequency (Hz)

$f(t)$ Stable function of time

$f(\tau)$ Unit impulse response of a stationary process

$f(\cdot)$ Probability density function

F, $F(s)$ Feedback transfer function, particularized by a subscript denoting the motion variable upon which it operates; also Laplace transform of $f(t)$ or $f(\tau)$

F_{sp} Pilot's stick force

g Gravitational acceleration; a polynomial coefficient

$g(s)$ A polynomial function of s

G, $G(s)$	Open loop transfer function, often particularized by a subscript; also G is an array involving the coefficients of $g(s)$
h	Altitude; a polynomial coefficient
$h(s)$	A polynomial function of s
H	Headwind velocity
$i(t)$	Stochastic input
I_{ij}	Infinite time integral of the product of two deterministic functions of time
I_x, I_y, I_z	Moments of inertia referred to stability axes
I_{xz}	Product of inertia referred to stability axes
I_{x_0}, I_{z_0}	Moments of inertia referred to principal axes
j,	$\sqrt{-1}$
$j\omega$	The imaginary portion of the complex variable $s = \sigma \pm j\omega$
k	Partial rate-weighting coefficient in first order extrapolation of sampled data
K	Gain, often particularized by a subscript
K_p	Human pilot's static gain; also roll rate feedback gain
ℓ_x	Distance along the X axis from the c.g., positive forward
ℓ_z	Distance along the Z axis from the c.g., positive down
L	Rolling acceleration due to externally applied torques; integral scale length of homogeneous isotropic atmospheric turbulence, often particularized by a subscript
L_β	$\rho S V_{T_0}^2 b\, C_{\ell_\beta}/2I_x$ in dimensional units of $(\text{time})^{-2}$
L_δ	$\rho S V_{T_0}^2 b\, C_{\ell_\delta}/2I_x$ in dimensional units of $(\text{time})^{-2}$
L_p	$\rho S V_{T_0} b^2 C_{\ell_p}/4I_x$ in dimensional units of $(\text{time})^{-1}$

xv

SYMBOLS (cont'd)

L_r $\rho S V_{T_o} b^2 C_{\ell_r}/4 I_x$ in dimensional units of $(\text{time})^{-1}$

L_v L_β/V_{T_o} in dimensional units of $(\text{time})^{-1}(\text{length})^{-1}$

L_i' $\dfrac{L_i + \dfrac{I_{xz}}{I_x} N_i}{1 - \dfrac{I_{xz}^2}{I_x I_z}}$ where i refers to any motion, or input, quantity

m Mass; integer

M Pitching acceleration due to externally applied torques; Mach number; integer

M_α $U_o M_w$ in dimensional units of $(\text{time})^{-2}$

$M_{\dot\alpha}$ $U_o M_{\dot w}$ in dimensional units of $(\text{time})^{-1}$

M_δ $\rho S U_o^2 c\, C_{M_\delta}/2 I_y$ in dimensional units of $(\text{time})^{-2}$

M_s Scanning workload margin $= (1 - W_s)$, dimensionless

M_q $\rho S U_o c^2 C_{M_q}/4 I_y$ in dimensional units of $(\text{time})^{-1}$

M_u $\rho S U_o c\, (C_M + C_{M_u})/I$ in dimensional units of $(\text{time})^{-1}$

M_u^* $M_u + T_u z_j\, m/I_y$

M_w $\rho S U_o c\, C_{M_\alpha}/2 I_y$ in dimensional units of $(\text{time})^{-1}(\text{length})^{-1}$

$M_{\dot w}$ $\rho S c^2 C_{M_{\dot\alpha}}/4 I_y$ in dimensional units of $(\text{length})^{-1}$

n Integer; vertical load factor; pilot's remnant, often particularized by a subscript

n_t Range-independent noise input to the measuring system

n_r Range-dependent noise input to the measuring system

N Yawing acceleration due to externally applied torques; integer

N_β $\rho S V_{T_O}^2 b \; C_{n_\beta}/2I_z$ in dimensional units of $(\text{time})^{-2}$

N_δ $\rho S V_{T_O}^2 b \; C_{n_\delta}/2I_z$ in dimensional units of $(\text{time})^{-2}$

$N_\delta^\lambda(s)$ Directly controlled airframe motion quantity/control deflection transfer function numerator

N_p $\rho S V_{T_O} b^2 \; C_{n_p}/4I_z$ in dimensional units of $(\text{time})^{-1}$

N_r $\rho S V_{T_O} b^2 \; C_{n_r}/4I_z$ in dimensional units of $(\text{time})^{-1}$

N_v N_β/V_{T_O} in dimensional units of $(\text{time})^{-1}(\text{length})^{-1}$

N_i' $\dfrac{N_i + L_i I_{xz}/I_z}{1 - I_{xz}^2/I_x I_z}$, where i refers to any motion, or input, quantity

p   Roll rate, angular velocity about the X axis, positive right wing going down; integer; the value of a real pole multiplied by (-1)

P   Probability, often particularized by a subscript; also the value of a real pole multiplied by (-1)

P_{A1} Probability of an accident, given that the window <u>is</u> attained

P_{A2} Probability of an accident, given continuation of an approach which does not attain the window

P_D Probability of the pilot's making the correct decision to discontinue the approach, given that he did not attain the window

P_{LAT} Probability of exceeding the window boundary in y

P_{LONG} Probability of exceeding the window boundary in d and/or u_{AS}

P_M Marginal probability of being inside the window on each approach

$P_{\bar{S}}$ Probability of an unsuccessful outcome of the approach

P_W	Probability of <u>not</u> attaining the window on any given approach
q	Pitch rate, angular velocity about the Y axis, positive nose going up; dynamic pressure, $\rho U_o^2/2$ or $\rho V_{T_O}^2/2$; integer
r	Yaw rate, angular velocity about the Z axis, positive nose going right
R	Range from a transmitting site to the aircraft
s	Laplace operator, $\sigma + j\omega$, a complex variable
S	Wing area
t	Time
$1/T_i$	Inverse time constant particularized by the subscript
T	Thrust; time interval; time "constant," particularized by a subscript
T_{d_e}	Effective dwell interval of the pilot's eye fixation
T_{d_f}	Foveal dwell interval of the pilot's eye fixation
T_I	Lag time "constant"
T_L	Lead time "constant"
T_o	Periodic sampling interval of a scanning beam measuring system; also lower bound on the domain of T_s
T_s	Human pilot's sampling interval in scanning his displays
T_u	$(1/m)\partial T/\partial V_T$ in dimensional units of $(\text{time})^{-1}$
u	Linear perturbed velocity along the X axis; unit white noise
U_o	Linear steady state velocity along the X axis
v	Linear perturbed velocity along the Y axis
V_o	Linear steady state velocity along the Y axis
V_T	Total true airspeed

V_{T_o}	Total steady state true airspeed
w	Linear perturbed velocity along the Z axis; also a complex variable
W	Weight
W_o	Linear steady state velocity along the Z axis
W_s	Dimensionless scanning workload $M_s + \sum_i \eta_{f_i}$
x	Output of a stationary process
X	Forward acceleration, along the X axis
X_α	$U_o X_w$; $\rho S U_o^2 (C_L - C_{D_\alpha})/2m$ in dimensional units of $(\text{length})(\text{time})^{-2}$
X_δ	$\rho S U_o^2 (-C_{D_\delta})/2m$ in dimensional units of $(\text{length})(\text{time})^{-2}$
X_u	$\rho S U_o (-C_D - C_{D_u})/m$ in dimensional units of $(\text{time})^{-1}$
X_u^*	$X_u + T_u \cos\xi_o$
X_w	$\rho S U_o (C_L - C_{D_\alpha})/2m$ in dimensional units of $(\text{time})^{-1}$
X_{CG}	Fuselage station of the center of gravity
Y	Side acceleration, along the Y axis; also $Y(s)$, particularized by a subscript
$Y(s)$	Transfer function, particularized by a subscript
$Y(j\omega)$	Describing function, particularized by a subscript
Y_β	$V_{T_o} Y_v$ in dimensional units of $(\text{length})(\text{time})^{-2}$
Y_δ	$\rho S V_{T_o}^2 C_{y_\delta}/2m$ in dimensional units of $(\text{length})(\text{time})^{-2}$
Y_δ^*	Y_δ/V_{T_o} in dimensional units of $(\text{time})^{-1}$
Y_p	$\rho S V_{T_o} b \, C_{y_p}/4m$; describing function of the human pilot
Y_{pg}	Transfer function of the roll rate response by a tilted yaw rate gyro

xix

SYMBOLS (cont'd)

Y_r — $\rho S V_{T_O} b\, C_{y_r}/4m$; also transfer function of a yaw rate gyro

Y_v — $\rho S V_{T_O}\, C_{y_\beta}/2m$ in dimensional units of $(\text{time})^{-1}$

z — The value of a real zero multiplied by (-1); damping coefficient in a first order extrapolator in which a share of the previous sampled derivative and the first back difference are used in computing the present sampled derivative

z_j — Perpendicular distance from the cg to the thrust line (positive for a nose-up pitching moment due to thrust)

Z — Vertical acceleration, along the Z axis; the value of a real zero multiplied by (-1)

Z_α — $U_O Z_w$ in dimensional units of $(\text{length})(\text{time})^{-2}$

Z_δ — $\rho S U_O^2(-\,C_{L_\delta})/2m$ in dimensional units of $(\text{length})(\text{time})^{-2}$

Z_q — $\rho S U_O c(-\,C_{L_q})/4m$ in dimensional units of $(\text{length})(\text{time})^{-1}$

Z_u — $\rho S U_O(-\,C_L - C_{L_u})/m$ in dimensional units of $(\text{time})^{-1}$

Z_u^* — $Z_u - T_u \sin \xi_O$

Z_w — $\rho S U_O(-\,C_{L_\alpha} - C_D)/2m$ in dimensional units of $(\text{time})^{-1}$

$Z_{\dot{w}}$ — $\rho S c(-\,C_{L_{\dot{\alpha}}})/4m$, dimensionless

α — Instantaneous angle of attack, w/U_O under no wind conditions

α_G — Gyro tilt angle measured from the X axis in the X-Z plane, positive up.

α_O — Angle of attack of body axis; also angle of attack of principal axis

β — Sideslip angle, v/V_{T_O} under no wind conditions

γ — Perturbed flight path angle, $\theta - \alpha$

xx

SYMBOLS (cont'd)

γ_o	Steady state flight path angle
Γ	Scanning beam angle in elevation for a terminal site measuring system
Γ_o	Nominal glide slope elevation angle
$\delta(t)$	Dirac delta function
δ	Control surface deflection, particularized by subscript; also normalized lower bound on the domain of T_s: T_o/T_s
δ_{ij}	Kronecker delta
Δ	Incremental prefix; also $\Delta(s)$
$\Delta(s)$	Denominator of airframe transfer functions; characteristic equation when set equal to zero
Δ_{lat}	Denominator of the lateral transfer functions; lateral characteristic equation when set equal to zero
Δ_{long}	Denominator of the longitudinal transfer functions; longitudinal characteristic equation when set equal to zero
Δ_s	Sampling coherence determinant of stability in the mean-square sense
ϵ	Incremental error
ϵ_H	Pitch flight director error presented on the horizontal pointer
ϵ_o	$\cos\theta_o + (W_o/U_o)\sin\theta_o$
ϵ_v	Roll flight director error presented on the vertical pointer
$\zeta,\ \zeta_i$	Damping ratio of linear second order system particularized by the subscript
η_e	Effective dwell fraction, T_{d_e}/T_s, of the pilot's eye fixation
η_f	Foveal dwell fraction, T_{d_f}/T_s, of the pilot's eye fixation

θ — Pitch angle, $\int q \, dt$ in straight and level flight

θ_o — Steady state pitch angle of the X axis with respect to the horizontal direction

λ — Lateral course angle of the aircraft in a horizontal plane; wavelength; a dummy variable

λ_d — d_e/R

λ_y — y_e/R

ξ — A directly controlled airframe motion quantity

ξ_o — Inclination of the thrust line with respect to the X axis in the plane of symmetry (positive for negative Z force)

π — 3.14159 ...

ρ — Mass density of air

$\rho(\cdot)$ — Probability density function

ρ_o — Mass density of air at sea level

σ — Standard deviation of a stochastic variable, often particularized by a subscript; the real portion of the complex variable $s = \sigma \pm j\omega$

τ — Time delay

$\tau_a, \tau_e, \tau_i, \tau_u$ — Human pilot's effective time delay, including transport delays and high frequency neuromuscular phase lags

φ — Roll angle, $(\cos \gamma_o \int p \, dt - \sin \gamma_o \int r \, dt)$ in rectilinear flight; polar phase angle of a complex variable

$\Phi(s)$ — Power spectral density, often particularized by a subscript

ψ — Perturbed heading angle of the X axis with respect to its trimmed value

ω_b — Half-power frequency bandwidth

SYMBOLS (cont'd)

ω_c	Crossover frequency
ω_i	Undamped natural frequency of a second order mode; particularized by the subscript
ω	Circular frequency in dimensions $(\text{rad})(\text{time})^{-1}$, often particularized by a subscript
ω_s	Pilot's circular scanning frequency, $2\pi f_s$
Ω	Average parafoveal to foveal gain crossover frequency ratio, $\omega_{c_p}/\omega_{c_f}$

Special Superscripts

*	Impulsively sampled value of a continuous function of time
°	Degrees

Special Subscripts

a	Roll control, e.g., aileron; accelerometer; actuator
a_y	Lateral acceleration
a_z	Normal acceleration
abs	Absolute (altitude)
A	Actuator
b	Bandwidth
B	Integral bypass
c	Crossover; controlled element; command
d	Dutch roll; dwell interval; glide slope displacement
e	Error; effective value; pitch control, e.g., elevator
f	Filter; foveal; flap
F	Flap

g	Atmospheric gust, when affixed to u, v, w, p, q, r, in particular, denotes corresponding component of air mass velocity
G	Gyro
h	Altitude
i, ι	Command input; index; input-correlated
ic	Initial condition
iT	Incidence of the horizontal tail (stabilator)
I	Lag
j	Index
k	Index
ℓ	Index
L	Lead
M	Margin
n	Index; remnant
N	Neuromuscular
o	Steady-state; trimmed (equilibrial) condition; periodic
p	Human pilot; phugoid; parafoveal; particular (fuselage station); roll rate
pg	Roll rate component measured by a tilted yaw rate gyro
r	Yaw control, e.g., rudder; yaw rate
R	Roll subsidence
s	Spiral mode; sample; scan; windshear
sp	Short period
T	Throttle
TH	Thrust
u	Airspeed
w	Steady wind

wo	Washout
x	Crossfeed
y	Lateral displacement
θ	Pitch angle
φ	Roll angle
ψ	Heading angle

Mathematical Symbols

(λ)	Real factor $(s + \lambda)$ of a polynomial in s
$[\zeta; \omega]$	Quadratic factor $[s^2 + 2\zeta\omega s + \omega^2]$ of a polynomial in s
$<$	Less than
$>$	Greater than
$\leq$	Less than or equal to
$\geq$	Greater than or equal to
$\ll$	Much less than
$\gg$	Much greater than
$\neq$	Not equal to
$\doteq$	Approaches; approximately equal to
$\equiv$	Identically equal to
$\rightarrow$	Fed to; approaches
$\Rightarrow$	Identified with
$-$	(Vinculum) average value; integrated value
$\cdot$	(Raised period) d/dt
$\cdot\cdot$	(Dieresis) d^2/dt^2
d	Differential operator
e	Naperian base, 2.71828 ...

E	Expectation operator
∂	Partial differential operator
$\int$	Integration operator
Σ	Summation operator
$\prod$	Multiplication operator
$\sqrt{}$	Square root operator
$+$	Addition operator; positive value suffix
$\otimes$	Difference operator
$-$	(Hyphen) subtraction operator; negative value prefix
$:$	In proportion to
$\mid, /$	Prefix is "conditional upon" suffix; solidus also separates the numerator from the denominator in a fraction when the use of a horizontal line would be inconvenient
adj	Prefix denoting the adjoint of a matrix, the transposed matrix of cofactors
$', '', iii, iv$	(single, double, triple, or quadruple superscript) on ζ, ω_n, $1/T$, Δ, and N_δ^ξ to denote closure of one, two or three loops, respectively; also affixed to symbol for displayed signal to denote closure of one, two or three <u>inner</u> loops, respectively
$\angle$	Angle
sgn	Signum function
det	Determinantal operator
$\vdots$	Partition between arrays in a matrix
$j,$	$\sqrt{-1}$
π	$3.14159 \ldots$
lim	limit of ...

$|\cdots|$	Absolute value of ...
%	Percent
∞	Infinity

Abbreviations

ABSV	Absolute value operator
ACC	Accident
AILS	Advanced Integrated Landing System
AN/CPU-80A	Military nomenclature for a specific flight director computer
APP	Approach
AR	Amplitude of a complex variable
ARR	Arrival
AS	Airspeed
Cat	Category
$\mathbb{C}$	Centerline
COV	Covariance
CTOL	Conventional take-off and landing
CW	Continuous wave
db, dB	Decibel ($20 \log_{10} AR$ or $10 \log_{10} PR$)
DC	"Direct current," meaning static or steady-state when used as an adjective modifying gain
DH	Decision height
DLC	Direct lift control
DME	Distance Measuring Equipment
FAA	Federal Aviation Agency
FM	Frequency modulation

SYMBOLS (cont'd)

Grnd	Ground
GS	Glide slope
ILS	Instrument landing system
LAT	Lateral
LE	Leading edge (flaps)
LIB	Library
LONG	Longitudinal
MA	Missed approach
MAC	Mean aerodynamic chord
NAFEC	National Aviation Facilities Experimental Center, Atlantic City, N. J.
NP1	Number of first order poles
NP2	Number of second order poles
NZ1	Number of first order zeros
NZ2	Number of second order zeros
OK	Safe landing
PDR	Damping ratio of (second order) pole
PNF	Undamped natural frequency of (second order) pole
PR	Power ratio
PRP	Pulse repetition period
REF	Reference
RHS	Right hand side
RMS	Root-mean-squared value
RPM	Revolutions per minute
RSS	Root-sum-squared value

SYMBOLS (cont'd)

RTCA	Radio Technical Commission for Aeronautics
RVR	Runway visual range
SC	Special Committee
SQ RT	Square root operator
STOL	Short take-off and landing
TACLAND	Tactical Landing System
TE	Trailing edge (flaps)
UHF	Ultra-high (radio) frequency (300 mHz to 3000 mHz)
VHF	Very high (radio) frequency (30 mHz to 300 mHz)
VTOL	Vertical take-off and landing
ZDR	Damping ratio of (second order) zero
ZNF	Undamped natural frequency of (second order) zero

SECTION I

INTRODUCTION

This report presents the results of an analytical investigation of measuring system requirements for instrument low-approach. It demonstrates the application of a general dynamic system model for aircraft low-approach operations so as to compute mathematical measures of performance, safety, and pilot acceptance which are appropriate to the determination of the requisite characteristics of the measuring system. (As distinct from the control system, the measuring system is here understood to comprise those elements of the landing guidance and control system which determine translational aircraft motion variables in earth-fixed coordinates.) The model is analyzed in connection with two typical aircraft together with their control systems so as to determine the variables to be measured, data rates required, and the influence of noise and bias errors in the measurements. The disturbing influence of wind gusts and is taken into account, and indeed is shown to be one of the principal determinants of performance.

A. PURPOSE OF THE INVESTIGATION

The United States Air Force has underway a program for the development of a tactical landing system (TACLAND) whose ultimate performance goal is to provide guidance information for zero visibility letdown, approach, go-around, flare, touchdown, roll out, take-off and climb out. The system will ultimately be used for all types of USAF aircraft (from VTOL to large supersonic) and at all types of bases from forward and combat operating bases to main permanent bases. Furthermore, it is intended that the development should be coordinated with national efforts to define a standardized replacement for the existing instrument low-approach system (e.g. the work of the Radio Technical Commission for Aeronautics Special Committee 117). An interim performance goal is to provide guidance information for low-visibility take-off and landing under weather minimum conditions of a 100 ft ceiling and 1/4 mile forward visibility. This interim goal would be substantially satisfied

1

by the achievement of a successful instrument low-approach capability.

While there have already been a number of "system" studies of TACLAND (Ref. 1 - 6), these have been primarily concerned with the characteristics of the ground-based equipment, and have, by and large, failed to address themselves directly to the question of the requirements and/or limitations which may be imposed on the measuring subsystem by the dynamics of the aircraft and their control subsystems, in response to commands and disturbances. Indeed, the whole question of what constitutes "successful" system performance may be a matter of debate, yet it is precisely at this point where we must begin, if we wish to distribute the error budget and to rationally determine specifications for subsystem and component performance.

The overall low-approach (or landing) system includes many elements: ground-based landing aids; airborne guidance equipment; communication, navigation, and identification channels; the aircraft; the flight control system; pilot (and flight crew); displays, etc. Performance of the overall low-approach system depends on the interaction among these components. Because of the tremendous variety of aircraft and control system dynamics, piloting techniques, manual or automatic flight operations, environmental conditions, and so forth which may be involved, the overall low-approach (or landing) system in which TACLAND is to play a part is enormously complex and varied. Generally, however, we may divide the system into two principal functional parts, the measuring system, and the control system.

The measuring system performs both sensing and guidance functions as needed to determine the course to be followed by the aircraft. The control system utilizes this guidance information to determine, develop, and apply appropriate forces and moments to the aircraft to execute the guidance commands. The measuring system is used to make such outer loop and/or low frequency measurements as position, altitude, glide path, distance, range rate, and flight path angle, using equipment which may fall into the categories of ground-based landing aids, airborne guidance equipment or ICNI (Integrated Communication Navigation and Identification) gear.

In this separation of functions and equipment the control system would include the aircraft, the flight control system, pilot, and displays.

As a practical matter the tactical landing system is essentially the measuring system as defined above. To determine meaningful, detailed performance specifications for the measuring system requires an allotment of the total system errors and a reflection of the overall system performance into the measuring and control subsystems. To accomplish this actually requires a detailed quantitative appreciation of the relationships between subsystem and overall system performance; but this is not presently available. Consequently, a need exists for orderly procedures to analyze subsystem requirements based upon specified overall landing system requirements. This leads to the essential purpose of the investigation reported here. It is:

> To develop and demonstrate an orderly method of analysis
> for determining measuring system requirements and for
> analyzing the interactions among the various elements
> of the measuring and control systems.

If this purpose is accomplished, it will be possible to analyze the effects of changes and interplay among the various elements in the total low-approach system. From the appreciation and understanding gained thereby, requirements can be established for the characteristics of the ground-based signals and their conversion to airborne control commands. This is a key item of system analysis support for TACLAND preliminary design. It is, however, only one element of several leading to the development of TACLAND performance specifications. As illustrated in Fig. 1 the investigation reported here covers the first block and a portion of the second with respect to the approach phase of the landing process. From the "Landing System and Subsystem Analysis Techniques" development the outputs are "Procedures" and "Measures." The "Procedures" cover system and subsystem analyses leading to estimates of measures for system and subsystem performance, safety, and pilot acceptance.
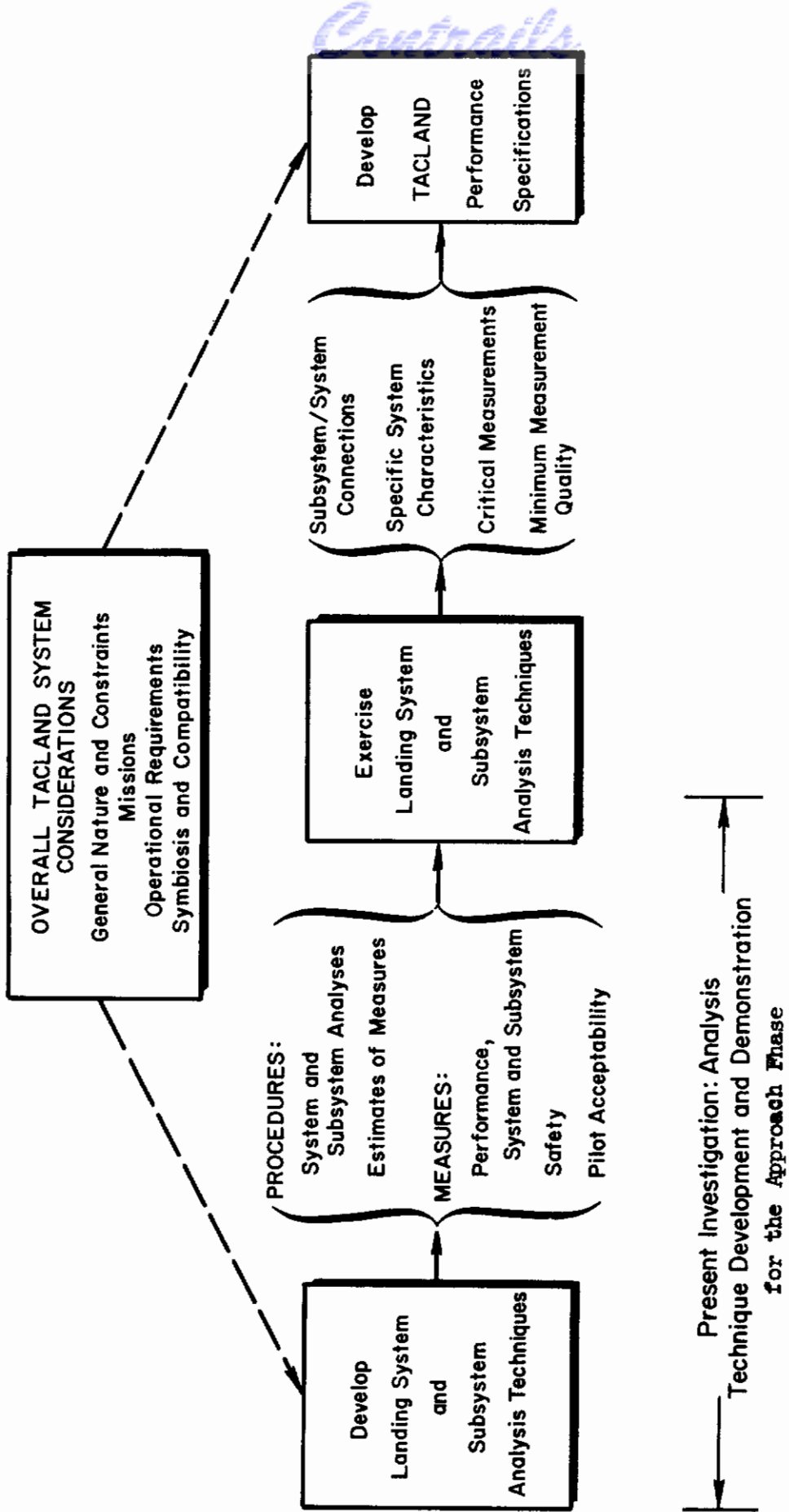
Figure 1. System Analysis Support for TACLAND Preliminary Design

4

B. SYNOPSIS OF THE ANALYSIS

The three part system model and procedure of Ref. 7 have been adapted to the purposes, described above, of the TACLAND measuring system requirements investigation. The three parts of the overall model are the dynamic system model, the performance measures and the probability tree outcome model. Each of these three elements is briefly introduced here, and the analytical procedures are described in terms of the flow diagram of Fig. 2.

The dynamic system model comprises the elements necessary to perform the steps enumerated as ① to ④ in Fig. 2.

Functions to be performed during the approach phase, for our purposes, consist primarily of capture and tracking of the localizer course and glide slope down to the decision height. (Capture of the localizer may typically take place 10 - 30 mi from the runway threshold and, in the present instance, the decision height will invariably be 100 ft.) Although there are other functions to be performed during approach, such as checklists, flap and landing gear extension, communications, etc., these aspects of system operation are beyond the scope of the present dynamic system model.

The airplane dynamics are represented by linearized, perturbation equations for the motions and the guidance system kinematics. The linearization is for trimmed flight in the neighborhood of the localizer course and the glide slope. As particular examples, the A-7D, a single-engined jet attack airplane, and the DC-8-60, a large jet transport, were selected to illustrate the application of the method in the investigation reported here.

Definition of the feedback control arrangements was accomplished in two different ways to show the scope of the procedure. The actual dynamics of the longitudinal and lateral primary control systems in the A-7D were accepted as limiting factors in its low-approach performance, and manual control of the approach, using a flight director, was taken to be the interesting mode of operation. Synthesis of the steering

① Determine Functions to be Performed During Approach Phase

② Define Airplane Dynamics

③ Define Feedback Control Arrangement (Manual and Automatic System Block Diagrams)

④ Select Inputs (Gusts, Shear, Beam Noise, Remnant, etc)

⑤ Exercise Model by Applying Inputs to System and Computing Performance Metrics (Means and σ's)

⑥ Define Approach Outcomes in Terms of Critical Values of Usual Variables in Numerical Terms

⑦ Define Figures of Merit (e.g. Approach Outcome Probabilities) In Terms of Performance Metrics and Critical Limits

⑧ Compute Numerical Values for Approach Outcome Probabilities (or Figures of Merit)

Figure 2. Outline of Analytical Steps Leading to Evaluation of Category II Approach Systems

6

laws for the flight director was constrained to the system configuration
of the AN/CPU-80A flight director computer installed in the airplane,
but an attempt was made to select gains and time constants which would
yield good approach performance with low pilot workload. In the case
of the DC-8, an advanced, high performance automatic pilot and approach
coupler were assumed in a deliberate effort to show how the demand for
very good approach tracking performance might impose severe requirements
on the measuring system. On the other hand the performance was restricted
in such a way that, for example, the control motions would be acceptable
to the pilot.

Inputs to the system, comprising winds, wind shears, random gusts,
pilot remnant in the case of manual control, and guidance system noise,
were selected from among the best sources available to be typical or
moderately severe. In all these cases, however, definitive data are
very hard to come by.

Step ⑤ in Fig. 2 is straightforward. It involves the computation
of performance metrics, such as the mean and standard deviation of
deviation from the glide slope in the presence of wind shear, random
gusts, guidance system bias and radio noise. Under the assumption of
Gaussianly distributed gust velocities and noise, and with deterministic
winds and shears, with linearized closed-loop aircraft guidance and control,
these calculations, in effect, yield the probability density functions of
any of the aircraft motion variables of interest.

Steps ⑥ and ⑦ are at the heart of the definition of approach
"success" in terms of performance, safety, and pilot acceptance. For
reasons which are fully developed in the body of the report, critical
values of the variables are defined in terms of the dimensions of the
Cat II "window" with the subsidiary conditions that, during the approach,
aircraft attitude angles and control deflections not be "excessive."
Then the principal figure of merit for the system is defined to be the
probability of passing through the window on any given approach.

Low-visibility landing categories defined by the International
Civil Aviation Organization (ICAO), are determined by reference to the

minimum runway visual range (RVR) and decision height (DH). Decision
height is a height above the runway elevation below which the pilot
may not descend in the absence of adequate visual references to land.
Without these he must initiate a missed approach at the decision height.
Category II-B conditions correspond to a RVR of 1,200 ft and a decision
height of 100 ft. (Note that these conditions closely approximate the
conditions appropriate to the interim goal for the TACLAND system
development.) Furthermore, it is recommended that a missed approach be
executed if the aircraft, at the decision height, is in a state which
deviates by more than specified amounts from the nominal or reference
condition. The specified amounts define the dimensions of the Cat II
window. These are illustrated in Fig. 3. The permissible normal deviation,
$\Delta d = \pm 12$ ft, and lateral deviation, $\Delta y = \pm 72$ ft, are limits recommended
by American and United Airlines for Cat II operations. They correspond,
at 100 ft, to 1 "dot" of glide slope error and to 1/3 "dot" of localizer
error on a standard ILS. The permissible airspeed deviation,
$\Delta AS = \pm 5$ kts $= \pm 8.45$ ft/sec, is a "guesstimate" by several airline
pilots as to an acceptable number for Cat II operations. (Ref. 7)

Other limits, such as the choice of what would constitute "excessive"
attitude angles or control deflections, could not be made quantitative
on the basis of present knowledge. They were finally and fuzzily set
on the basis of rough judgment.

Ultimately, at Step 8 , the results from Steps 5 and 7 are used
in a probability tree outcome model to compute:

- the probability that an approach will pass through
  the window (performance)

- the number of approaches required to land, given
  an arrival in the terminal area (safety)[*] and to
  estimate:

- the probability that attitude angles and control
  deflections will not be considered excessive
  (pilot acceptance)

---

[*] The reasons for this choice of a figure of merit are developed in the
body of the report.
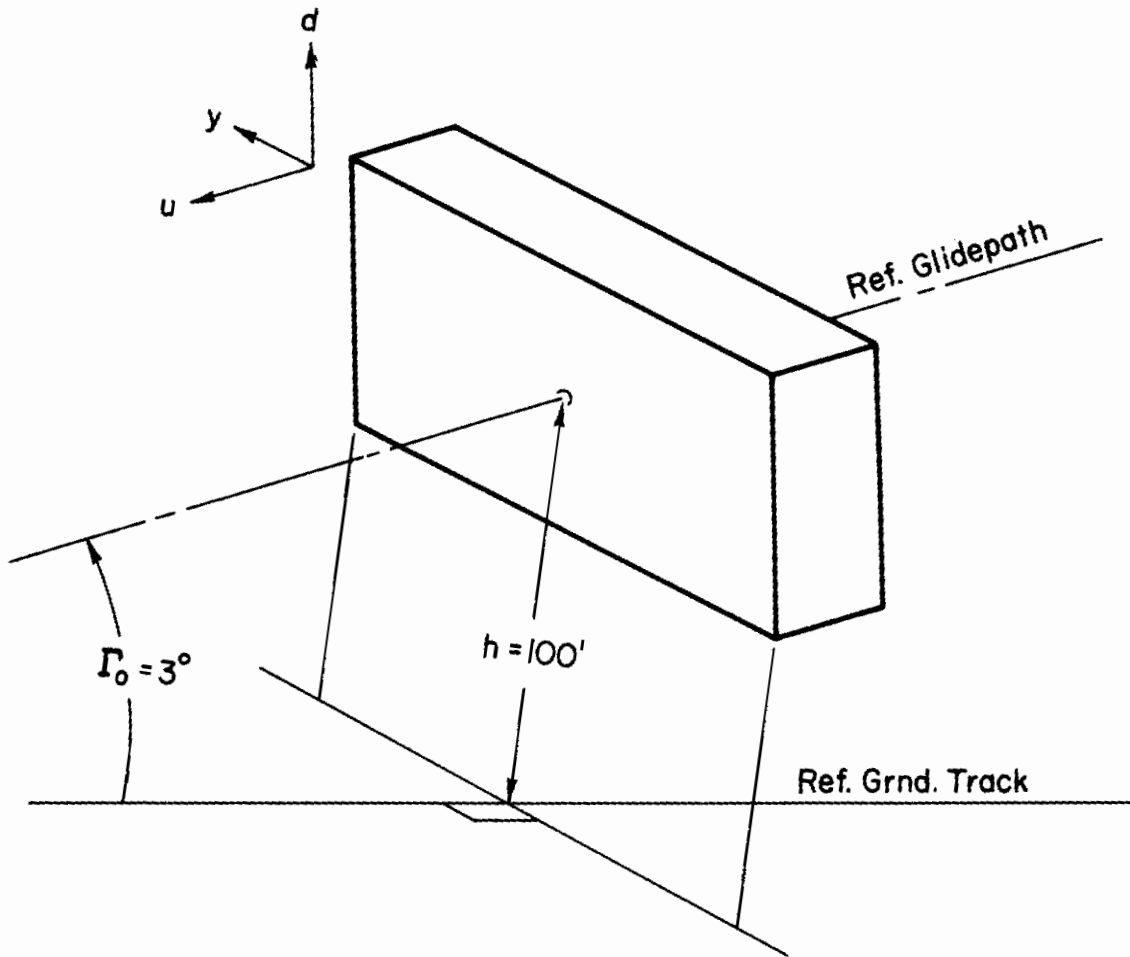
$$\Delta d = \pm 12 \text{ ft}$$
$$\Delta y = \pm 72 \text{ ft}$$
$$\Delta AS = \pm 5 \text{ kts} = \pm 8.45 \text{ ft/sec}$$

Figure 3. The Recommended Category II Window

9

The result of all this then is a set of performance metrics and outcome probabilities for a specific aircraft guidance and control system arrangement subjected to a given input and disturbance environment. Variations on the system can be tried in a way which makes their effect clear, and this provides a route to the formulation of requirements. (See Fig. 1.)

C. OUTLINE OF THE REPORT

The organization of the remainder of the report follows the flow chart of Fig. 2 and the discussion above.

Linearized equations of motion, as well as geometrical, inertial, and dimensional stability derivative data for the two example aircraft are presented in Section II.

Section III discusses feedback control arrangements for approach guidance in four parts under two headings. First longitudinal-vertical control is considered in general terms, and then the exposition is specialized to the cases of manual-flight director control of the A-7D and advanced automatic pilot control of the DC-8-60. Next lateral-directional control is, in turn, considered in general terms, and, again, the development is made specific in connection with both manual flight-director control of the A-7D and advanced automatic pilot control of the DC-8-60.

System inputs are described in Section IV, and the actual choice of mathematical models for winds, wind shears, gusts, beam anomalies and bias errors, fluctuation noise, missed sample effects, and human pilot remnant are recorded there.

The formulation of appropriate measures of performance, safety and pilot acceptance is accomplished in Section V. Immediately thereafter, in Section VI, the background for the computation of these measures is explored and the results of the computation are displayed.

Section VII addresses itself to the computation of the probabilities of the outcomes of an approach and presents the results for the examples of manual-flight director and automatic pilot controlled approaches.

Insofar as they are revealed by only the two examples which were analyzed, the principal implications of the results with respect to requirements on the measuring subsystem are dealt with in Section VIII.

Conclusions which were drawn from the investigation are summarized in Section IX.

A series of Appendices to the report presents certain details of the analysis which are necessary for a complete understanding of the work which was done, but which would interfere with the continuity of the body of the report if they were included there.

11

SECTION II

AIRCRAFT DYNAMICS

The controlled element for the landing approach task actually includes the airframe and the flight control subsystem. In the investigation reported here two different aircraft together with their control systems were considered as examples. These were the A-7D, a single-engined attack airplane and the DC-8-60, a large jet transport. This Section conveniently presents the dynamics of the example aircraft without stability augmentation. Later, in analyzing the A-7D flight director for manual guidance and control, we shall represent the actual manual "control augmentation" subsystem which modifies the dynamics of the airframe as a portion of the feedback control arrangement. Consideration of the automatic flight control system for the DC-8 as a portion of the feedback control arrangement is straightforward.

Each of the example aircraft can be adequately represented in the (trimmed) landing approach flight condition by ordinary linear differential equations of motion with constant coefficients (Ref. 8). This is because the approach task itself is one of regulating against disturbances from a desired rectilinear path in space, and the changes in altitude do not importantly change the flight condition. The linearization permits the efficient and powerful methods of system transfer function calculations to be applied subsequently.

In steady (trimmed) rectilinear flight the (linearized) differential equations of perturbed longitudinal, vertical and pitching motions can be separated from the equations describing the lateral, rolling and yawing motions. All these motions are then described by two sets of three simultaneous differential equations. The two sets are respectively termed "longitudinal" and "lateral."

In the process of linearization, the choice of the initial (trimmed) orientation of the body-fixed axis system is made for convenience.

The Laplace-transformed longitudinal set of equations is displayed in Table I in "body" axes with zero initial conditions (Ref. 9). These

12

TABLE I
LONGITUDINAL EQUATIONS OF MOTION

$$[\,A\,]\,\{u,\ w,\ \theta,\ \dot h,\ a_z,\ a_z',\ \dot h_p\}^T \;=\; [\,B\,]\,\{\delta_1,\ \dots,\ \delta_n,\ u_g,\ w_g\}^T$$

Left-hand matrix $[A]$ (state vector $u,\ w,\ \theta,\ \dot h,\ a_z,\ a_z',\ \dot h_p$):

u	w	θ	$\dot h$	a_z	a_z'	$\dot h_p$
$s - X_u^*$	$-X_w$	$W_o s + g\cos\theta_o$				
$-Z_u^*$	$(1-Z_{\dot w})s - Z_w$	$-U_o s + g\sin\theta_o$				
$-M_u^*$	$-M_{\dot w}s - M_w$	$s^2 - M_q s$				
$-\sin\theta_o$	$\cos\theta_o$	$-U_o\cos\theta_o - W_o\sin\theta_o$	1			
	$-s$	$U_o s - g\sin\theta_o$		1		
	$-s$	$\ell_{x_a}s^2 + U_o s - g\sin\theta_o$			1	
$-\sin\theta_o$	$\cos\theta_o$	$-\ell_{x_p}s^2 - U_o\cos\theta_o - W_o\sin\theta_o$				1

Right-hand matrix $[B]$ (input vector $\delta_1,\ \dots,\ \delta_n,\ u_g,\ w_g$):

δ_1	$\dots$	δ_n	u_g	w_g
X_{δ_1}	$\dots$	X_{δ_n}	$-X_u^*$	$-X_w$
Z_{δ_1}	$\dots$	Z_{δ_n}	$-Z_u^*$	$-Z_{\dot w}s - Z_w$
M_{δ_1}	$\dots$	M_{δ_n}	$-M_u^*$	$-M_{\dot w}s + \dfrac{M_q}{U_o}s - M_w$

$\dot h$ may be replaced by $\dot d$ or $\dot h_p$ by $\dot d_p$, if θ_o is replaced by $(\theta_o - \Gamma_o)$ in their respective equations.

See the list of symbols for the definition of constants and variables appearing in the table.

a_z and a_z' are accelerometer signals which cannot distinguish between gravitational and inertial acceleration.

13

equations are directly suitable for the expression of transfer functions.

Table II presents the Laplace-transformed lateral set of equations in "body" axes (Ref. 9).

The equations in Tables I and II may be simplified by initially orienting the body axis system to make $W_O = 0$. Such an orientation results in a "stability" axis system for which the X-axis in the steady state is collinear with the trimmed velocity, which may be initially inclined with respect to the local horizontal plane at the flight path angle γ_O. Since $\theta_O = \gamma_O + \alpha_O$ and $\alpha_O = \arctan W_O/U_O = 0$, $\theta_O = \gamma_O$ for "stability" axes (Ref. 8).

The equations in Tables I and II are especially adaptable to approach studies. For example, the vertical speed at the center of mass $(\dot{h})$ and at a fuselage station which is a distance x_p positive forward of the center of mass $(\dot{h}_p)$ may be converted to variables representing glide slope beam rate by substituting $(\theta_O - \Gamma_O)$ in place of θ_O only in the equations for $\dot{h}$ and $\dot{h}_p$, i.e. in the fourth and seventh rows. (The distance x_p is convenient for representing a forward glide slope receiving antenna location with respect to the center of mass.) The acceleration of the aircraft center of mass with respect to the localizer course may be found from the equation for $\dot{\lambda}$ in Table II by substituting $(\theta_O - \Gamma_O)$ in place of θ_O and by multiplying the entire equation by V_{T_O}. Lateral acceleration with respect to the beam at an antenna location a distance ℓ_x positive forward of and a distance ℓ_z positive below the center of mass may be found from the equation for $a_y^{(1)}$ by omitting the gravitational acceleration, i.e., by substituting $g = 0$.

Transfer functions for the response, ξ, to control or disturbance inputs, δ, are written in the form:

$$\frac{\xi(s)}{\delta(s)} = \frac{N_\delta^\xi(s)}{\Delta(s)}$$

The numerator $N_\delta^\xi(s)$ is obtained from the Laplace-transformed equations

TABLE II

LATERAL EQUATIONS OF MOTION

$$
\begin{bmatrix}
s-Y_v & -\dfrac{W_o}{V_{TO}} & \dfrac{U_o}{V_{TO}} & -\dfrac{g\cos\theta_o}{V_{TO}} & & & \\[2ex]
-L'_\beta & s-L'_p & -L'_r & & & & \\[2ex]
-N'_\beta & -N'_p & s-N'_r & & & & \\[2ex]
& -1 & -\tan\theta_o & s & & & \\[2ex]
-V_{TO}\,s & \ell_z s + W_o & -\ell_x s - U_o & g\cos\theta_o & 1 & & \\[2ex]
-\dfrac{V_{TO}}{U_o\epsilon_o}\,s & \dfrac{W_o}{U_o\epsilon_o} & -\dfrac{1}{\epsilon_o} & & & 1 & \\[2ex]
-\sin\alpha_G & & -\cos\alpha_G & & & & 1
\end{bmatrix}
\begin{bmatrix}
\beta \\[2ex] p \\[2ex] r \\[2ex] \varphi \\[2ex] a_y^{(1)} \\[2ex] \dot\lambda \\[2ex] r_G
\end{bmatrix}
=
\begin{bmatrix}
Y^*_{\delta_1} & \cdots & Y^*_{\delta_n} & -Y_v & \\[2ex]
L'_{\delta_1} & \cdots & L'_{\delta_n} & -L'_\beta & -L'_p \\[2ex]
N'_{\delta_1} & \cdots & N'_{\delta_n} & -N'_\beta \;-N'_r\,g\,s & -N'_p \\[2ex]
& & & & \\[2ex]
& & & & \\[2ex]
& & & & \\[2ex]
& & & &
\end{bmatrix}
\begin{bmatrix}
\delta_1 \\[2ex] \vdots \\[2ex] \delta_n \\[2ex] \beta_g \\[2ex] p_g
\end{bmatrix}
$$

λ = heading of aircraft velocity vector (measured in horizontal plane)

$\epsilon_o = \cos\theta_o + (W_o/U_o)\sin\theta_o$

$\ddot y^{(1)} = a_y^{(1)} = a_y + \varphi_g\cos\theta_o$, because $a_y^{(1)}$ is measured by an accelerometer which cannot distinguish between gravitational and inertial acceleration

See the list of symbols for other definitions of constants and variables appearing in the table.

of motion by Cramer's rule. The denominator is the (characteristic) determinant of the coefficients of the dependent variables.

Coupling numerators which appear in multiloop analysis (Ref. 8, 10) depend on two response and two "control" variables, one of which may be a control input and other either an additional control or a disturbance. The coupling numerator is found by a process analogous to Cramer's rule in which two columns of the characteristic determinant, Δ, (associated with the two response variables of concern) are respectively replaced by the columns of coefficients of the two inputs of concern. The awkward but descriptive symbol $N_{\delta_1 \delta_2}^{\xi_1 \xi_2}$ is intended to suggest this replacement.

Numerical values for the coefficients of the equations in Tables I and II and for the polynomial factors of the characteristic denominators, numerators and selected coupling numerators are presented in Tables III and IV. Table III is for the A-7D airplane alone and Table IV is for the DC-8 airplane. Appendix A presents a simplified equivalent representation of the A-7D pitch axis manual control system with "control augmentation." Explanatory notes show how to interpret the arrangement of the results in the tables. These results will be used in analyzing the feedback control arrangements to be discussed in Section III which follows.

16

TABLE III

A-7D PARAMETERS FOR LANDING APPROACH CONFIGURATION

GEOMETRY & INERTIA		LONGITUDINAL STABILITY AXES		LATERAL STABILITY AXES	
C_{L_o}	0.693	X_u (1/sec)	-0.0457	Y_v (1/sec)	-0.251
h (ft)	0	X_w (1/sec)	0.0833	$Y_{\delta_a}^*$ (1/sec)	-0.0258
M	0.226	$X_{\delta_{TH}}$ (ft/sec²/lb thrust)	15.3×10^{-4}	$Y_{\delta_r}^*$ (1/sec)	-0.0453
V_{T_o} (ft/sec)	253.0	Z_u (1/sec)	-0.244	L_β (1/sec²)	-11.8
γ_o (deg)	-2.8	Z_w (1/sec)	-0.708	L_p (1/sec)	-2.24
q (lb/ft²)	76.0	$Z_{\delta_{iT}}$ (ft/sec²/rad)	-28.0	L_r (1/sec)	0.915
S (ft²)	375.0	$Z_{\delta_{TH}}$ (ft/sec²/lb thrust)	-2.83×10^{-4}	L_{δ_a} (1/sec²)	14.4
b (ft)	38.73	M_u (1/sec-ft)	-0.000121	L_{δ_r} (1/sec²)	2.24
c (ft)	10.84	M_w (1/sec-ft)	-0.00990	N_β (1/sec²)	2.43
W (lb)	20,600.	$M_{\dot{w}}$ (1/ft)	-0.000295	N_p (1/sec)	-0.143
m (slugs)	642.0	M_q (1/sec)	-0.388	N_r (1/sec)	-0.405
I_x (slug-ft²)	0.1332×10^5	$M_{\delta_{iT}}$ (1/sec²)	-3.86	N_{δ_a} (1/sec²)	0.645
I_y (slug-ft²)	0.6657×10^5	$M_{\delta_{TH}}$ (1/sec²/lb thrust)	0.0407×10^{-4}	N_{δ_r} (1/sec²)	-1.69
I_z (slug-ft²)	0.7370×10^5	M_α (1/sec²)	-2.50		
I_{xz} (slug-ft²)	-0.2046×10^4	$M_{\dot{\alpha}}$ (1/sec)	-0.0746		
X_{CG} (% c)	29.04				
δ_{F_o} (deg)	40 (T.E.); 42 (L.E.)				
α_o (deg)	5.36				
δ_{iT_o} (deg)	-2.63				

I_x, I_y, I_z, and I_{xz} are given for Stability Axes. α_o is the angle between the X-body axis and X-stability axis. Derivatives not listed are assumed zero. $U_o = V_{T_o}$, $W_o = 0$, and $\Gamma_o = \gamma_o = \theta_o$.

TABLE III (cont'd)

LONGITUDINAL TRANSFER FUNCTIONS FOR THE A-7D IN LANDING APPROACH CONFIGURATION

Abbreviated notation is used for polynomial factors in root locus form:

Real factor (λ) means $(s + \lambda)$

Quadratic factor $[\zeta, \omega]$ means $[s^2 + 2\zeta\omega s + \omega^2]$

Denominator

$$\Delta = [0.114, 0.164][0.353, 1.668]$$

Numerators

δ_{iT} Control Input

$$N^{\theta}_{\delta_{iT}} = -3.854(0.601)(0.082)$$

$$N^{\hbar}_{\delta_{iT}} = 28.01(4.957)(-4.477)(0.029)$$

$$N^{\dot{d}}_{\delta_{iT}} = N^{\hbar}_{\delta_{iT}} - \Gamma_o N^{u}_{\delta_{iT}}$$

$$N^{u}_{\delta_{iT}} = -2.333(-19.649)(1.726)$$

δ_{TH} Control Input

$$N^{u}_{\delta_{TH}} = 15.32(-0.043)[0.358, 1.671]$$

Coupling Numerators

$$N^{u \quad \theta}_{\delta_{TH}\delta_{iT}} = -59.02(0.621)$$

$$N^{u \quad \hbar}_{\delta_{TH}\delta_{iT}} = 428.9(4.982)(-4.519)$$

18

TABLE III (cont'd)

LATERAL TRANSFER FUNCTIONS FOR THE A-7D IN LANDING APPROACH CONFIGURATION

Abbreviated notation is used for polynomial factors in root locus form:

Real factor (λ) means $(s + \lambda)$

Quadratic factor $[\zeta, \omega]$ means $[s^2 + 2\zeta\omega s + \omega^2]$

Denominator

$$\Delta = (2.527)(0.037)[0.094, 1.869]$$

Numerators

δ_a Control Input

$$N_{\delta_a}^r = 0.2451(2.282)[-0.782, 3.123]$$

$$N_{\delta_a}^\varphi = 14.4[0.205, 1.759]$$

$$N_{\delta_a}^{\lambda} = -0.02583(9.793)(-7.476)[0.102, 1.698]$$

$$s^2 N_{\delta_a}^y = V_{T_o} N_{\delta_a}^{\lambda}$$

δ_r Control Input

$$N_{\delta_r}^{\lambda} = 0.04533(-2.475)(2.272)[0.531, 2.699]$$

$$N_{\delta_r}^r = -1.765(2.53)[-0.003, 0.645]$$

$$N_{\delta_r}^\varphi = 2.512(-2.549)(2.323)$$

Coupling Numerators

$$N_{\delta_a \delta_r}^{\psi\, p} = 26.03(0.191)$$

$$N_{\delta_a \delta_r}^{\lambda\, r} = 0.03446(-8.034)(11.963)$$

$$N_{\delta_a \delta_r}^{p\, \lambda} = 0.7178(2.832)(-2.447)$$

TABLE IV
DC-8 PARAMETERS FOR LANDING APPROACH CONFIGURATION

GEOMETRY & INERTIA		LONGITUDINAL STABILITY AXES		LATERAL BODY AXES	
C_{L_O}	1.0	X_u (1/sec)	-0.0373	Y_v (1/sec)	-0.0887
h (ft)	0	X_w (1/sec)	0.136	Y_p (ft/sec)	±0.245
M	0.204	X_{δ_T} (ft/sec^2/% RPM)	0.106	Y_r (ft/sec)	2.45
V_{T_O} (ft/sec)	228.0	Z_u (1/sec)	-0.283	$Y_{\delta_a}^*$ (1/sec)	0
γ_O (deg)	-2.8	Z_w (1/sec)	-0.750	$Y_{\delta_r}^*$ (1/sec)	0.031
q (lb/ft^2)	61.8	Z_{δ_e} (ft/sec^2/rad)	-9.25	L_β (1/sec^2)	-1.40
S (ft^2)	2758.0	Z_{δ_T} (ft/sec^2/% RPM)	-0.00097	L_p (1/sec)	-1.04
b (ft)	142.4	M_u (1/sec-ft)	0	L_r (1/sec)	0.474
c (ft)	22.16	M_w (1/sec-ft)	-0.00461	L_{δ_a} (1/sec^2)	1.13
W (lb)	180,000.0	$\dot{M}_w$ (1/ft)	-0.00085	L_{δ_r} (1/sec^2)	0.159
m (slugs)	5,580.0	M_q (1/sec)	-0.594	N_β (1/sec^2)	0.368
I_x (slug-ft^2)	3.2 x 10^6	M_{δ_e} (1/sec^2)	-0.923	N_p (1/sec)	-0.029
I_y (slug-ft^2)	3.8 x 10^6	M_{δ_T} (1/sec^2/% RPM)	0.000623 X_{δ_T}	N_r (1/sec)	-0.257
I_z (slug-ft^2)	6.6 x 10^6	M_α (1/sec^2)	-1.05	N_{δ_a} (1/sec^2)	0
I_{xz} (slug-ft^2)	0	$\dot{M}_\alpha$ (1/sec)	-0.1936	N_{δ_r} (1/sec^2)	-0.368
X_{CG} (% c)	25.2				
δ_{F_O} (deg)	50				
α_O (deg)	0.62				

I_x, I_y, I_z, and I_{xz} are given for Body Axes. α_O is the angle between the X-body axis and X-stability axis. Derivatives not listed are assumed zero. $U_O = V_{T_O}$, $W_O = 0$, and $\Gamma_O = \gamma_O = \theta_O$.

TABLE IV (cont'd)

LONGITUDINAL TRANSFER FUNCTIONS FOR THE DC-8 IN LANDING APPROACH CONFIGURATION

Denominator

$$\Delta = [0.10, 0.167][0.626, 1.231]$$

Numerators

δ_e Control Input

$$N_{\delta_e}^u = -1.258(4.03)(-4.082)$$

$$N_{\delta_e}^w = -9.25(23.34)[0.107, 0.198]$$

$$N_{\delta_e}^\theta = -0.9151(0.101)(0.646)$$

$$N_{\delta_e}^{\dot h} = 9.239(0.042)(-3.607)(4.397)$$

$$N_{\delta_e}^{\dot d} = 9.25(0.035)(-3.606)(4.396)$$

u_g Gust Input

$$N_{u_g}^u = 0.0373(1.543)[0.599, 0.857]$$

$$N_{u_g}^w = 0.283(0)(0)(0.594)$$

$$N_{u_g}^\theta = -0.0002406(0)(5.424)$$

$$N_{u_g}^{\dot h} = -0.2845(0.007)[0.386, 1.027]$$

$$N_{u_g}^{\dot d} = -0.283(0)[0.384, 1.025]$$

w_g Gust Input

$$N_{w_g}^u = -0.1360(0)[0.486, 0.795]$$

$$N_{w_g}^w = 0.3498(4.379)[0.118, 0.166]$$

$$N_{w_g}^\theta = -0.001755(0)(-1.475)(-0.000464)$$

$$N_{w_g}^{\dot h} = -0.7425(1.243)[0.081, 0.214]$$

$$N_{w_g}^{\dot d} = -0.75(1.234)[0.091, 0.214]$$

Coupling Numerators

$$N_{\delta_e u_g}^{\theta\,u} = -0.03413(1.751)$$

$$N_{\delta_e u_g}^{\theta\,w} = -0.2612(0)$$

$$N_{\delta_e u_g}^{u\,w} = 0.345(1.102)(22.243)$$

$$N_{\delta_e w_g}^{\theta\,u} = 0.1223(0)$$

$$N_{\delta_e w_g}^{\theta\,w} = -0.01624(0.092)(39.955)$$

$$N_{\delta_e w_g}^{u\,w} = -1.258(-0.696)(23.626)$$

21

TABLE IV (cont'd)

LATERAL TRANSFER FUNCTIONS FOR THE DC-8 IN LANDING APPROACH CONFIGURATION*

Denominator

$$\Delta = (1.176)(0.041)[0.116, 0.725]$$

Numerators

δ_a Control Input

$$N_{\delta_a}^p = 1.13(-0.001)[0.277, 0.626]$$

$$N_{\delta_a}^{a_y'} = -0.5636(0.283)[0.023, 2.279]\dagger$$

$$N_{\delta_a}^r = -0.03277(-1.363)(1.315)$$

$$N_{\delta_a}^\lambda = 0.01216(13.143)[.196, 0.606]$$

$$N_{\delta_a}^y = \frac{V_{T_o}}{s^2} N_{\delta_a}^\lambda$$

$$N_{\delta_a}^\psi = \frac{N_{\delta_a}^r}{\cos(\alpha_o + \gamma_o)s}$$

δ_r Control Input

$$N_{\delta_r}^p = 0.159(-2.313)(1.29)(-0.001)$$

$$N_{\delta_r}^r = -0.368(1.176)[-0.086, 0.386]$$

$$N_{\delta_r}^{a_y'} = 0.7384(3.58)(-1.729)(1.155)(-0.109)\dagger$$

$$N_{\delta_r}^\lambda = 0.031(-1.095)(1.263)[0.46, 1.227]$$

Coupling Numerators

$$N_{\delta_a \delta_r}^{p\ r} = -0.4158(0)(0.058)$$

$$N_{\delta_a \delta_r}^{p\ \lambda} = 0.03503(0.977)(-0.720)$$

$$N_{\delta_a \delta_r}^{r\ \lambda} = -0.001016(-57.553)$$

$$N_{\delta_a \delta_r}^{p\ a_y'} = 0.8344(3.726)(-1.759)(-0.002)\dagger$$

$$N_{\delta_a \delta_r}^{a_y'\ \lambda} = -0.01747(-1.505)[0.785, 5.419]\dagger$$

$$N_{\delta_a \delta_r}^{r\ a_y'} = -0.2316[0.07, 1.826]\dagger$$

* Abbreviated notation is used for polynomial factors in root locus form:

       Real factor (λ) means $(s + \lambda)$

       Quadratic factor $[\zeta, \omega]$ means $[s^2 + 2\zeta\omega s + \omega^2]$

† Accelerometer location 17.2 ft forward of c.g. @ 25.2% MAC

SECTION III

FEEDBACK CONTROL ARRANGEMENTS

A. LONGITUDINAL-VERTICAL CONTROL

A block diagram of a typical longitudinal-vertical approach measuring and control system is shown in Fig. 4.

At the top of Fig. 4 a distinction is drawn between the measuring subsystem and the control subsystem, although the boundary may be arbitrary and possibly subject to interpretation. As illustrated, however, the measuring subsystem emphasizes the (continuous or sampled, radio or radar) transmission of guidance data from a terminal site on the ground together with the airborne decoding of these data into commands for the control subsystem. In Fig. 4 the radiated guidance reference path is termed the "Beam Command."

Consider that the approach path is intended to be rectilinear. Then the beam command d_i will be identically zero and the guidance and kinematic relationships reduce to their simplest form. In these circumstances a noise-free glidepath signal would be directly proportional to the perpendicular error from the beam, d_e, i.e., $\lambda_d = d_e/R$. The variation with range gives an increased sensitivity as the aircraft approaches the aiming point. In contemporary low approach and landing systems, the time-varying gain introduced by the range variation is undesirable for stability, monitoring, and precision of control. Consequently, its effect is removed in the computer by changing the gain of G_{λ_d} with range (or altitude or time, which are roughly equivalent to range when on a constant speed approach down a straight path) during the final portions of the approach.

Besides the function of range de-sensitization, the receiver/decoder/ computer combination serves to demodulate the ground transmitted glidepath signal, reconstruct the signal if it is sampled (as with a scanning beam system), provide smoothing, and send an $\dot{h}_c$ control command to the control subsystem.

23
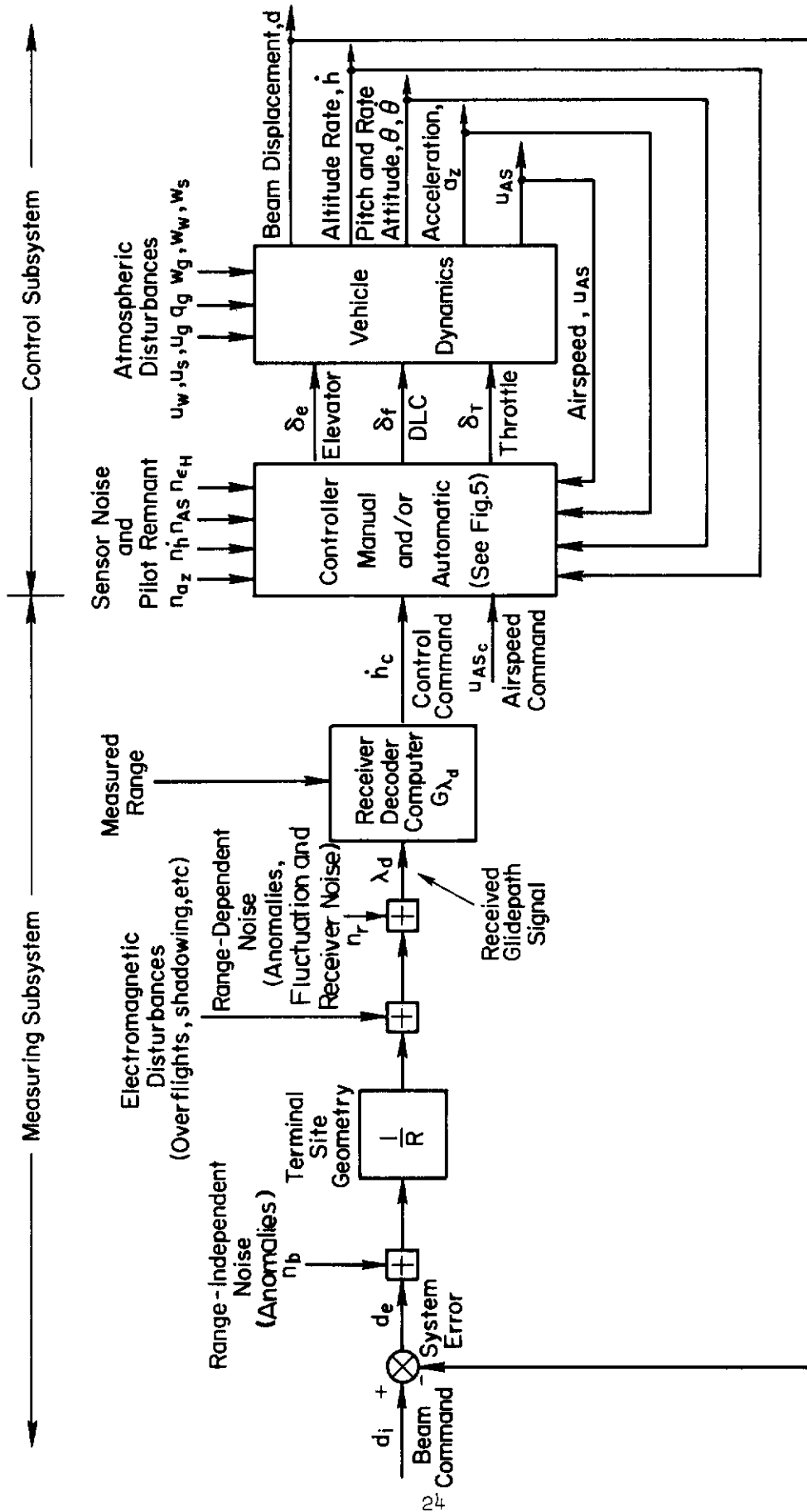
Figure 4. Measuring and Control System for Vertical Plane Approach

The measuring subsystem has three important, unwanted quantities. Two are noises, conveniently divided into range-dependent, n_r, and range-independent, n_b, quantities. The noise, n_r, represents those quantities which are approximately stationary when represented as angles (hence, range-dependent), whereas n_b represents noises which are approximately stationary when represented as lengths (hence, range-independent). Range-dependent noise includes the effective receiver noise, which tends to have a constant RMS value and thus is largest relative to the desired signal at the longer ranges. Other examples of range-dependent noise are the anomalies in the glidepath beam due to multipath transmissions from side lobes. These are insignificant at long ranges, but can become troublesome at short ranges where the side lobe power and hence its multipath transmission becomes more significant. An example of range-independent noise might be main beam multipath transmissions. In the vertical plane these are caused primarily by fixed structures, changes in ground reflection coefficients due to stratified wet and dry layers in the ground ("fixed" for a particular approach), and other deviations of the ground plane from an ideal reflecting surface where the ground reflecting surface is fundamental to the measuring system as in VHF-UHF ILS. Such effects appear as essentially stationary noise when referred to a ground dimension. The third unwanted input shown in Fig. 4 is the result of electromagnetic disturbances. These can come from lead aircraft creating an electromagnetic shadow on following aircraft on the same approach beam pathway, from multipath transmissions of overflying craft (either direct, as the current VHF-UHF ILS, or from side lobes with higher frequency transmissions), and so forth. Great emphasis is placed on these noise and distrubance sources because of their potentially limiting character in the measuring subsystem. Means of smoothing, rejecting, or partially ignoring these are important considerations for the TACLAND preliminary design.

Although the altitude rate feedback signal for damping the path-following dynamics is depicted in Fig. 4 within the control subsystem, part of or all of it might be supplied in the measuring subsystem. The development of a vertical velocity signal can, in general, be accomplished

using radio, barometric, and inertial[*] elements with complementary filtering and mixing to reduce the effect of beam noises. Development of a normal velocity signal exclusively from beam rate, however, has great appeal for general aviation and interurban service as well as possibly for tactical applications.

The airspeed command (in Fig. 4) usually comprises the longitudinal control reference for CTOL and STOL vehicles. Longitudinal position, however, can be an important additional landing system outer loop for VTOL aircraft.

Unwanted inputs to the controller in Fig. 4 are sensor noise errors and human pilot remnant in the case of manual control.

The remainder of the diagram in Fig. 4 shows that as many as three controls may be involved, if direct lift control (DLC) is available, and that as many as seven components of atmospheric disturbances might be considered. The disturbances act directly on the aircraft and the measurement of their effect is confused by vehicle motions in response to control inputs. The seven components of atmospheric disturbances are longitudinal tailwind (u_w), longitudinal windshear (u_s), longitudinal random gusts (u_g), pitching gusts (q_g) induced by the longitudinal gradient of normal random gusts (w_g), normal component of tailwind (w_w) and windshear (w_s).

Figure 5 provides a more detailed view of the controller block diagram of Fig. 4 and illustrates the difference between the signal flow for manual and/or automatic control. The only new signals shown are the outputs from the displays to the human pilot. For clarity only necessary control signals are shown which proceed from a flight director $(\epsilon_{DLC}$ and $\epsilon_H)$, and from an airspeed display (u_{AS}). In actuality, there will be a multitude of other displayed signals for the human pilot (and

---

* A single strapped-down accelerometer may suffice in lieu of a signal from a more complex inertial platform, velocity sensor, or navigation system.
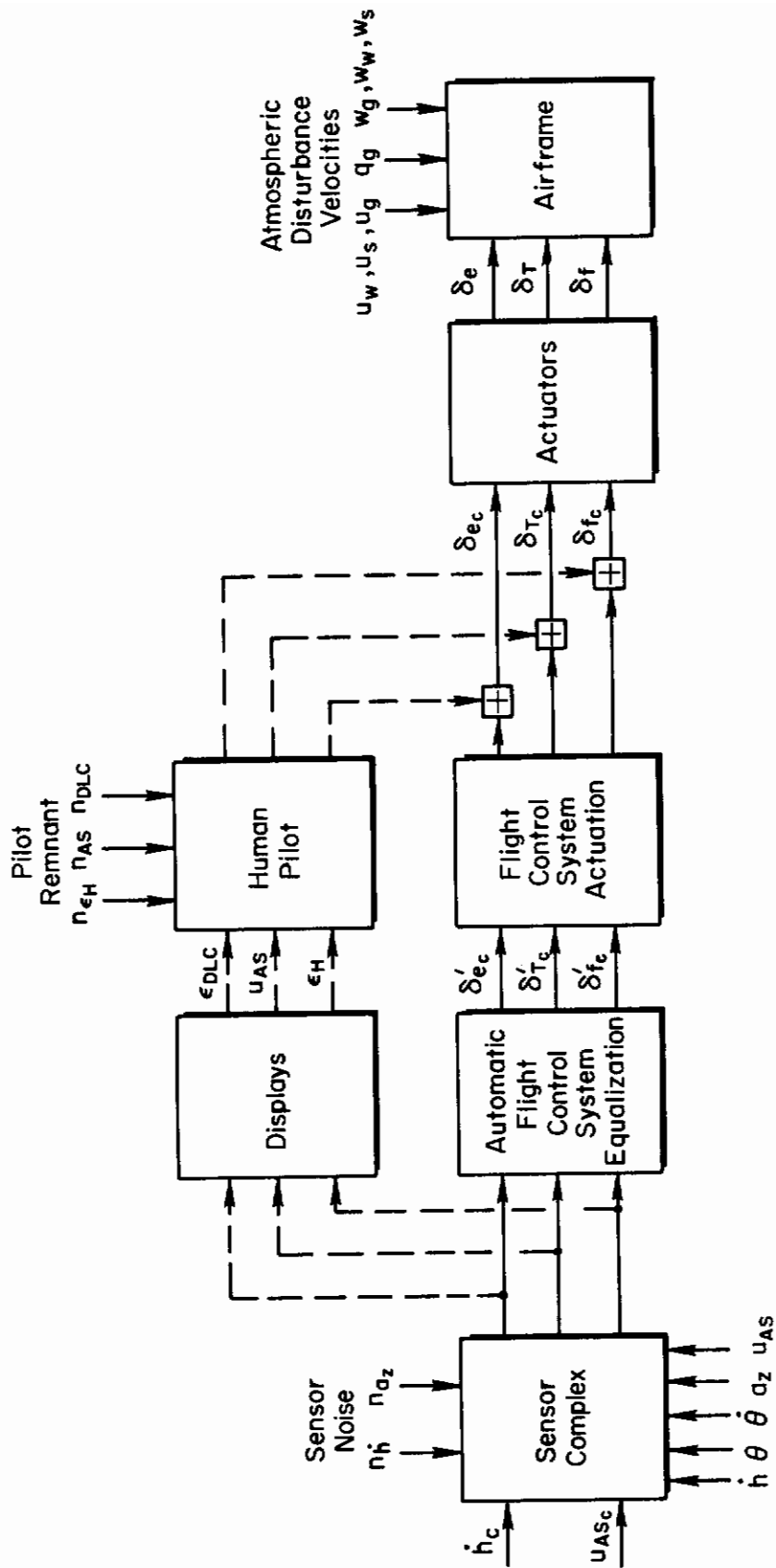
Figure 5. Controller Block Diagram (Longitudinal-Vertical)

copilot in the case of the DC-8 to monitor which may contribute to scanning workload and pilot remnant.

In the first example of feedback arrangement analysis we shall discuss techniques for optimizing the performance of a conventional flight director for manual approach control in the A-7D aircraft. No DLC is employed. In the second example we shall illustrate feedback system analysis with an advanced "windproofed" automatic flight control system in the DC-8 aircraft. The second example will illustrate superior approach tracking performance without employing direct lift control. This is achieved by abandoning some traditional notions about the regulation of pitch attitude and heading.

1. Manual Approach Glidepath Control of the A-7D Aircraft

The steps in optimizing the director/display/pilot/control interface for manual approach control of the A-7D can be listed in deceptively simple terms:

- select the proper signals for the director

- combine these signals with appropriate gains, equalization and filtering to obtain the required director commands

- display the director commands with appropriate sensitivity

- verify the system acquisition and tracking performance and disturbance regulation effectiveness

The system analysis here will address only the first two steps and will defer the verification of performance until Section VI. In selecting the proper signals for the director, we shall be guided by the specification for the AN/CPU-80A flight director (Ref. 11). However, we shall not be restricted by Ref. 11 in adopting the appropriate gains, equalization and filtering. Since the details of the calculations are lengthy, we shall confine the discussion here to the techniques, and to the presentation of the results.

A simplified equivalent system block diagram of the AN/CPU-80A approach glidepath flight director applied to the A-7D airframe and manual control system is given in Fig. 6. Certain elements of the feel and control augmentation systems are here represented by the approximation developed in Appendix A.

Fair glidepath tracking control can be accomplished with only horizontal "stabilator" control (δ_{iT}) in the A-7D by virtue of its trimmed approach at a speed in excess of that for trim response reversal. In such an approach condition fair speed regulation will accompany glidepath tracking through horizontal stabilator control with a very low gain throttle (δ_{TH}) control.

It is important to note in connection with Fig. 6 that the longitudinal feel and stability augmentation system includes bobweights which supply an acceleration, a_z, feedback and a pitch damper which supplies a rate, $\dot{\theta}$, feedback. These feedbacks modify the pilot's control displacement (δ_{ip}), which is in turn applied to the horizontal stabilator through a gain and low pass pitch rate attenuation filter. The low pass filter is designed to attenuate the peak normal acceleration in high dynamic pressure flight, but it is retained in the control system during approach. Since the filter time constant $T_f = 0.55$ sec, it will severely limit the glidepath tracking loop gain which can be used.

The zeros of the pitch attitude response (θ)-to-horizontal stabilator (δ_{iT}) input transfer function of the A-7D in approach are favorably located to provide inner loop lead equalization in the phugoid frequency range in parallel with the glidepath displacement (d)-to-pitch attitude command (θ_c) outer loop via radio guidance. (See Appendix B.) Therefore the only feedback signals strictly necessary for pilot/flight director glidepath tracking control are θ and d. The AN/CPU-80A flight director computer does not derive beam rate to provide path damping. Instead, it employs washed-out barometric height rate, but only after passing the middle marker. Thus, Fig. 6, for convenience, shows the $\dot{h}$-feedback signal represented in terms of its equivalent linear combination of glide slope rate $(\dot{d})$ and longitudinal velocity (u) in stability axes:
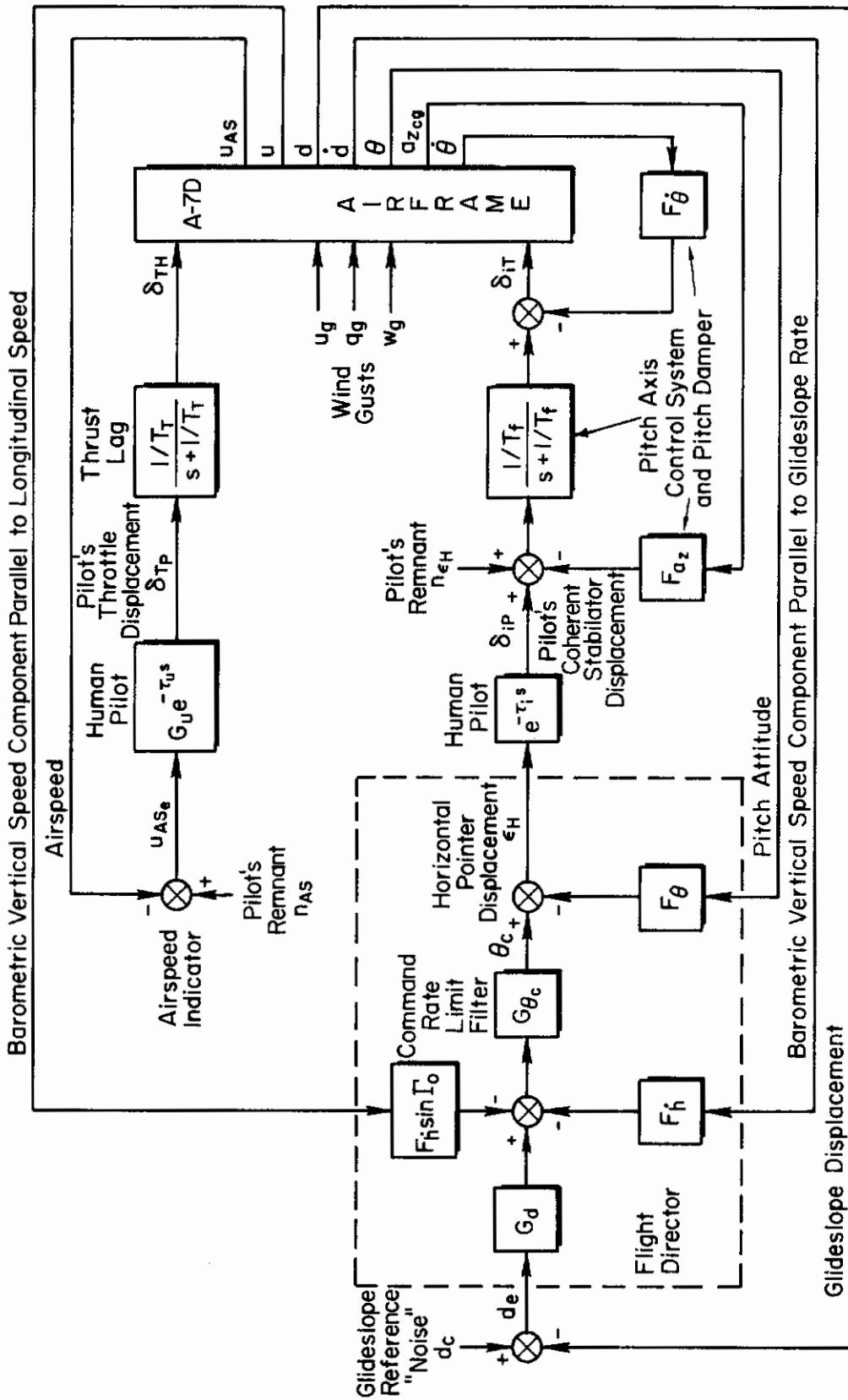
Figure 6. Equivalent Block Diagram for Manual Airspeed and Glidepath Displacement Control in the A-7D Aircraft (Pilot's gain is combined with flight director gains)

$\dot{h} = \dot{d} + u \sin \Gamma_0$, where Γ_0 is the trimmed glidepath angle.

The describing functions, gains, and time constants which appear in Fig. 6 are summarized in Table V.

For manual glide slope control the describing functions to be determined are denoted by F_θ, G_{θ_c}, $F_{\dot{h}}$, G_d, and G_u. An appropriate describing function characterizing the dynamic behavior of the human pilot in tracking tasks will be of the form (Ref. 12, 13):

$$Y_p(j\omega) \quad = \quad K_p \frac{(j\omega T_L + 1)}{(j\omega T_I + 1)} e^{-j\omega \tau_e}$$

where

K_p = pilot's static gain

T_L = lead time constant (relative rate-to-displacement sensitivity)

T_I = lag time constant

τ_e = effective time delay, including transport delays and high frequency neuromuscular phase lags.

These describing functions are analogous to the transfer functions which describe airframe and control system behavior.

In general, according to the rule of thumb of servomechanism analysis, the lead and lag equalization (T_L and T_I) are adjusted by the analyst to achieve the -20 db/decade slope of K/s in the range of $|s|$ where open-loop unit gain crossover is desired. The gain K_p is then adjusted to determine the required value of crossover frequency, ω_c.

The method for designing F_θ, G_{θ_c}, $F_{\dot{h}}$ and G_d, however, depends upon a very important result from engineering psychology (Ref. 12). This is namely that Y_p will consist of the pilot's effective time delay, $\tau_e \doteq 0.3$ sec, and a pure gain, K_p, when the flight director gains and equalization are optimum (that is, when the combination of the director, control system and aircraft dynamics together have a glide slope displacement loop transfer function which is approximately K/s in the region of open-loop unit gain crossover).

31

TABLE V

GAINS AND TIME CONSTANTS FOR MANUAL AIRSPEED AND
GLIDEPATH DISPLACEMENT CONTROL IN THE A-7D AIRCRAFT

Feedforward Terms		Feedback Terms		Remarks
G_u	$K_u T_u (s + 1/T_u)\ \dfrac{rad}{ft/sec}$			$K_u = 0.001\ \dfrac{rad}{ft/sec}$ $T_u = 0$ $e^{-\tau_u s} \doteq -\dfrac{(s - 6)}{(s + 6)}$ $h_{abs} = 100$ ft
τ_u	$0.36 - 0.08\left(\dfrac{1.75}{\sqrt[3]{h_{abs}}}\right)$ sec			
T_T	1.0 sec			
		F_θ	$-0.358\ \dfrac{(s + 2.54)}{(s + 1/T_f)}\ \dfrac{rad}{rad/sec}$	$T_f = 0.55$ sec
T_f	0.55 sec	$F_{a_{z_{cg}}}$	$2.12 \times 10^{-3}\ \dfrac{rad}{ft/sec^2}$	
τ_i	$0.36 - 0.08\left(\dfrac{253\sqrt{3}}{h_{abs}}\right)$ sec	F_θ	$K_\theta T_\theta (s + 1/T_\theta)\ \dfrac{T_{\theta_{wo}} s}{T_{\theta_{wo}} s + 1}$	$e^{-\tau_i s} \doteq -\dfrac{(s - 10)}{(s + 10)}$ $h_{abs} = 212$ ft
G_{θ_c}	$\dfrac{1/T_{\theta_c}}{s + 1/T_{\theta_c}}$	$F_{\dot{h}}$	$K_{\dot{h}}\ \dfrac{s}{(s + 1/T_{\dot{h}})}$	$K_{\dot{h}} = 0$, except after passing middle marker
G_d	$K_d\ \dfrac{1/T_d}{(s + 1/T_d)}$	$T_{\dot{h}}$	1.0 to 4.0 sec (MIL-C-83014)	
SELECTED GAINS AND CONSTANTS				
K_d	-0.00063 rad/ft	$K_{\dot{h}}$	$-0.001\ \dfrac{rad}{ft/sec}$	
T_d	0.25 sec	$T_{\dot{h}}$	22.2 sec	values required by spec. for $T_{\dot{h}}$ unusable
T_{θ_c}	1.0 sec	K_θ T_θ $T_{\theta_{wo}}$	-0.515 0.486 sec 20.0 sec	

32

The gains of the pilot's describing function for stabilator control in Fig. 6 will remain arbitrarily distributed among the unknown describing functions, F_θ, $F_{\dot{h}}$, and G_d, in our analysis, because the static gain of G_{θ_c} has been defined to be unity, and because for our purpose here it will not be necessary to show how to display the director commands with appropriate sensitivity. The pilot's time delay for stabilator control is shown separately with unit gain in Fig. 6 as $e^{-\tau_1 s}$, where $s = j\omega$. Thus, F_θ, G_{θ_c}, $F_{\dot{h}}$ and G_d become, in fact, the flight director transfer functions for unit pilot gain ($K_p = 1$). Furthermore F_θ, G_{θ_c}, $F_{\dot{h}}$ and G_d will then be determined so as to enable the human pilot to adopt the most desirable form for Y_p, a pure gain and time delay.

The analyses of the feedback arrangement of Fig. 6 are summarized in Appendix B.

A very low pure gain manual throttle control loop is closed first so as to regulate airspeed. This closure will also slightly augment phugoid damping, reduce $-1/T_{\theta_2}$ and increase $-1/T_{\theta_1}$, which are the zeros of the pitch attitude response-to-stabilator input transfer function. The effectiveness of this closure and the modification of the aircraft's transfer function singularities is limited by the one-second thrust lag time constant which is assumed for the simplified first-order propulsion dynamics. The analysis of this closure is not, in fact, illustrated in Appendix B which begins with the modified singularities for the pitch attitude closure through the feedback transfer function, F_θ.

In terms of the transfer functions illustrated in Fig. 6, and beginning with the innermost loops, it has already been pointed out that $F_{\dot{\theta}}$, F_{a_z} and $1/T_f$ are fixed by the characteristics of the longitudinal control system for the A-7D (see Appendix A and Table V), and that G_u is determined arbitrarily.

Consider next F_θ which provides a necessary inner loop equalization in parallel with the outer displacement loop. A steady-state pitch attitude washout (high-pass) filter is required to remove the effects of varying trimmed pitch attitude from the flight director display.

The value selected for the high-pass time constant is $T_{\theta_{WO}} = 20$ sec (Table V). This value is large enough so as not to interact with pitch attitude control loop dynamics in the crossover frequency range near the closed loop short period mode. Therefore it is not included in the analysis in Appendix B. Its inverse time constant $(1/T_{\theta_{WO}} = 0.05$ rad/sec) is chosen to be slightly larger than the magnitude of the smallest zero in the displacement (d)-to-pitch command (θ_c) response transfer function of the A-7D. This smallest zero determines the upper limit of closed loop trim response bandwidth. A phase lead filter is also required in the pitch attitude feedback signal to overcome the lag of the low pass pitch rate attenuation filter in the manual control system discussed previously. The value selected for the phase lead filter is $T_\theta = 0.486$ sec (Table V). The gain, K_θ, is determined in Appendix B so as to provide ample closed loop phugoid damping and slight increase in effective phugoid frequency bandwidth while maintaining a margin of short period stability. (See Table V for the gains and time constants which were selected as a result of the analysis.)

The intermediate washed-out barometric feedback function F_h provides path damping after passing through the pitch command rate limiting filter G_{θ_c}. Since the vehicle pitch axis control system already has a command rate attenuation filter, the inclusion of another filter in the flight director is actually redundant. If the filter in the flight director were to have any effect without drastically reducing the glide slope crossover frequency, Appendix B shows that the filter time constant should be provided by $0.5 \leq T_{\theta_c} \leq 1.0$ sec. $T_{\theta_c} = 1$ sec is chosen in the analysis so as to illustrate how it acts to depress glide slope crossover frequency which, in turn, degrades approach tracking performance.

The inverse wash-out time constant in F_h is $1/T_h$. It is chosen approximately equal to $1/T_{h_1}$, the smallest zero in the airframe vertical speed response to stabilator displacement, so as to wash out the trimmed sink rate on the glidepath. (Again see Table V.)

Finally consider G_d, the director glidepath displacement transfer function. It contains a pure gain K_d and a low pass beam noise

attenuation filter with time constant, $T_d = 0.25$ sec. This low pass filter affects higher frequencies than the low pass pitch rate attenuation filters in the director and manual control systems. Therefore, its effect on path control is effectively negligible and the beam noise filter has been omitted from the analysis in Appendix B. The gain, K_d, is determined in Appendix B to provide the highest possible bandwidth for tracking glidepath displacement and gust disturbance suppression which is consistent with adequate stability margins and the least sensitivity to pilot gain and time delay variation. Optimization of the gain K_d and final selection of the pilot gain K_p involve a compromise between smooth glidepath acquisition and least tracking error on glide slope. (The value of K_d chosen as a result of the analysis is displayed in Table V.)

Table VI summarizes the main features of the dynamics of the manual glide slope displacement control system of Fig. 6. Particularly

TABLE VI

A-7D MANUAL GLIDE SLOPE DISPLACEMENT CONTROL DYNAMICS
IN LANDING APPROACH WITH AN/CPU-80A FLIGHT DIRECTOR

		(Recommended by RTCA SC-79)
Crossover frequency	0.17 rad/sec	
Dominant path-following damping ratio	0.35	$(0.2 \leq \zeta \leq 2.0)$
Dominant path-following undamped natural frequency	0.28 rad/sec	
Dominant path-following undamped natural wavelength	1.1 mi	$(\lambda_1 \leq 1.1 \text{ mi})$
Short-period damping ratio	0.37	
Short-period undamped natural frequency	2.5 rad/sec	

important to note are the rather low crossover frequency and path-following damping ratio as well as the long path-following wavelength.

35

These features of the system dynamics are intimately related. Their improvement is limited by the fixed characteristics of the manual control system, most particularly by the filter time constant, T_f. Observe, however, that the performance of the system is just barely within the limits recommended by RTCA SC-79 for automatically coupled approaches (Ref. 14). By this standard, the performance on approach should be "satisfactory." Whether it, in fact, is, or is not, will be considered again in detail in Section VII.

The most important and useful closed loop transfer functions for disturbance and command inputs for the multiple closed loop system of Fig. 6 are summarized in Table VII.

2. Automatic Approach Glidepath Control of the DC-8 Aircraft

A simplified block diagram representing an approach coupler and automatic pilot for glidepath displacement control in the DC-8-60 aircraft is presented in Fig. 7. Note, however, that this figure does not represent the actual approach coupler and automatic pilot which are installed in the DC-8-60. In the first place, detailed information on that equipment could not be readily obtained, and in the second place, it was thought to be desirable to study the potential performance of advanced, "windproof" systems such as the ones which are scheduled to be installed on the new wide-body transports. (The performance of the advanced system is compared to the performance of more conventional designs in Ref. 7 where, furthermore, the choice of feedback variables and equalization is justified in more detail.)

The principal considerations in the system synthesis parallel the ones already outlined in connection with the A-7D. There are, however, some important differences. These revolve around the much higher bandwidths which can be achieved because the filter time constant associated with the AFCS actuator, T_a, is small, as well as in the features which make the system relatively windproof.

As in the A-7D, the approach flight condition for the DC-8 is at a trim speed above the one for trim response reversal, and both glidepath

TABLE VII

LONGITUDINAL CLOSED LOOP TRANSFER FUNCTIONS FOR A-7D

Abbreviated notation is used for polynomial factors in root locus form:

Real factor (λ) means $(s + \lambda)$

Quadratic factor $[\zeta; \omega]$ means $[s^2 + 2\zeta\omega s + \omega^2]$

Denominator:

$(0.0368)(0.0428)(0.895)(0.977)(2.127)(6.01)(10.38)*$

$*[0.366;0.284][0.3506;2.403]$

$$\frac{d}{u_g} = \frac{-0.244(0)(0.04354)(1.602)(6.03)(10.375)[0.999;0.987][0.384;2.203]}{\text{Denominator}}$$

$$\frac{d}{w_g} = \frac{-0.7204(0.0436)(0.174)(0.934)(1.0)(1.247)(6.01)(10.3)* \quad *[0.713;1.545]}{\text{Denominator}}$$

$$\frac{d}{d_{command}} = \frac{0.0321(-4.451)(-10.0)(0.045)(0.0454)(0.977)(4.931)(6.01)}{\text{Denominator}}$$

$$\frac{u}{u_g} = \frac{0.0457(0.0538)(0.106)(0.326)(0.889)(4.97)(10.37)* \quad *[0.992;1.99][0.371;2.344]}{\text{Denominator}}$$

$$\frac{u}{w_g} = \frac{-0.0833(0.0487)(0.896)(1.0)(2.16)(6.0)(10.36)* \quad *[-0.0382;0.282][0.196;0.2498]}{\text{Denominator}}$$

$$\frac{u}{d_{command}} = \frac{-0.002674(0)(-10.0)(-19.51)(0.045)(1.0)(1.722)(6.0)}{\text{Denominator}}$$

$$\frac{u_{AS}}{u_g} = \frac{-(0)(0.0488)(0.894)(1.0)(2.126)(6.0)(10.37)* \quad *[0.375;0.239][0.351;2.402]}{\text{Denominator}}$$

37

Figure 7. Block Diagram of Automatic Glidepath Displacement Control of the DC-8 Aircraft

tracking and speed regulation can be achieved with elevator control alone. For this reason neither an automatic nor manual throttle control is assumed.

The requirement for short-period damping and the possibility of extending the path-following bandwidth suggest the feedback of pitch rate, $\dot{\theta}$, to the elevator, δ_e. A conventional feedback of pitch attitude, θ, so as to achieve short-period attitude stiffness together with path damping is modified by a washout with a comparatively small time constant, T_{wo}. This has the effect of retaining the short-period attitude stiffness, but it trades path damping for a much reduced response to normal gusts. The analysis of this first set of loop closures is illustrated in Appendix B, and the appropriate gains and time constants are displayed in Table VIII.

TABLE VIII

SELECTED GAINS AND TIME CONSTANTS FOR
AUTOMATIC GLIDEPATH DISPLACEMENT CONTROL FOR THE DC-8

Pitch Rate and Attitude Stability Augmentation

$$1/T_a = 15 \text{ rad/sec}$$
$$1/T_{wo} = 0.7 \text{ rad/sec}$$
$$K_{\dot{\theta}} = -2.0 \text{ sec}$$
$$K_{\theta} = -2.0$$

Path-Following Regulation and Control

$$1/T_f = 2.0 \text{ rad/sec}$$
$$K_d = -0.00867 \text{ rad/ft}$$
$$K_{\bar{d}}/K_d = 1/T_{d_1} = 0.0887 \text{ sec}^{-1}$$
$$K_{\dot{d}}/K_d = T_{d_2} = 29.5 \text{ sec}$$

Letting go of the absolute attitude reference now, however, requires that a high quality path damping signal be provided. In practice, this may be the derived beam rate, $\dot{d}$, the incremental altitude rate, $\dot{h}$, or the result of a complementary filtering which indeed may further include the

39

output of a normal accelerometer. Figure 7, and the analysis presented
in Appendix B, assumes that in a high performance system, and on a
relatively shallow glidepath, such as -3.0 deg, the complementary
filtering can be performed in such a way that, over the bandwidth of
the path following loop, a pure $\dot{d}$ signal can be provided.

A straight-through beam displacement signal is, of course, required
for path acquisition and stiffness, and to this is added the integral
of the beam displacement signal. The latter will serve to keep the
aircraft on the reference glidepath in the presence of a headwind or a
long wavelength updraft. The gain on the integral term, however, is
necessarily limited by considerations of path following stability, so
that its effectiveness is only felt in regulating against at most
slowly changing winds. Both the beam displacement and integral signals
are shown, in Fig. 7, to be filtered by a low-pass filter with a time
constant, T_f. This filter is representative of the combined impedance
of the filter capacitor and the receiver conventionally used in the
VHF-UHF ILS, or alternatively it can be taken to closely approximate
the combined characteristics of a receiver boxcar hold and ripple
filter such as might be employed in connection with a microwave
scanning beam system.

Analysis of the second closure comprising the $\dot{d}$, d, and $\int d\ dt$ paths
shown in Fig. 7 is also presented in Appendix B. There it is assumed
that the total feedback transfer function for the outer loop closure
with $d_c = 0$ is:

$$Y_d = \frac{K_{\bar{d}} + K_d s}{s(T_f s + 1)} + K_{\dot{d}} s = \frac{K_{\dot{d}}[s^3 + (1/T_f)s^2 + (K_d/K_{\dot{d}}T_f)s + K_{\bar{d}}/K_{\dot{d}}T_f]}{s(s + 1/T_f)}$$

$$= \frac{K_{\dot{d}}(s + 1/T_{d_1})(s + 1/T_{d_2})(s + 1/T_{d_3})}{s(s + 1/T_f)}$$

where

$$\frac{1}{T_{d_1}} \doteq \frac{K_{\bar{d}}}{K_d} \ , \quad \frac{1}{T_{d_2}} \doteq \frac{K_d}{K_{\dot{d}}} \ , \quad \frac{1}{T_{d_3}} \doteq \frac{1}{T_f}$$

40

Table IX summarizes the characteristic closed loop glide slope displacement control dynamics for the DC-8 in the landing approach with a windproofed autopilot. Here note that the path-following damping ratio and wavelength are well within the recommendations of RTCA SC-79 for automatically-coupled approaches (Ref. 14).

TABLE IX

DC-8 AUTOMATIC GLIDE SLOPE DISPLACEMENT CONTROL DYNAMICS
IN LANDING APPROACH WITH A WINDPROOFED AUTOMATIC PILOT

(Recommended by
RTCA SC-79)

Crossover frequency	0.75 rad/sec	
Dominant path-following damping ratio	0.66	$(0.2 \leq \zeta \leq 2.0)$
Dominant path-following undamped natural frequency	0.7 rad/sec	
Dominant path-following undamped natural wavelength	0.4 mi	$(\lambda \leq 1.1 \text{ mi})$
Short-period damping ratio	0.67	
Short-period undamped natural frequency	1.4 rad/sec	
Trim response:		
Damping ratio	> 1.0	
Time constant	28 sec	
Characteristic distance	1.2 mi	

Closed loop transfer functions between the most interesting and important inputs and outputs for the automatic glide slope tracking system for the DC-8 are shown in Table X.

B. LATERAL-DIRECTIONAL CONTROL

A block diagram of a typical lateral-directional approach measuring and control system is shown in Fig. 8. This figure is analogous to

TABLE X

LONGITUDINAL CLOSED LOOP TRANSFER FUNCTIONS FOR DC-8

Abbreviated notation is used for polynomial factors in root locus form:

Real factor (λ) means $(s + \lambda)$

Quadratic factor $[\zeta ; \omega]$ means $[s^2 + 2\zeta\omega s + \omega^2]$

Denominator:

$(0.036)(0.123)(0.582)(2.462)(13.232)[0.657;0.699][0.673;1.428]$

$$\frac{d}{u_g} = \frac{-0.283(0)(0)(0.174)(2.0)(12.918)[0.767;2.215]}{\text{Denominator}}$$

$$\frac{d}{w_g} = \frac{-0.75(0)(2.0)(13.75)[0.464;0.103][0.936;2.018]}{\text{Denominator}}$$

$$\frac{d}{d_{command}} = \frac{-2.406(0.035)(0.089)(0.7)(-3.606)(4.396)}{\text{Denominator}}$$

$$\frac{u}{u_g} = \frac{0.0373(0.136)(1.596)(2.777)(13.261)[0.5;0.276][0.58;1.918]}{\text{Denominator}}$$

$$\frac{u}{w_g} = \frac{-0.136(0.153)(0.215)(2.409)(13.262)[-0.082;1.023][0.872;1.492]}{\text{Denominator}}$$

$$\frac{u}{d_{command}} = \frac{0.3272(0)(0.089)(0.7)(-4.082)(4.03)}{\text{Denominator}}$$

$$\frac{u_{AS}}{u_g} = \frac{-(0.08)(0.111)(2.458)(13.232)(0.449)[0.68;1.394][0.668;0.814]}{\text{Denominator}}$$

42
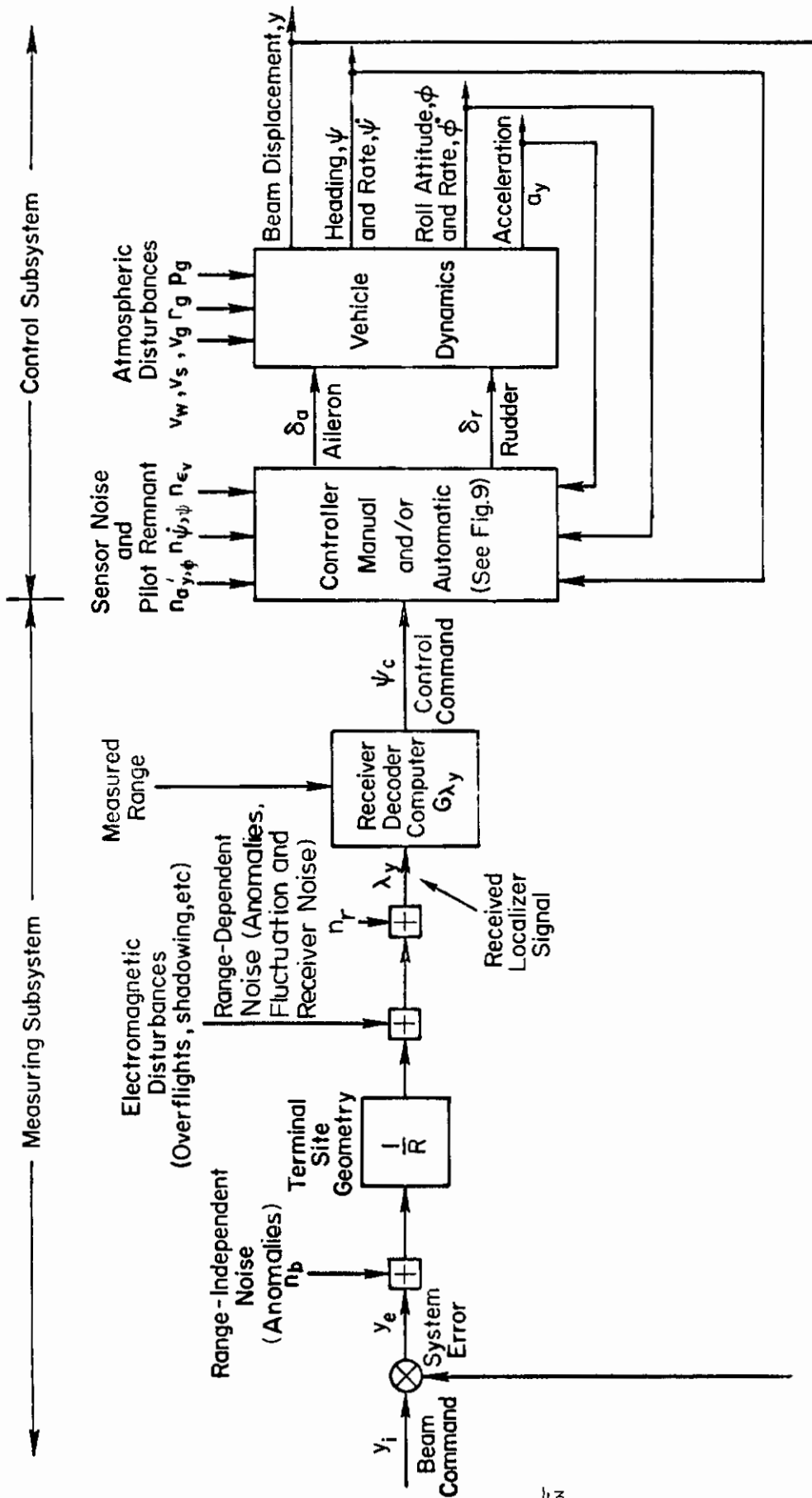
Figure 8. Measuring and Control System for Lateral Plane Approach

43

Fig. 4 for the longitudinal-vertical system, except that lateral beam displacement (y in Fig. 8), instead of glide slope displacement (d in Fig. 4), forms the outer loop feedback; heading, roll attitude, their derivatives, and lateral acceleration form candidates for inner loop feedbacks, and only two control points, aileron and rudder, are available.

When lateral guidance is provided by a localizer, y_i is the runway centerline extension and thus is identically equal to zero. When lateral guidance is provided by a microwave scanning beam measuring subsystem, a curved approach course is possible and y_i may establish a course command. We shall not, however, consider this possibility.

In general, a lateral velocity signal for course damping (not shown) can be obtained from beam rate, $\dot{y}$, or alternatively from an inertial system, if available, or from washed-out heading and so forth. Here again, however, development of a lateral velocity signal for course damping exclusively from beam rate offers an important simplification which has great appeal for general aviation and interurban service as well as for tactical applications.

Five atmospheric disturbances act directly on the aircraft. They are cross wind (v_w) cross windshear (v_s), lateral random gusts (v_g), yawing gusts (r_g) induced by the longitudinal gradient of lateral random gusts, and rolling gusts (p_g) induced by the spanwise gradient of normal random gusts.

It is assumed here, as it was in the longitudinal case, that the dependence on range of the guidance system sensitivity is automatically removed.

Figure 9 provides a more detailed view of the controller block diagram in Fig. 8 and illustrates the difference between the signal flow for manual and/or automatic control. Again the only new signals shown are the outputs from the displays to the human pilot. Although, in practice many signals will be displayed, only two control signals are shown which proceed from a flight director (ϵ_v) to aileron control (δ_{a_c}),
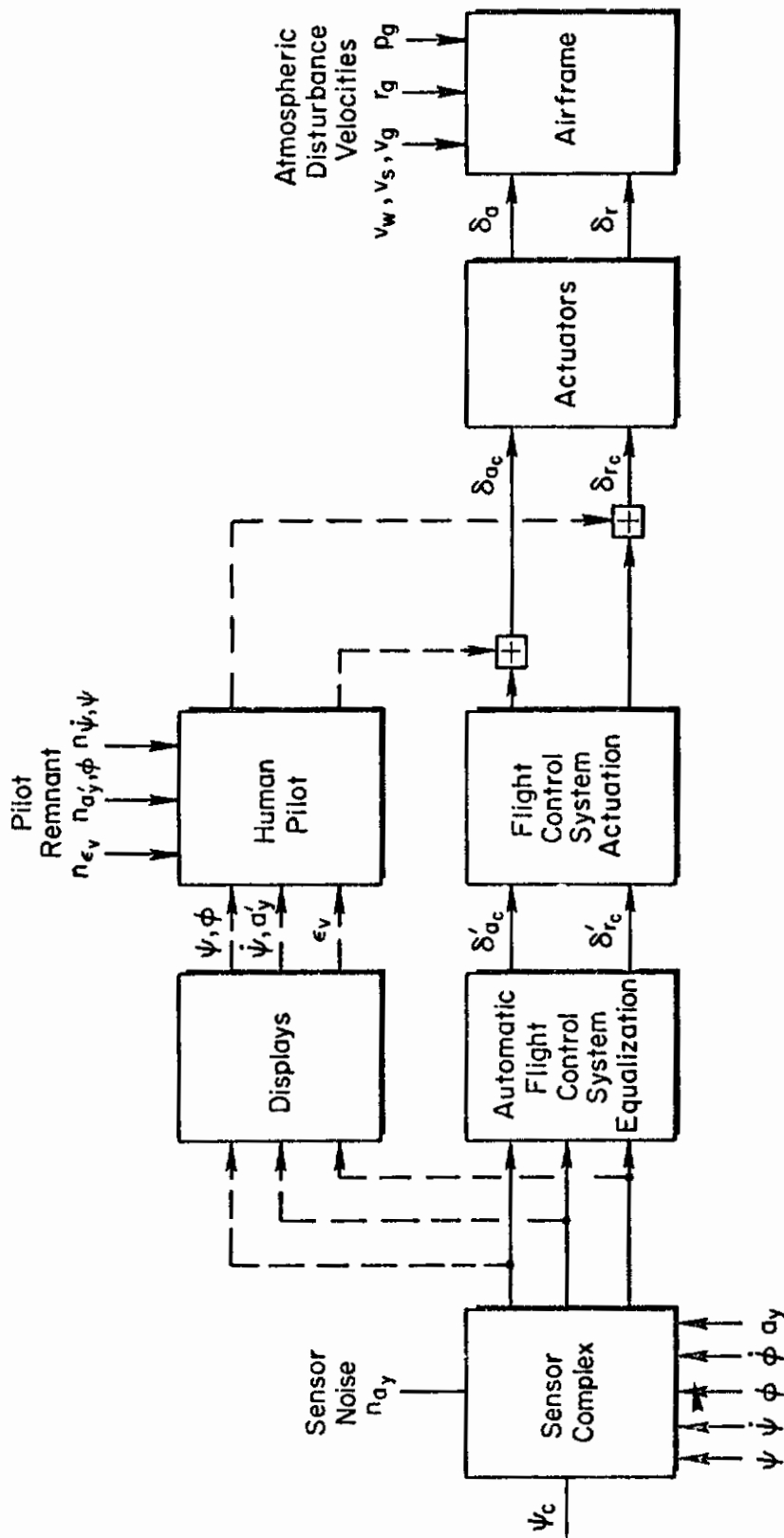
Figure 9. Controller Block Diagram (Lateral-Directional)

45

and from lateral acceleration (a_y') or yaw rate $(\dot{\psi})$ to rudder control (δ_{r_c}) for the case of manual control of the approach.

In the following analyses of the feedback arrangement for lateral-directional control, we shall first discuss techniques for optimizing the flight director for manual control of approach in the A-7D, and then discuss an advanced windproofed automatic flight control system for approach in the DC-8.

1. Manual Approach Lateral Displacement Control of the A-7D Aircraft

A simplified equivalent system block diagram of the AN/CPU-80A approach lateral flight director applied to the A-7D airframe and manual control system is given in Fig. 10. Fair localizer tracking control can be accomplished with only aileron control (δ_a) in the A-7D by virtue of its coupled roll-and-yaw rate stability augmentation system. (Refer to Table XI for numerical values of parameters in Fig. 10.)

The manual roll axis control system for the A-7D with stability augmentation is illustrated in Fig. 10. The pilot's control displacement (δ_{a_p}) is applied to the aileron through a gain and low pass roll rate attenuation filter. Whereas the low pass filter is designed to attenuate peak roll rate, p, at high dynamic pressure flight conditions, the low pass filter is retained in the control system during approach. Since the filter time constant $T_f = 0.33$ sec (Cf. Table XI), it will limit the ultimate gain of the localizer tracking loop.

The complex zeros of the roll attitude (φ)-to-aileron (δ_a) response transfer function of the A-7D in approach are favorably located to provide modest Dutch roll damping but only a slight increase in Dutch roll frequency when the feedback is in parallel with the heading (ψ)-to-roll attitude command (φ_c) intermediate loop and localizer displacement (y)-to-heading command (ψ_c) outer loop via radio guidance. Therefore the only feedback signals necessary for pilot/flight director glidepath tracking control are φ, ψ, and y. The describing functions to be determined are denoted by F_φ, F_ψ, and G_y. The describing function characterizing the dynamic behavior of the human pilot with unit gain

46
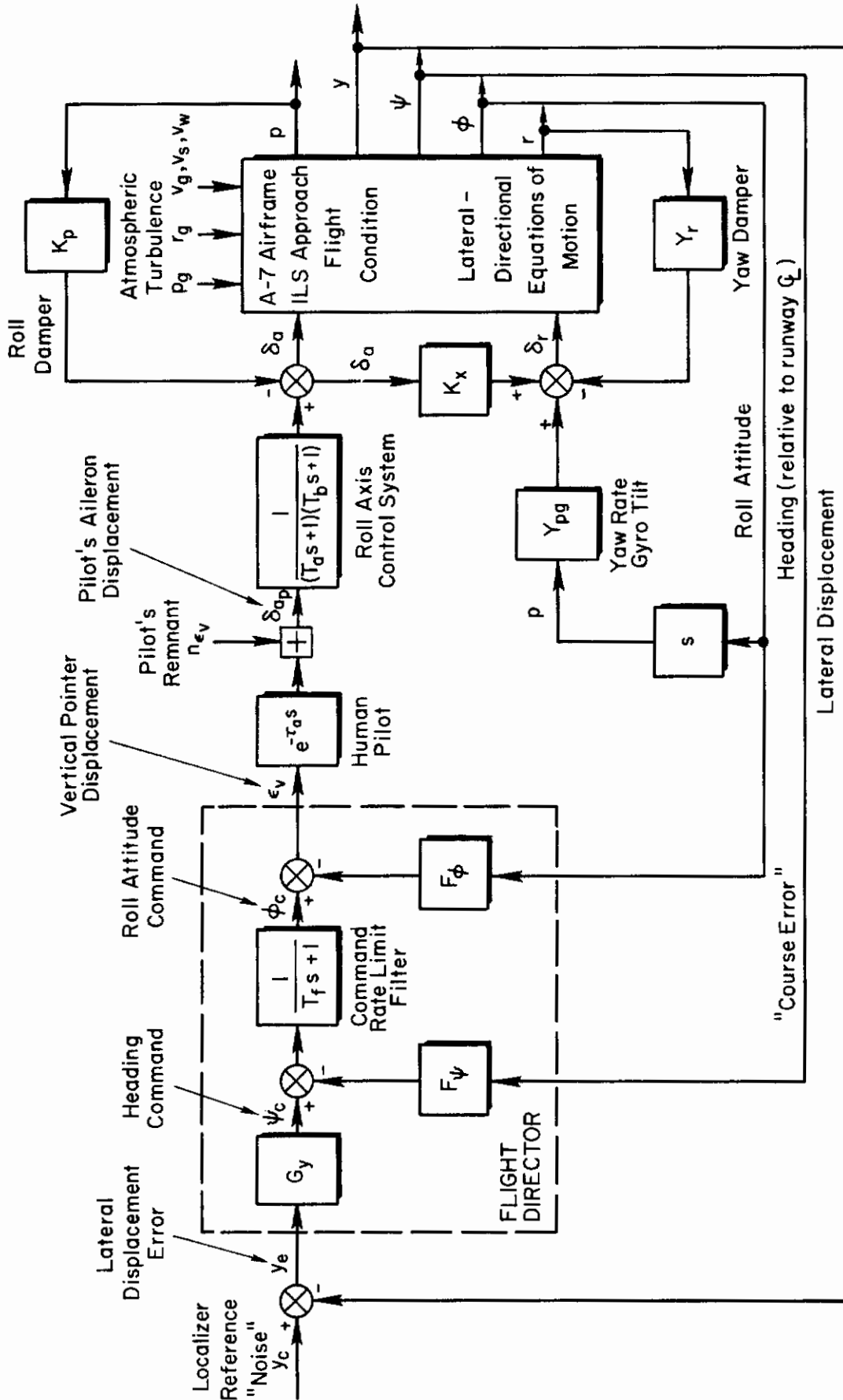
Figure 10. Block Diagram for Manual Lateral-Directional Approach Control in the A-7D Aircraft

47

TABLE XI

GAINS AND TIME CONSTANTS FOR MANUAL
LATERAL-DIRECTIONAL APPROACH CONTROL
IN THE A-7D AIRCRAFT

	Feedforward Terms		Feedback Terms	Remarks
τ_a	$0.36 - 0.08\left(\dfrac{253\sqrt{3}}{h_{abs}}\right)$ $= 0.2$ sec			$h_{abs} = 212.0$ ft $e^{-\tau_a s} \doteq -\dfrac{(s-10)}{(s+10)}$
K_x	-0.075	K_p	0.4 sec	
T_a	0.33 sec	Y_r	$-\dfrac{s}{s+1}\cos(\alpha_o - 2.5^o)$	$\alpha_o = 5.36^o$
T_b	0.1 sec	Y_{pg}	$\dfrac{s}{s+1}\sin(\alpha_o - 2.5^o)$	
T_f	0.30 sec	F_φ	$K_\varphi T_\varphi (s + 1/T_\varphi)\dfrac{T_{\varphi_{wo}}s}{T_{\varphi_{wo}}s + 1}$	$T_f = T_3$ in spec. MIL-C-83014
G_y	$K_y \dfrac{(s + 1/2T_\psi)}{(s + 1/T_\psi)}$	F_ψ	$\dfrac{K_\psi s}{s + 1/T_\psi}$	$T_\psi = T_1$ in spec. MIL-C-83014

SELECTED GAINS AND CONSTANTS

K_y	0.00055 rad/ft	T_φ	0.43 sec
		K_φ	0.4
		$T_{\varphi_{wo}}$	20.0 sec
		T_ψ	10.0 sec
		K_ψ	0.63

is denoted by $e^{-\tau_a s}$, where $s = j\omega$. These describing functions are analogous to the transfer functions which describe airframe and control system behavior. In fact, F_φ, F_ψ, and G_y become the flight director transfer functions for unit pilot gain. Furthermore, F_φ, F_ψ, and G_y will be determined so as to enable the human pilot to adopt the most desirable form for Y_p, a pure gain and time delay. The method for designing F_φ, F_ψ, and G_y is analogous to the one described previously for glidepath control.

The analysis of the multiloop system of Fig. 10 is summarized in Appendix B. The best forms and values for F_φ, F_ψ, and G_y are given in Table XI.

Consider F_φ first, since it provides necessary inner loop equalization in parallel with the heading and lateral displacement loops. A steady-state roll attitude washout (high-pass) filter is required to remove from the flight director display the effects of varying steady roll attitude in turns. The value selected for the high-pass time constant is $T_{\varphi_{wo}} = 20$ sec (Table XI). This value is large enough so as not to interact with roll attitude control loop dynamics in the crossover frequency range above the closed loop Dutch roll mode. Therefore, the effect of the washout is not included in the analysis in Appendix B. A phase lead filter is also required in the roll attitude feedback signal to overcome the lag of the low pass roll rate attenuation filter in the manual control system. The value selected for the phase lead filter is $T_\varphi = 0.4$ sec (Table XI). The gain, K_φ, is determined in Appendix B to provide ample roll tracking bandwidth, adequate closed loop Dutch roll damping and slight increase in Dutch roll frequency while maintaining a margin of roll control system stability.

A washout filter is also required for the heading feedback transfer function, F_ψ, to remove effects of a steady-state crab angle from the director display during the approach. The washout time constant is $T_\psi = 10$ sec. Besides the gain K_ψ in F_ψ, the heading (ψ)-to-roll command (φ_c) channel of the flight director contains a low pass filter for peak roll rate command attenuation. The value selected for the low pass filter time constant is $T_f = 0.3$ sec, nearly the same value as for the similar

49

filter in the roll axis of the manual control system. No additional lag of the smoothing filters can be tolerated in this channel near or below a frequency of 3 rad/sec. The gain, K_ψ, is determined in Appendix B to provide the highest possible heading tracking control bandwidth consistent with a margin for closed loop roll stability. Since both yaw damper inverse washout time constant (1 rad/sec) and decreasing closed loop roll damping set an upper bound on heading bandwidth, selection of the gain, K_ψ, involves a compromise between heading bandwidth and adequate roll damping ratio. Reference 11 illustrates that the heading washout filter provides essential low frequency lead for the outer lateral displacement loop closure. Therefore the value chosen for T_ψ (10 sec) depends on the sensitivity of both "lateral phugoid" and roll damping to variation in displacement loop gain.

Now we can consider G_y, the director lateral displacement describing function. The analysis in Appendix B shows that even the largest achievable closed loop localizer tracking bandwidth (0.2 rad/sec) is too low for significant gust disturbance suppression. For example, the tracking error suppression bandwidth is only about one-fourth of the average lateral gust disturbance bandwidth at 500 ft altitude and is an even smaller fraction at lower altitudes. Thus we may expect RMS localizer tracking errors on the same order of magnitude as RMS lateral gust disturbances for a wide range of lateral displacement gain. Therefore, selection of an "optimum" gain in the sense of offering "best" RMS disturbance suppression is impossible. Instead gain selection is governed by stability limitations.

Under the circumstances of relatively low achievable localizer tracking bandwidth limited by stability, the design of G_y also depends upon another result from engineering psychology (Ref. 12). This is that the pilot will prefer to adopt a relatively low tracking bandwidth and a greater margin of stability when it is not possible to achieve high tracking bandwidth relative to disturbance bandwidth. The way to provide a relatively low localizer tracking bandwidth and a greater margin of stability (greater closed loop tracking damping ratio) through

50

G_y is to add low frequency lead-lag equalization to the localizer deviation signal. This is why the heading washout time constant, T_ψ is selected to be 10 sec inside the outer marker. Selection of the gain K_y is then made for a "lateral phugoid" damping ratio on the order of 0.6. The damping ratio of the roll oscillation is increased to nearly 0.7, because of the favorable location of the complex zeros, $[\zeta_y, \omega_y]$.

Table XII summarizes the characteristic closed loop manual lateral displacement control dynamics for the A-7D in the landing approach with an AN/CPU-80A flight director. Course-following damping ratio and wavelength are within the recommendations of Ref. 14 for automatically-coupled approaches.

TABLE XII

A-7D MANUAL LATERAL DISPLACEMENT CONTROL DYNAMICS IN LANDING APPROACH WITH AN/CPU-80A FLIGHT DIRECTOR

		(Recommended by RTCA SC-79)
Crossover frequency	0.15 rad/sec	
Dominant course-following damping ratio	0.59	$(0.4 \leq \zeta \leq 1.5)$
Dominant course-following undamped natural frequency	0.2 rad/sec	
Dominant course-following undamped natural wavelength	1.5 mi	$(\lambda \leq 2 \text{ mi})$
Roll response damping ratio	0.68	
Roll response undamped natural frequency	0.65 rad/sec	
Dutch roll damping ratio	0.42	
Dutch roll undamped natural frequency	1.6 rad/sec	

51

TABLE XIII

LATERAL CLOSED LOOP TRANSFER FUNCTIONS FOR A-7D

Abbreviated notation is used for polynomial factors in root locus form:

Real factor (λ) means $(s + \lambda)$

Quadratic factor $[\zeta; \omega]$ means $[s^2 + 2\zeta\omega s + \omega^2]$

Denominator:

$(0.0853)[0.604;0.205][0.697;0.666][0.406;1.587][0.989;3.071][0.994;6.647]$

$$\frac{y}{v_g} = \frac{0.270(0.00163)(1.322)(4.587)[-0.506;0.638][0.615;2.358][0.975;6.676]}{\text{Denominator}}$$

$$\frac{y}{p_g} = \frac{6.25(0.102)(12.93)[0.435;1.110][0.966;2.80][0.92;3.733]}{\text{Denominator}}$$

$$\frac{y}{y_{command}} = \frac{0.0175(-10.0)(-6.824)(0.05)(2.358)(9.65)[0.397;1.11]}{\text{Denominator}}$$

Important and useful closed loop transfer functions for disturbance and command inputs for the multiple closed loop system of Fig. 10 are summarized in Table XIII.

2. Automatic Approach Lateral Displacement Control of the DC-8 Aircraft

A simplified block diagram representing an approach coupler and automatic pilot for lateral control to the localizer course in the DC-8-60 aircraft is presented in Fig. 11. This figure does not represent the approach coupler and automatic pilot which are actually installed in the DC-8-60, but instead, in the absence of detailed information on that equipment, we have studied an advanced "windproof" system of very high performance.
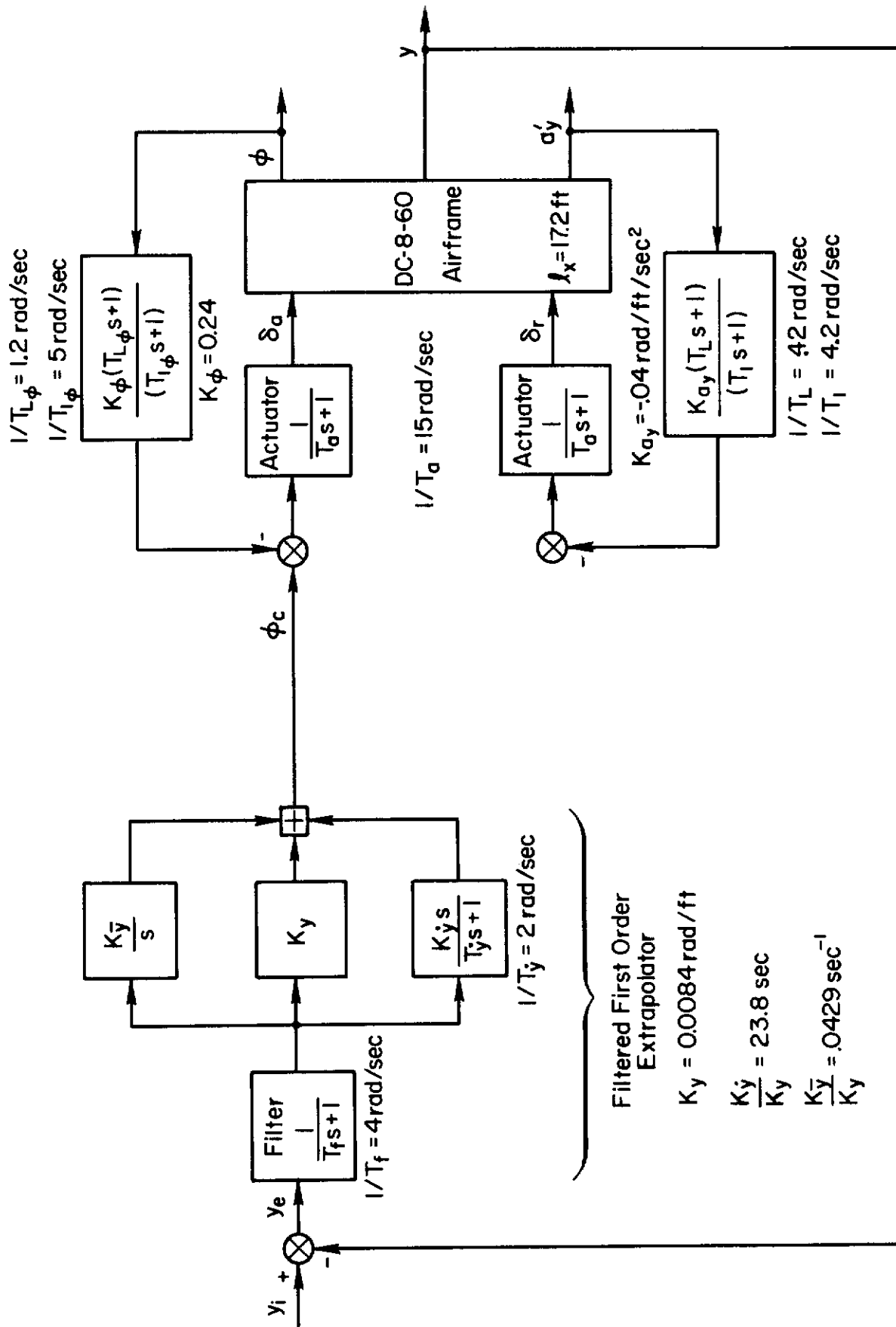
Figure 11. Block Diagram of Automatic Lateral Control to the Localizer in the DC-8 Aircraft

Reference 7 has explored the main considerations in the synthesis of automatic lateral control to the localizer course, which here, in general, parallel the ones already outlined in connection with the A-7D. Dutch roll stability augmentation is required, and bank angle feedback must be employed as an inner loop in parallel with the feedback of deviation from the localizer course. Path damping is supplied by the use of a derived beam rate signal, stiffness by the direct feedback of deviation from the centerline, and the integration of the beam signal removes any possible steady-state errors. Heading is not required as a feedback signal until just before touchdown when it might be employed to assure alignment of the aircraft wheel path with the runway.

Analysis of successive loop closures for the multiple loop system of Fig. 11 is presented in Appendix B.

Directional stability, short term windproofing and turn coordination are provided by the feedback of side acceleration to the rudder. Dutch roll damping is provided by lead-lag compensation on the side acceleration measured at a location approximately one chord length ahead of the aircraft center of gravity. The accelerometer location is chosen slightly aft of the rigid airframe's center of rotation in response to rudder displacement to provide appropriate damping of the dutch roll oscillation. (In practice, the accelerometer location should probably be based on flexible DC-8 equations of motion including at least the first two fuselage side bending modes. However, since the purpose here is only to illustrate the principles of windproofing as they affect the measuring subsystem, we have simplified the analysis by basing it on rigid airframe equations of motion.) No aileron crossfeed is required with this sideslip stability augmenter since adequate turn coordination is inherently available.

A thorough discussion of the design of a sideslip stability augmentation loop with acceleration feedback is given in Ref. 15. A suitable location for the lateral accelerometer can be found to accommodate fore-aft c.g. movement in the DC-8 provided that the reciprocal lag equalization time constant $1/T_I$ varies so as to remain in

the neighborhood of $1/T_{a_{y_3}}$, the largest left-half plane zero in the numerator of the lateral acceleration response to rudder displacement. $1/T_{a_{y_3}}$ varies with the distance between accelerometer and c.g. locations as shown in Table XIV, where correspondingly suitable values for $1/T_I$ are given. The accelerometer location is chosen 2 ft aft of the center of rotation shown to reduce the sensitivity of lag equalization to c.g. shift. In this respect the most aft c.g. location is critical, since it might increase the separation of the fixed accelerometer and c.g. to 19.2 ft which would effectively place the accelerometer again at the center of rotation. Since a 2 ft c.g. shift corresponds to nine percent of the mean aerodynamic chord, the chosen accelerometer location will amply accommodate an aft c.g. location up to 25.2 + 9.0 = 34.2 percent of the mean aerodynamic chord.

The inverse lead equalization time constant is then chosen to be less than the Dutch roll undamped natural frequency so as to provide damping, and the controller gain is then selected to provide modest increases in damping and natural frequency of the Dutch roll with reasonable levels of rudder activity in the presence of heavy turbulence.

The gains and time constants for the rudder control loop which were selected on the basis of the analysis of Appendix B are displayed in Table XIV. A high bandwidth and excellent performance are achievable in part because of the low actuator time constant, $T_a = 0.067$ sec. The value of this parameter is, however, not at all unrealistic for a hydraulic servo-actuator.

Roll attitude regulation and control for attitude stiffness, roll damping, and the suppression of rolling gust effects is accomplished by feedback of the bank angle, φ, to the ailerons, δ_a with lead-lag equalization. The inverse lead time constant is chosen in the neighborhood of the rolling subsidence, and the inverse lag time constant, on the order of twice the desired closed loop undamped natural frequency of the rolling oscillation. The resulting roll loop crossover frequency is about 1.8 rad/sec with a gain of about 0.24 deg/deg. (See Appendix B and Table XIV.)

TABLE XIV

SELECTED GAINS AND TIME CONSTANTS
FOR AUTOMATIC CONTROL TO THE LOCALIZER IN THE DC-8

Sideslip Stability Augmentation $\quad a_y' \rightarrow \delta_r$

$$1/T_a \;=\; 15 \text{ rad/sec}$$

$$1/T_L \;=\; 0.42 \text{ rad/sec}$$

$1/T_I$	∞	4.2	2.0 rad/sec
Accelerometer distance forward of c.g.	19.2 (Center of Rotation)	17.2	15.2 ft (2 ft = 9% MAC)
$1/T_{ay_3}$	554.	3.58	2.29 rad/sec

$$K_{a_y'} \;=\; -0.04 \text{ rad/ft/sec}^2 \quad (\text{corresponding to } q = 61.8 \text{ lb/ft}^2)$$

accelerometer location 17.2 ft forward of c.g. @ 25.2% MAC

Roll Attitude Regulation and Control $\quad \varphi \rightarrow \delta_a$

$$1/T_a \;=\; 15 \text{ rad/sec}$$

$$1/T_{L_\varphi} \;=\; 1.2 \text{ rad/sec (corresponding to rolling subsidence)}$$

$$1/T_{I_\varphi} \;=\; 5 \text{ rad/sec}$$

$$K_\varphi \;=\; 0.24$$

Course-Following Regulation

$$1/T_f \;=\; 4 \text{ rad/sec}$$

$$1/T_{\dot{y}} \;=\; 2 \text{ rad/sec}$$

$$K_y \;=\; 0.0084 \text{ rad/ft}$$

$$K_{\dot{y}}/K_y \;=\; 23.8 \text{ sec}$$

$$K_{\overline{y}}/K_y \;=\; 0.0423 \text{ sec}^{-1}$$

Finally, the lateral displacement measuring system outer loop is closed to provide ample course-following bandwidth and damping with automatic cross wind trim control. Again, as in the glide slope displacement closure, the equalization has both a rate and an integral term in addition to the possibly sampled azimuth beam decoder noise filter, whose half-power frequency is taken to be 4 rad/sec. The beam rate is further smoothed with a lag filter with a time constant $T_{\dot{y}} = 0.5$ sec. At very low frequencies, the open-loop system looks like K/s^3 because of the integral bypass path. The system configuration, however, allows the choice of equalization gains so as to provide complex second order lead and an open loop logarithmic amplitude-frequency gradient of about -20 dB/decade in the desired region of unit gain crossover (0.23 rad/sec) for precision course-following in turbulence. The crossover frequency in the lateral displacement control loop is primarily limited by the available rudder and aileron authority. Control system authority in landing approach for the DC-8 has been taken from Ref. 16 as: aileron (δ_a) ± 17.5 deg, rudder (δ_r) ± 18 deg. For the loop closure analysis see Appendix B and for the selected gains and time constants consult Table XIV.

The second order lead equalization effectively determines the damping ratio (0.7) and undamped natural wavelength (3.6 mi) of the automatic crosswind trim oscillation, which will provide about two wavelengths of trimming dynamics over a 7.2 mi approach. The resulting dominant closed loop dynamic modes are represented in Table XV and the closed loop transfer functions are displayed in Table XVI. The dominant course-following damping ratio and undamped natural wavelength satisfy the criteria set forth in Ref. 14 for pilot acceptance of automatically coupled approaches.

TABLE XV

DC-8 AUTOMATIC LATERAL DISPLACEMENT CONTROL DYNAMICS
IN LANDING APPROACH WITH A WINDPROOFED AUTOMATIC PILOT

(Recommended by
RTCA SC-79)

Crossover frequency	0.23 rad/sec	
Dominant course-following damping ratio	0.71	$(0.4 \leq \zeta \leq 1.5)$
Dominant course-following undamped natural frequency	0.32 rad/sec	
Dominant course-following undamped natural wavelength	0.8 mi	$(\lambda \leq 2 \text{ mi})$
Roll response damping ratio	0.75	
Roll response undamped natural frequency	2.7 rad/sec	
Dutch roll damping ratio	0.53	
Dutch roll undamped natural frequency	1.1 rad/sec	
Cross trim response:		
Damping ratio	0.71	
Undamped natural period	83 sec	
Undamped natural wavelength	3.6 mi	

58

TABLE XVI

LATERAL CLOSED LOOP TRANSFER FUNCTIONS FOR DC-8

Abbreviated notation is used for polynomial factors in root locus form:

Real factor (λ) means $(s + \lambda)$

Quadratic factor $[\zeta; \omega]$ means $[s^2 + 2\zeta\omega s + \omega^2]$

Denominator:

$(1.673)(2.465)(4.078)(4.862)(9.205)(15.0)(15.74)*$

$*[0.711;0.0756][0.709;0.324][0.533;1.086][0.754;2.709]$

$$\frac{y}{v_g} = \frac{0.089(2.0)(1.673)(0.0055)(0.122)(4.0)(15.74)(0)(15.0)(42.4)*\ *[0.970;2.137][0.578;2.561]}{\text{Denominator}}$$

$$\frac{y}{p_g} = \frac{23.703(0)(1.673)(2.0)(4.0)(15.0)(15.69)*\ *[0.420;0.955][0.974;3.159][0.0769;5.397]}{\text{Denominator}}$$

$$\frac{y}{y_{command}} = \frac{4.626(1.673)(3.103)(5.0)(15.0)*\ *[0.702;0.059][0.437;0.896][0.575;13.6]}{\text{Denominator}}$$

59

SECTION IV

SYSTEM INPUTS

Performance of the feedback control arrangements described in Section III will be dependent on the environment in which they operate. In particular it is necessary to define an appropriate set of inputs and disturbances for the approach measuring system and the airplane. Since the approach speed is initially "trimmed" and the approach guidance reference is rectilinear, the "command" inputs to the measuring system are identically zero, if the measuring system is perfectly boresighted. However, as has already been noted in connection with the block diagrams, at least seven types of disturbances encountered during an approach should be considered. These are:

- Steady winds
- Windshears
- Stochastic atmospheric gusts
- Beam anomalies and bias errors
- Scanning beam fluctuation noise
- Missed samples in scanning beam detection
- Pilot's scanning remnant

Models for atmospheric disturbances are discussed in some detail in Ref. 7, which presents the justification for the choice of particular levels and shaping. Table XVII presents a summary of selected atmospheric disturbances used to predict errors at the approach "window." It may be noted that a choice of other levels of the disturbance and/or other temporal or spectral shapes would alter the results.

Values for steady wind velocity and shearing gradient displayed in Table XVII represent a consensus of the airline industry's unofficial thinking on environmental limits for automatic approach and landing (Ref. 7). The magnitudes may be considered somewhat arbitrary, but they do represent experience. It may be noted, however, that much larger shears are not infrequently encountered.

TABLE XVII

SUMMARY OF "SEVERE" ATMOSPHERIC DISTURBANCES FOR
LANDING APPROACH

Type of Disturbance	Component	Disturbance Velocity		Altitude (h) or Integral Scale (L) of Turbulence (ft)	Half-Power Frequency (Dryden Form) rad/sec	Source of Model
		kt	ft/sec			
Steady Wind	Head (H)	25	42.2		- -	Air Transport Association Recommendations to FAA to prove Cat IIIA performance
	Tail (-H)	10	16.9	(Throughout Entire Approach)		
	Cross (C)	15	25.4			
Shear	(typical) $\pm \frac{dH}{dh}$ and $\pm \frac{dC}{dh}$ or $\pm \dot{H}$ and $\pm \dot{C}$ (95% confidence)	0	0	$h \geq 200$	- -	
		$4 \frac{kt}{100\ ft}$	$0.0675\dot{h}_o \frac{ft}{sec^2}$	$100 \leq h \leq 200$		
		$8 \frac{kt}{100\ ft}$	$0.135\dot{h}_o \frac{ft}{sec^2}$	$50 \leq h \leq 100$		
Stochastic Turbulence	u_g	(RMS) 5.92	(RMS) 10.0	$L_u = 672$	U_o/L_u	MIL-F-008785A (USAF) (Ref. 17)
	v_g	5.92	10.0	$L_v = 672$	$\sqrt{3}U_o/L_v$	
	w_g	3.85	6.5	$L_w = 100$	$\sqrt{3}U_o/L_w$	
	p_g	lateral gradient of w_g	Refer to σ_{wg}	$L_w = 100$	$U_o\pi/20b$	
	q_g	longitudinal gradient of w_g	Refer to σ_{wg}	$L_w = 100$	$U_o\pi/4b$ or $\sqrt{3}U_o/L_w$, whichever is less	
	r_g	longitudinal gradient of v_g	Refer to σ_{vg}	$L_v = 672$	$U_o\pi/3b$ or $\sqrt{3}U_o/L_v$, whichever is less	

The stochastic turbulence model is drawn from Ref. 18. There the gust components are represented as stationary random processes which are formed by passing white noise through an appropriate linear constant coefficient filter (Dryden form). Thus the six components of the stochastic turbulence are represented by six power spectral densities and each component is characterized by a mean square value and break frequency. The spectra in terms of temporal frequency are:

$$\Phi_{u_g}(\omega) = \sigma_u^2 \frac{2L_u}{\pi U_o} \frac{1}{1 + \left(\frac{L_u \omega}{U_o}\right)^2}$$

$$\Phi_{v_g}(\omega) = \sigma_v^2 \frac{L_v}{\pi U_o} \frac{1 + 3\left(\frac{L_v \omega}{U_o}\right)^2}{\left[1 + \left(\frac{L_v \omega}{U_o}\right)^2\right]^2}$$

$$\Phi_{w_g}(\omega) = \sigma_w^2 \frac{L_w}{\pi U_o} \frac{1 + 3\left(\frac{L_w \omega}{U_o}\right)^2}{\left[1 + \left(\frac{L_w \omega}{U_o}\right)^2\right]^2}$$

$$\Phi_{p_g}(\omega) = \frac{\sigma_w^2}{4U_o L_w} \frac{\sqrt{\pi L_w / b}}{1 + \left(\frac{20b\omega}{\pi U_o}\right)^2} \quad *$$

$$\Phi_{q_g}(\omega) = \frac{\omega^2 / U_o^2}{1 + \left(\frac{4b\omega}{\pi U_o}\right)^2} \Phi_{w_g}(\omega)$$

$$\Phi_{r_g}(\omega) = \frac{\omega^2 / U_o^2}{1 + \left(\frac{3b\omega}{\pi U_o}\right)^2} \Phi_{v_g}(\omega)$$

---

* This form of $\Phi_{p_g}(\omega)$ from Ref. 18 has since been superseded by a different form in Ref. 19.

where L_u, L_v, L_w = scale length (ft)

$\qquad U_O$ = airplane's mean (trim) airspeed (ft/sec)

$\qquad \omega$ = frequency (rad/sec)

$\qquad \sigma$ = standard deviation

Scale lengths are not well established at low altitudes. The entries in Table XVII are the result of choosing scale lengths appropriate to an altitude of 100 ft. On the other hand, the choice of mean square intensities appropriate to an altitude of 100 ft, as recommended by Ref. 19, led to RMS values which were thought to be excessive. For this reason the RMS gust velocities were chosen to be the ones from Ref. 19 appropriate to an altitude of 500 ft.

The probability of encountering clear-air turbulence bears an inverse relationship to altitude and increases to 0.8 at 100 ft (Ref. 19). Given an encounter with clear-air turbulence, the probability that the RMS gust velocity will equal or exceed the values given in Table XVII is only 0.02 (Ref. 19). Thus we may view the gust disturbances presented in Table XVII as "severe" and as nearly a "worst case" for approach and landing.

Models for the remaining three system disturbances were difficult to derive. Reference 7 has presented some summary data for VHF-UHF ILS. The TACLAND measuring system, however, will probably comprise a microwave scanning beam. For that category of equipment only theoretical predictions and very limited preliminary measurements are available as a basis for disturbance models (Ref. 20). Experimental flight tracking measurements from which missed sample probabilities and guidance system noise power spectral densities might be found are possibly available in raw form at the National Aviation Facilities Experimental Center (NAFEC). Some data have been accumulated there in connection with the AILS equipment manufactured by Airborne Instruments Laboratory Division of Cutler-Hammer, Inc. However these data are not in a form suitable for modeling the position-measuring system disturbances at this writing.

Tables XVIII and XIX present calculated results from Ref. 20 which suggest that crystal drift (Items 1 and 2) and reflection

TABLE XVIII

ESTIMATED CONTRIBUTIONS TO ROOT-SUM-SQUARED ERRORS IN THE 2.5 DEG ELEVATION ANGLE OF A MICROWAVE SCANNING BEAM RECEIVED AT 100 FEET ALTITUDE (Ref. 20)

The effective number of hits/beamwidth (H) reduces resultant effects of six fluctuation errors as noted below. In this table H = 16 hits/beamwidth. The root-mean-squared value of the source of fluctuation error is given in parentheses; after the source error has been divided by H, the effective root-mean-square d value is listed without parentheses.

Type of Error	Effective Half-Power Bandwidth of Power Spectral Density (rad/sec)	Source of Contribution		Probability Distribution	Source Error (deg)	ITEM	RMS Source Error (deg)	Effective RMS Error (deg)	Sub-total Root-Sum-Squared Error (deg)	Grand Total Root-Sum Squared Error (deg)
Bias	$\doteq 0$		Ground Crystal Drift	Gaussian	(Not Applicable))	1	0.0005		0.0283	0.0341
	(Effectively static errors during an approach)		Air Crystal Drift			2	0.001			
			Angle Pickoff Bias			3	0.02			
			Boresight Bias			4	0.02			
Reflection Bias	Usually much less than the glide slope displacement loop crossover		Multipath Reflection Anomalies			5	0	(Not reduced by averaging over hits/beamwidth)	0	
Fluctuation	$\dfrac{2.8\ \text{rad}}{T_0}\ \text{sec}$ where T_0 is updating interval (sec)	Perturbation	Receiver Noise	Gaussian	(Not Applicable)	6	(0.05)	0.0031	0.019	
			Ground Circuit Jitter			7	(0.015)	0.0009		
			Air Circuit Jitter			8	(0.015)	0.0009		
		Pulse Increment Errors	Angle Pickoff Increment	Uniform	(0.125)	9	(0.0361)*	0.0023		
			Encoder Clock Increment		(0.125)	10	(0.0361)*	0.0023		
			Decoder Clock Increment		(0.25)	11	(0.0722)*	0.0045		
		Beam-Data Increment Error	(Beam packing error) Scan Degrees per Hit	Uniform	(0.062 deg/transmission)	12	0.0179†	(Not reduced by averaging)		

* RMS Value is (Increment) $\div \sqrt{12}$

† RMS Value is (Deg/Transmission) $\div \sqrt{12}$

TABLE XIX

ESTIMATED CONTRIBUTIONS TO ROOT-SUM-SQUARED ERRORS IN THE APPROACH CENTERLINE AZIMUTH ANGLE OF A MICROWAVE SCANNING BEAM RECEIVED AT 100 FEET ALTITUDE (Ref. 20)

The effective number of hits/beamwidth (H) reduces resultant effects of six fluctuation errors as noted below. In this table H = 22 hits/beamwidth. The root-mean-squared value of the source of fluctuation error is given in parentheses; after the source error has been divided by H, the effective root-mean-squared value is listed without parentheses.

Type of Error	Effective Half-Power Bandwidth of Power Spectral Density (rad/sec)	Source of Contribution		Probability Distribution	Source Error (deg)	RMS Source Error (deg)	ITEM	Effective RMS Error (deg)	Sub-total Root-Sum-Squared Error (deg)	Grand Total Root-Sum Squared Error (deg)
Bias	≈ 0		Ground Crystal Drift	Gaussian		0.0008	(1)		0.0283	0.0332
	(Effectively static errors during an approach)		Air Crystal Drift			0.0008	(2)			
			Angle Pickoff Bias		(Not	0.02	(3)	(Not reduced by averaging over hits/beamwidth)		
			Boresight Bias			0.02	(4)			
Reflection Bias	Usually much less than the lateral displacement loop crossover		Multipath Reflection Anomalies	Gaussian	Applicable)	0.01	(5)		0.01	
Fluctuation			Receiver Noise	Gaussian	(Not	(0.05)	(6)	0.0023	0.0141	
		Perturbation	Ground Circuit Jitter		Applicable)	(0.02)	(7)	0.0009		
			Air Circuit Jitter			(0.015)	(8)	0.0007		
	2.8 rad / T₀ sec where T₀ is updating interval (sec)	Pulse Increment Errors	Angle Pickoff Increment	Uniform	(0.25)	(0.0722)*	(9)	0.0033		
			Encoder Clock Increment		(0.25)	(0.0722)*	(10)	0.0033		
			Decoder Clock Increment		(0.25)	(0.0722)*	(11)	0.0033		
		Beam-Data Increment Error	(Beam packing error) Scan Degrees per Hit	Uniform	(0.044)	0.0127†	(12)	(Not reduced by averaging)		

where T₀: $\frac{2.8 \text{ rad}}{T_0 \text{ sec}}$

* RMS Value is (Increment) ÷ $\sqrt{12}$

† RMS Value is (Deg/Transmission) ÷ $\sqrt{12}$

65

anomalies (Item 5) will contribute less bias error than the root-sum-square of angle pickoff bias (Item 3) and boresight bias (Item 4), both of which are systematic, <u>static</u> errors. These latter errors should be capable of reduction in an operational system (Ref. 21). Further since the path-following crossover frequency is expected to substantially exceed the bandwidth of any multipath reflection anomalies, we may assume for the present example that the root-sum-square (RSS) anomaly and bias errors exert a negligible influence on <u>dynamic</u> tracking errors in glide slope and lateral displacement at the decision height.

The remaining errors in Tables XVIII and XIX (Items 6 through 12) are here called "fluctuation noise from sample to sample." This is a dynamic error which is expected on theoretical grounds to exhibit a broad-band power spectral density relative to path-following crossover frequencies. In fact, the best estimate of its spectral characteristics is based on the assumption that the noise is a boxcar sequence in time with an interval between samples which is the inverse of the scan frequency. The half-power bandwidth of fluctuation noise will then be about one-half the scanning frequency. The root-sum-square (RSS) fluctuation errors in Tables XVIII and XIX may double in operational practice (Ref. 21). Therefore we shall adopt for the present example the RSS fluctuation errors in Table XX.

The probability of a missed sample has been estimated as 0.001 (Ref. 21). Reference 41 shows that the influence of a missed sample on the total root-sum-square (RSS) tracking error is negligible, even for a missed sample probability as high as 0.2. The effect of missed samples, therefore, is to be entirely neglected.

A model for the pilot's multiloop control-display scanning remnant is derived in Ref. 22 and has been experimentally validated for two separated display-control tracking tasks in Ref. 23. The resulting model of scanning (sampling) remnant is summarized in Table XXI together with definitions of the symbols which appear there. The average level of noise power contributed by the pilot's visual scanning of a particular display is proportional to the product of at

TABLE XX

ANTICIPATED OPERATIONAL FLUCTUATION ERRORS
(Values are for a microwave scanning beam
at a 100 ft decision height.)

	Angle (mrad)	Distance (ft)
1:20 Glide slope	0.66	1.32
Centerline azimuth	0.5	7.0

Power spectral density for both coordinates

$$\Phi(\omega) \doteq \Phi(0) \left[\frac{\sin \frac{\omega T_o}{2}}{\frac{\omega T_o}{2}} \right]^2 \quad ; \quad \text{where } \Phi(0) = \frac{T_o}{\pi} \sigma^2 \frac{(\text{units})^2}{\text{rad/sec}}$$

$$\text{if } \sigma^2 = \int_0^\infty \Phi(\omega) d\omega$$

Sampling time interval $\quad T_o$ (sec)

Half-power frequency $\quad \omega_{1/2} \doteq \frac{2.8}{T_o}$ (rad/sec)

Sampling frequency	$1/T_o$	2	4	8	16	Hz
Half-power frequency	$\omega_{1/2}$	5.6	11.2	22.4	44.8	rad/sec

N.B. $\Phi(\omega)$ was approximated by $\dfrac{\Phi(0)}{1 + \left(\dfrac{\omega T_o}{2.8}\right)^2}$ in the analysis

67

TABLE XXI

SAMPLING REMNANT POWER SPECTRAL DENSITY

$$\sigma^2 = \int_0^\infty \Phi(\omega)\, d\omega$$

Definition of sampling remnant power spectral density:

$$\Phi_{nn}(\omega) = \frac{\overline{T}_s(1-\overline{\eta}_e)(1-\delta)\sigma^2}{\pi\left[1 + \left(\dfrac{\omega\overline{T}_{d_e}}{2}\right)^2\right]}\left(\frac{\text{units}^2}{\text{rad/sec}}\right)$$

where σ^2 is total mean-squared signal to be sampled

$\overline{T}_s$ is mean sampling interval

$\overline{\eta}_e$ is effective dwell fraction = $\overline{T}_{d_e}/\overline{T}_s$

$\overline{T}_{d_e}$ is effective dwell interval

δ is normalized lower bound on the domain of T_s: $T_0/\overline{T}_s$

$(1-\delta)$ is approximately $\sigma_{T_s}/\overline{T}_s$, the sampling variability ratio

σ_{T_s} is standard deviation in T_s

Assume sampling variability ratio $(\sigma_{T_s}/\overline{T}_s) \leq 0.5$ for skilled pilots.
Effective dwell fraction is related to foveal dwell fraction, η_f, if para-
foveal perception is possible during intersample fraction, $1-\overline{\eta}_f$, by the
expression

$$\overline{\eta}_e = \overline{\eta}_f + (1-\overline{\eta}_f)\frac{\omega_{c_p}}{\omega_{c_f}}$$

where ω_{c_p} is crossover frequency with continuous parafoveal
attention and

ω_{c_f} is crossover frequency with continuous foveal attention

Typically, $\dfrac{\omega_{c_p}}{\omega_{c_f}} \leq \dfrac{1}{2}$ for K/s controlled element with separated displays

(Refer to Ref. 22 for complete theory of sampling remnant applied to
crossover model of human operator tracking.)

least three factors:

(1) the total mean-squared value of the displayed signal, σ^2

(2) the average effective time interval during which the pilot is <u>not</u> looking at the display [the average effective intersample or "non-dwell" interval, $\overline{T}_s(1 - \overline{\eta}_e)$]

(3) the sampling interval variability ratio, $\sigma_{T_s}/\overline{T}_s$.

The half-power (cut-off) frequency of the low-pass first order noise process which characterizes sampling remnant is inversely proportional to the average effective time interval during which the pilot is looking at the display (the average effective sample dwell interval, $\overline{T}_{d_e}$). Corroborating experimental justification for representing the human operator's remnant in single and multiloop tracking tasks by a first order noise process which scales with the mean-squared value of the displayed signal is presented in Ref. 24 from a variety of diverse sources and in Ref. 25 for flight director control tasks during simulated landing approaches with a transport aircraft.

In the examples to be discussed here, we shall inject a first order noise process, whose power spectral density is described as in Table XXI, at each point in the multiloop control topology where the pilot views a display. For example, there are two scanning remnant injection points in Fig. 6. One is at the airspeed indicator and the other following the flight director horizontal pointer displacement summing junction and the pilot's time delay. In Fig. 10, on the other hand there is only one scanning remnant injection point. This is following the flight director vertical pointer displacement summing junction and the pilot's time delay. Then, following the procedure of Ref. 42 here, we shall predict the average scanning statistics for the pilot's visual attention which is required on the flight director and airspeed displays for tracking control and also for monitoring other situation displays throughout the landing approach.

The prediction of average scanning statistics forms part of the procedure for estimating approach tracking error variances and covariances.

Although it scales with displayed signal variance, the injected noise which represents sampling remnant produces a component of approach tracking error variance which is relatively uncorrelated with the independent input forcing functions. This uncorrelated portion of the approach tracking error is here termed <u>incoherent</u> error to distinguish it from the coherent error caused by the independent inputs. The total (coherent <u>and</u> incoherent error) covariance matrix bears a tensor relationship to the coherent covariance matrix. However, since the sampling remnant scales with only the displayed signal variances (and not the covariances), a more practical approach is to predict average scanning statistics in terms of the relationship between the total variance vector and the coherent variance vector.

A rearrangement of the definition of sampling remnant power spectral density in Table XXI is useful in practice. If we substitute the assumed upper limit of the sampling variability ratio, $\sigma_{T_s}/\overline{T}_s = 0.5$ (for skilled pilots) the power spectral density in Table XXI becomes

$$\Phi_{nn}(\omega) \;=\; \frac{(1 - \overline{\eta}_e)}{\omega_s} \; \frac{\sigma^2}{\left[1 + \left(\dfrac{\omega \overline{T}_{d_e}}{2}\right)^2\right]} \left(\frac{units^2}{rad/sec}\right) \tag{1}$$

where $\omega_s = 2\pi/\overline{T}_s$ and the other symbols are as defined in Table XXI. The total variance vector $\left\{\overrightarrow{\epsilon^2}\right\}$ is then related to the coherent variance vector $\left\{\overrightarrow{\epsilon_\iota^2}\right\}$ by the equation

$$\left[\Delta_s\right] \left\{\overrightarrow{\epsilon^2}\right\} \;=\; \left\{\overrightarrow{\epsilon_\iota^2}\right\} \tag{2}$$

where $\left[\Delta_s\right]$ is a square coherence matrix containing elements

$$\Delta_{s_{\epsilon_i \epsilon_j}} \;=\; \left[\delta_{ij} - \frac{(1 - \overline{\eta}_{\epsilon_j})}{\omega_{s_{\epsilon_j}}} \int_0^\infty \left|\frac{\epsilon_i}{n_{\epsilon_j}}\right|^2 \frac{d\omega}{\left[1 + \left(\dfrac{\omega \overline{T}_{d_{\epsilon_j}}}{2}\right)^2\right]}\right] \tag{3}$$

with j displayed variables and i states in the variance vector and where

$\delta_{ij} = \begin{Bmatrix} 1; & i = j \\ 0; & i \neq j \end{Bmatrix}$ is the Kronecker delta.

The determinant of $[\Delta_s] \equiv \Delta_s$ is called the characteristic determinant of stability in the mean-square sense, or the coherence determinant. Each component of the coherent variance vector has the form

$$\overline{\epsilon^2_{\iota_1}} = \sum_{k=1}^{N} \int_0^\infty \left| \frac{\epsilon_i}{\iota_k} \right|^2 \Phi_{\iota_k} \, d\omega \tag{4}$$

where $\iota_k = d_c, u_g, w_g$ $(u_c \equiv 0)$, for example, for $N = 3$ independent longitudinal inputs. Thus the vector $\left\{ \overline{\epsilon^2_\iota} \right\}$ will, in general, be a column matrix of linear combinations of input-correlated mean-squared errors. The formal result for the total variance vector is

$$\left\{ \overline{\epsilon^2} \right\} = \frac{\text{adj}[\Delta_s]}{\Delta_s} \left\{ \overline{\epsilon^2_\iota} \right\} \tag{5}$$

Now the adopted scanning behavior is unknown. It depends, for example, on satisfying performance requirements for $\left\{ \overline{\epsilon^2} \right\}$ and the physical upper bound on cumulative visual foveal fixation dwell fraction (scanning workload) expressed in the following equation of constraint.

$$M_s + \sum_{j=1}^{M} \eta_j = 1 \; ; \quad \text{M separate displays; with an optional} \atop \text{scanning workload margin } M_s \text{ for} \atop \text{non-control tasks} \tag{6}$$

This equation is called the "scanning workload constraint." The adopted scanning behavior may be discovered by seeking values of ω_s and η_e which minimize $\left\{ \overline{\epsilon^2} \right\}$, subject to the scanning workload constraint.

In practice the minimization procedure can be accomplished by simultaneous solution of Eq 7 and 8 subject to an assumed value for the effective sampling-to-crossover frequency ratio, S.

$$\eta_e = \cfrac{1}{1 + \cfrac{\pi}{S\omega_c\tau_e} \left\{ \tan\left[\cfrac{2S\,(2-\omega_c\tau_e)}{(2+\omega_c\tau_e)(3+\omega_c\tau_e)} \right] \right\}} \tag{7}$$

71

$$\omega_s = S\,\omega_c(1 - \eta_e)\ (\text{rad/sec}) \tag{8}$$

Equation 8 is merely the definition for S. The product, $\omega_c\tau_e = (\pi/2) - \varphi_M$, where φ_M is the phase margin of stability for the crossover model. Experimental results in Ref. 23 have suggested the following ranges of values for S:

$4 < S \le 6$ for separate displays among which **parafoveal perception is inhibited**

$6 < S < 10$ for combined displays among which **parafoveal perception may be significant.**

Then the coefficient, $(1 - \eta_e)/\omega_s$, of the incoherent power integral in each element of Δ_s in Eq 3 can be related to the adopted crossover frequency ω_c (or to the displayed signal bandwidth ω_b) by rearranging equation 8:

$$\frac{(1 - \eta_e)}{\omega_s} \doteq \frac{1}{S\,\omega_c}$$

The average scanning frequency, (f_s), scanning interval $(\bar{T}_s)$, and effective dwell interval $(\bar{T}_{d_e})$ follow from their definitions.

$$f_s = \omega_s/2\pi\ (\text{Hz}) \tag{9}$$

$$\bar{T}_s = 1/f_s\ (\text{sec}) \tag{10}$$

$$\bar{T}_{d_e} = \eta_e\bar{T}_s\ (\text{sec}) \tag{11}$$

Sometimes the sum of the effective dwell fractions will exceed unity in the scanning workload constraint. More often the sum will exceed $(1 - M_s)$, where M_s is a margin of scanning workload for communication, navigation, search, identification, fuel management and supervisory tasks. Effective dwell fractions, the sum of which apparently exceeds the scanning workload constraint can be achieved with lower foveal dwell fractions if parafoveal perception of the appropriately displayed signals is not inhibited. A reduced foveal dwell fraction can be estimated from the equation

72

$$\eta_f = \frac{\eta_e - \Omega}{1 - \Omega} \qquad (0 \leq \Omega < 1) \qquad\qquad (12)$$

where $\Omega \equiv \omega_{c_p}/\omega_{c_f}$, the average parafoveal-to-foveal gain crossover frequency ratio from Table XXI.

Ω is largest on a combined display with two signals and homogeneous equalization. Increasing display separation reduces Ω and increasing the number of displays also reduces Ω. The cumulative dwell fraction (scanning workload) will be based on a sum of _foveal_ dwell fractions, η_f, whereas the coherence determinant, Δ_s, will be based on _effective_ dwell fractions, η_e, which are greater than or equal to η_f.

The coherence determinant governs multiloop stability in the mean-square sense; therefore, it must be greater than zero. A value for the determinant which is much less than unity means that incoherent error power due to sampling remnant will be much greater than the coherent error power due to inputs and disturbances. If the coherence determinant approaches unity (its upper bound), the error power will become increasingly coherent.

The coherence determinant depends on the display scanning statistics as well as the closed loop frequency responses to sampling remnant. Therefore, it is desirable to obtain the coherence determinant in analytic form first, so that the average scanning statistics can be estimated in conjunction with their influence on scanning workload (cumulative dwell fraction) and mean-squared errors.

Some savings in labor will result if preliminary coherence tests of Δ_s (to ascertain whether or not it is greater than 0.4, for example) are based on only the principal diagonal elements of Δ_s. Experience has shown that all members of one set of off-diagonal elements will usually be negligible; thus, the value of the determinant is practically equal to the value of its principal diagonal. Computation of the principal diagonal elements is sufficient to define a scanning behavior. All of the elements of the determinant, are, of course, required to verify that $\left\{ \overline{\epsilon^2} \right\}$ has been minimized and satisfies approach performance requirements.

73

In the example of manual control of the A-7D approach with a flight director, the control tasks explicitly require only three displayed signals, airspeed error, u_{AS_e}, flight director pitch error (horizontal pointer) ϵ_H, and flight director roll error(vertical pointer) ϵ_v. A complete analysis of the adopted display scanning behavior would also include all of the situation and status displays required in the landing approach. Such an analysis, however, is beyond the scope of this example. Therefore we shall illustrate the predictions of scanning statistics which have been made for the pilot's visual attention on the three primary control signals by subsuming the scanning workload for status information within the margin, M_s.

The results are shown in Table XXII.

Since the two flight director signals are presented on a combined indicator in the A-7D, the predicted combined foveal dwell fraction is the sum of 0.40 and 0.33 or 0.73. This fraction, coupled with a foveal dwell fraction of only 0.05 on the separate airspeed display and a margin of 0.22 for status displays satisfies the unit scanning workload constraint. All of the predicted statistics shown here are roughly comparable to experimental results measured in a simulated DC-8 flight director approach in Ref. 26.

Since each coherence determinant is greater than 0.9, we may expect that sampling remnant will contribute little incoherent power to the total error variance. This is perhaps as one would expect, if the flight director is so designed that it can be properly used.

The pilot's scanning remnant is now defined for the purpose of inclusion as an input in the system analysis.

TABLE XXII

PREDICTED SCANNING STATISTICS FOR MANUAL APPROACH CONTROL IN THE A-7D WITH A FLIGHT DIRECTOR

Displayed Signal	Effective Bandwidth ω_b (rad/sec)	Normalized Scanning Ratio $S = \dfrac{\omega_s}{\omega_b(1-\eta_e)}$	Average Scanning Frequency $\omega_s \left(\frac{rad}{sec}\right)$	Average Scanning Frequency f_s (Hz)	Average Effective Dwell Fraction η_e	Parafoveal-to-Foveal Gain Ratio Ω	Foveal Dwell Fraction η_f	Average Scanning Interval T_s (sec)	Average Foveal Dwell Interval T_{d_f} (sec)	Average Effective Dwell Interval T_{d_e} (sec)
Airspeed Error u_{AS_e}	0.1	5.0	0.45	0.072	0.1	0.05	0.05	14.0	0.7	1.4
Flight Director Pitch Error ϵ_H	1.0	9.0	1.8	0.286	0.8	0.67	0.40	3.5	1.4	2.8
Flight Director Roll Error ϵ_v	0.6	9.0	1.6	0.256	0.7	0.55	0.33	3.9	1.3	2.7

Scanning workload margin M_s for combined status displays   0.22

Total scanning workload   1.00

Longitudinal Coherence Determinant

$$\Delta_s = \begin{vmatrix} \Delta_{s_{d_e d_e}} & \Delta_{s_{d_e u_{AS_e}}} & \Delta_{s_{d_e \theta}} & \Delta_{s_{d_e \epsilon_H}} \\ \Delta_{s_{u_{AS_e} d_e}} & \Delta_{s_{u_{AS_e} u_{AS_e}}} & \Delta_{s_{u_{AS_e} \theta}} & \Delta_{s_{u_{AS_e} \epsilon_H}} \\ \Delta_{s_{\theta d_e}} & \Delta_{s_{\theta u_{AS_e}}} & \Delta_{s_{\theta \theta}} & \Delta_{s_{\theta \epsilon_H}} \\ \Delta_{s_{\epsilon_H d_e}} & \Delta_{s_{\epsilon_H u_{AS_e}}} & \Delta_{s_{\epsilon_H \theta}} & \Delta_{s_{\epsilon_H \epsilon_H}} \end{vmatrix} = \begin{vmatrix} 1 & -0.0379 & 0 & -48600.0 \\ 0 & 0.996 & 0 & -48.0 \\ 0 & -1.36 \times 10^{-8} & 1 & -6.73 \\ 0 & -6.05 \times 10^{-9} & 0 & 0.943 \end{vmatrix} = 0.94$$

Lateral-Directional Coherence Determinant

$$\Delta_s = \begin{vmatrix} \Delta_{s_{y_e y_e}} & \Delta_{s_{y_e \psi}} & \Delta_{s_{y_e \phi}} & \Delta_{s_{y_e \epsilon_v}} \\ \Delta_{s_{\phi y_e}} & \Delta_{s_{\phi \psi}} & \Delta_{s_{\phi \phi}} & \Delta_{s_{\phi \epsilon_v}} \\ \Delta_{s_{\psi y_e}} & \Delta_{s_{\psi \psi}} & \Delta_{s_{\psi \phi}} & \Delta_{s_{\psi \epsilon_v}} \\ \Delta_{s_{\epsilon_v y_e}} & \Delta_{s_{\epsilon_v \psi}} & \Delta_{s_{\epsilon_v \phi}} & \Delta_{s_{\epsilon_v \epsilon_v}} \end{vmatrix} = \begin{vmatrix} 1 & 0 & 0 & -160100.0 \\ 0 & 1 & 0 & -0.437 \\ 0 & 0 & 1 & -0.0739 \\ 0 & 0 & 0 & 0.926 \end{vmatrix} = 0.926$$

75

SECTION V

MEASURES OF PERFORMANCE, SAFETY AND PILOT ACCEPTANCE

Appropriate measures of TACLAND system performance must be sensitive to variables indicative of landing success and minimally affected by quantities difficult to define exactly such as accident rates. Introduction of a criterion for continuing an approach based upon "making a window" in terms of allowable deviations in airspeed, and normal and lateral displacement from the reference glidepath, is a device which makes it possible to obtain a performance measure with the desired properties. The key performance parameter is the average number of approaches required to land, given an arrival at the terminal. It further turns out that this measure is proportional to both system effectiveness (minimum average time between landings) and system safety (accident <u>potential</u>). This measure may be used with a fixed window size and corresponding accident rates when <u>relative</u> comparisons of competing system performance are desired. When absolute performance is the concern for a <u>single</u> system the window size should be optimized for maximum system effectiveness and safety in view of the best <u>relevant</u> estimates of accident rates.

The average number of approaches required to land is derived from a probability tree outcome model. Its complexity is held to the minimum appropriate for obtaining a sensitive measure. The model consists of a network of various system centered, pilot centered, and window centered probabilities which act to determine estimates of the probability of the various alternative outcome events (safe landing, accident, missed approach, etc.) occurring. Certain key probabilities (accidents per arrival, missed approaches per approach) which are highly sensitive to system centered probabilities and relatively insensitive to pilot centered and window centered probabilities can be computed using the probability tree outcome model.

The analytical viewpoint which may be adopted for system analysis is closely constrained by the nature of what might be termed an

76

"acceptably performing" TACLAND system. This is because an acceptable system may have an appreciable missed approach rate even though accidents may be very rare indeed.[*] It turns out that this is both a curse and a blessing. It is a curse because it prevents straight-forward propagation of the covariances to the point where the covariances of certain variables define accident probabilities. On the other hand, it forces us to take a simpler view of the problem. A first reaction might be that this would render the result obtained considerably less interesting. Fortunately, however, with a proper physical interpretation of the simplified problem statistics, this is not the case. In actual fact, the result of the simpler problem is what is actually needed - and is what would probably be used in any event regardless of model complexity - since it is the most <u>sensitive</u> <u>system-centered</u> measure of system performance and safety.

The key simplification is that of determining missed approach rates based upon the statistics of "making a window." The quality of a particular system can then be judged relatively and with confidence based upon the missed approach rates. Why is this so? To answer this, we shall derive a performance measure and a safety measure from the probabilistic measures of "making a window."

System performance is here interpreted in a sense of effectiveness. That is, performance is equated with the minimum average time between landings

$$(\text{min. av. time between landings}) = \frac{\Delta T}{1 - P_{MA}}$$

where ΔT is the average time separation required between approaching

---

[*] An appreciable missed approach rate distorts the random variable distribution governing accidents from the Gaussian distribution. This makes analysis considerably more difficult if not infeasible as a practical matter.

aircraft and P_{MA} is the probability of a missed approach on any given approach.

$$P_{MA} = P_W P_D$$

That is, the probability of a missed approach on any given approach is the probability of _not_ making the window on any given approach, P_W, multiplied by the probability of the pilot making the (correct) decision to discontinue the approach, P_D, given that he did not make the window.

A preliminary selection of an overall system requirement for approach system performance would be a preliminary to the development of subsystem performance requirements. We selected a requirement, subject to Air Force approval, which was expressed in terms of the expected or probable number of missed approaches, given an arrival at the terminal:

$$P_{MA/ARR} \leq 0.05$$

This requirement is related to P_{MA}, the probability of a missed approach on any given approach by the expression

$$P_{MA/ARR} = \frac{P_{MA}}{1 - P_{MA}} \leq 0.05$$

from which $\qquad P_{MA} \leq 0.0476$

and the factor $\qquad (1 - P_{MA})^{-1} \leq 1.05$

We shall see from subsequent numerical examples that, _in the selected disturbance environment_, this is a very stringent performance requirement. No numerical requirement such as this is presently applied in civil or military operations.

Safety is interpreted in terms of accident potential. For the probability tree which, in our judgment, best fits the situation, the

78

probable number of accidents given an arrival at the terminal, $P_{ACC/ARR}$, can be approximated as:

$$P_{ACC/ARR} \doteq \frac{P_{A1}}{1 - P_{MA}}$$

where P_{A1} is the probability of an accident given that the window <u>is</u> attained. The approximation arises because of the assumption that P_{A1} is equal to the probability that an accident results when the window is <u>not</u> attained. This assumption, however, tends to be valid because of the fact that the relatively high probability of an accident given continuation of an approach which does not make the window, P_{A2}, is offset by the very low probability, $1 - P_D$, that such an approach would be continued. In equation form, this amounts to:

$$P_{A1} \doteq (1 - P_D)P_{A2}$$

The implicit assertion is that when a pilot decides to continue an approach which does not make the window it is because in his experienced opinion there is no greater risk, $(1 - P_D)P_{A2}$, than the risk, P_{A1}, which would obtain when continuing an approach which does make the window.*

The key factor in <u>both</u> the measure of performance and the measure of safety is $(1 - P_{MA})^{-1}$. This can be identified as the average number of approaches which must be made to achieve one landing per arrival at the terminal, or alternatively, as the accident exposure multiplier because of missed approaches. This measure is sensitive only to the system

_____

* This evaluation is made with a restricted viewpoint. It is shown in Ref. 27 that this policy is not optimum, but is very close to optimum when the missed window rate, P_W, and/or the accident ratio P_{A1}/P_{A2} are low.

centered probability, P_W, and hence is a measure ideally suited to our purpose. It will be minimum for the optimum system.

Given a window of fixed "size" reasonably close to the runway threshold and a single aircraft type, the statistics for each type of accident, or for all types considered collectively, can be expected to be invariant for all approaches which attain the window. This is not to imply that these accident statistics are or must be known in any other way. However, it is clear that accident rates must be very small to be tolerable. These rates would be governed mainly by window size given that the window is attained. The exact window size is not critical for making system performance comparisons on a relative basis. Window size must be optimized for best performance and safety only when absolute performance is of interest.

For the sake of being definitive, and proceeding in a way consonant with current airline practice for Cat II approaches, we shall assume that most, but not all, approaches which do not make the window result in missed approaches. All those which make the window are assumed to be continued. Those approaches which do not make the window but are continued anyway will also be assumed to result in an invariant (but substantially higher) accident rate for a given type of aircraft. Since the accident rates per approach for making or not making the window are considered fixed, variability in the accident rates per arriving aircraft depends only upon the window attainment probability and the correct decision probability. Probability of window attainment depends directly upon the overall landing system quality for a given disturbance environment.

The above features are incorporated in the probability tree outcome model of Fig. 12. All types of accidents are considered collectively in Fig. 12 although the same structure would be applicable for considering any one type of accident.

Probabilities for the events of interest can be derived directly from Fig. 12. Several are derived below. The key probabilities are:

Figure 12. Probability Tree Outcome Model
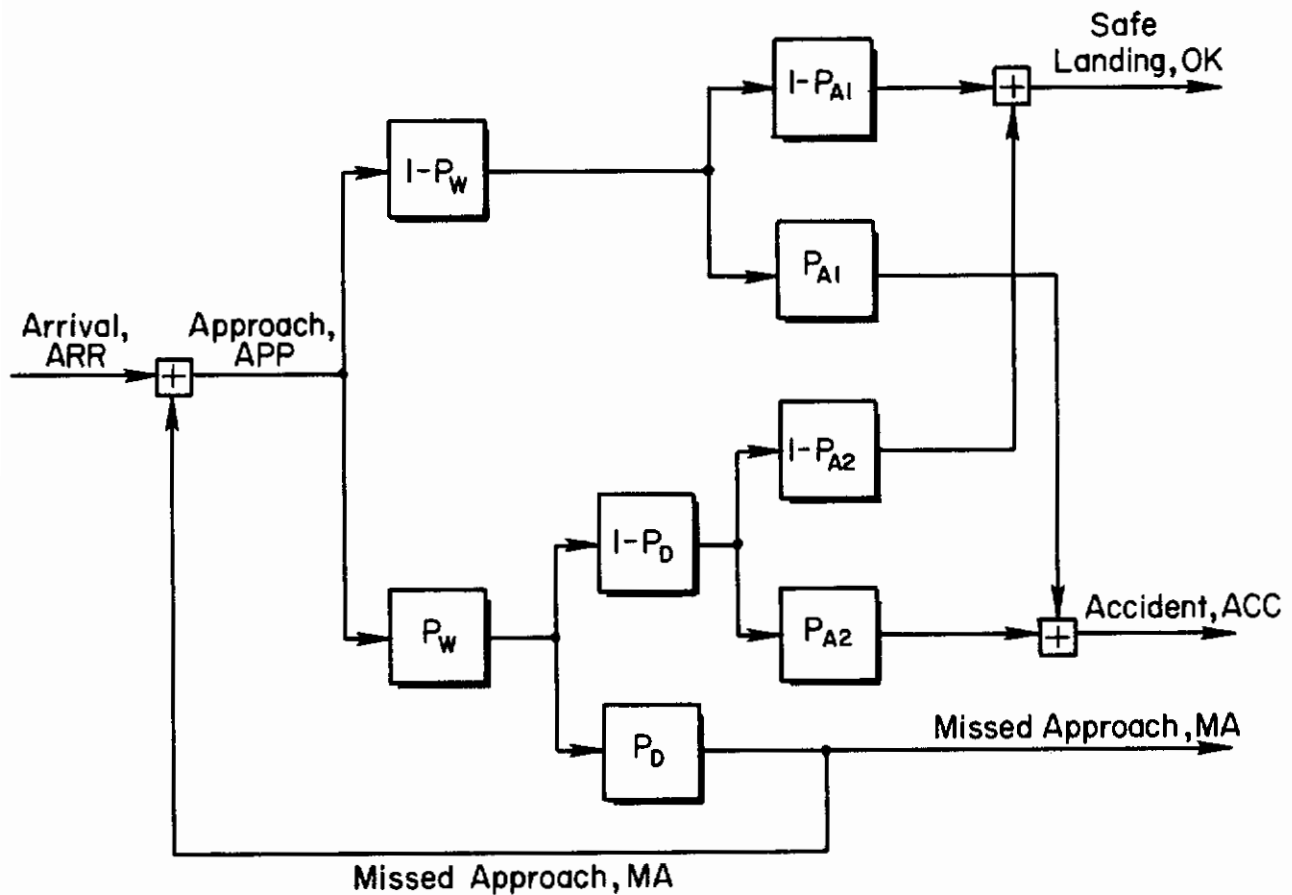
Legend for Probabilities

P_W -   Prob. of being outside window

P_D -   Prob. of discontinuing approach if outside window

P_{MA} -   Prob. of missed approach on any one approach. $P_{MA} = P_W P_D$

P_{A1} -   Prob. of accident if inside window

P_{A2} -   Prob. of accident if outside window

Abbreviations for Events

OK   -   Safe landing

ACC -   Landing accident

MA   -   Missed approach

APP -   Approach

ARR -   Arrival at terminal area

$P_{APP/ARR}$ - Probable number of approaches given an arrival

$P_{MA/ARR}$ - Probable number of missed approaches given an arrival

$P_{ACC/ARR}$ - Probable number of accidents given an arrival

$$P_{APP/ARR} = \frac{1}{1 - P_W P_D} = \frac{1}{1 - P_{MA}}$$

$$P_{ACC/APP} = P_{A1} + (P_{A2} - P_{A1})P_W - P_{A2}P_D P_W$$

$$P_{ACC/ARR} = \frac{P_{A1} + (P_{A2} - P_{A1})P_W - P_{A2}P_D P_W}{1 - P_{MA}} \doteq \frac{P_{A1}}{1 - P_{MA}}$$

$$P_{MA/APP} = P_W P_D = P_{MA}$$

$$P_{MA/ARR} = \frac{P_W P_D}{1 - P_W P_D} = \frac{P_{MA}}{1 - P_{MA}}$$

It is clear that the probabilities when referred to arrivals are amplified by $(1 - P_{MA})^{-1}$ times the comparable quantities referred to approaches. We should be concerned with the statistics based upon arrivals in distinction to those based upon approaches. (This distinction, however, becomes significant only as the missed approach rate becomes significant, say five percent or more.) For TACLAND, this will probably be an important consideration because missed approaches tend to occur more frequently as visibility levels are lowered, other things being equal.

The missed approach rate per approach depends upon a pilot decision centered probability, P_D, which tends toward unity, and a system centered probability, P_W, which is highly dependent upon overall system quality of performance. The pilot centered probability can be chosen to be a fixed number near unity, say 0.95, without affecting performance comparisons of competing systems on a relative basis. It is demonstrated in Ref. 27 that, if P_D is nearly unity, it does not have a significant affect on the other measures of performance and safety in any case.

Thus only the system centered probability, P_W, remains as a function of system design, but the closely related measure $P_{APP/ARR}$ is the proper measure to use for comparative purposes. This measure is the one selected here as a measure of performance and safety. It reflects the influence of system performance quality on both the minimum average time between landings and on accident rates.

Measures of pilot acceptance fall into quantitative and qualitative classifications. These measures are of secondary importance to performance measures for the first screening of competing systems, but are a prime consideration along with performance measures for the second and subsequent screenings.

Quantitative measures of pilot acceptance consist of the variances of attitude deviations, attitude rates, accelerations, airspeed fluctuations and control deflections; the maximum values of pitch and bank angles and rate of descent* required; and the margin from stall. The qualitative measures include pilot opinion, pilot workload estimates, and degree of consonance between automatic and manual control techniques (for ease of monitoring automatics, for rapid failure detection and for rapid takeover in the event of a failure).

Some "maximum permissible" values for the quantitative measures are given in Table XXIII below. These are taken from Ref. 14 and are appropriate for autopilot-coupled approaches. No comparable authoritative quantitative reference has been found for acceptable control defections. Presumably these measures can be taken to comprise some of the other measures, such as margin from the stall.

Some qualitative measures may possibly be evaluated in numerical terms, such as by calculating predicted pilot opinion rating or scanning workload, but in connection with the example systems considered in this investigation, neither of these two measures was thought to be at all critical. Furthermore the problem of consonance between automatic and

---

* Maximum rate of descent is a critical parameter only for so-called steep approaches which may typify V/STOL operations.

manual control techniques did not arise as it perhaps would in connection with an airplane equipped with direct lift control. For these reasons the formulation of qualitative measures of pilot acceptance was passed over, and no attempt was made to actually evaluate them.

TABLE XXIII

SOME QUANTITATIVE MEASURES OF PILOT ACCEPTANCE
FOR AUTOMATIC APPROACHES

Maximum permissible value of a measure with respect to its trimmed value*	Landing Approach Phase		
	From localizer capture to a point 2 mi inbound from outer marker	From a point 2 mi inside outer marker to Decision Height	Glide slope capture-stabilization and steady-state tracking
Roll angle, φ (deg)	±30.0 deg	±6.0 deg	-
Roll rate, p (deg/sec)	±10.0 deg/sec	±10.0 deg/sec	-
Heading, ψ (deg)	±10.0 deg	±5.0 deg	-
Pitch angle, θ (deg)	-	-	±6.0 deg
Normal acceleration, $\frac{a_z}{g}$ "g"	-	-	±0.5 g

* Maximum permissible values of a Gaussian random variable are often interpreted as that value which will never be exceeded with probability 0.9974. For this interpretation the "maximum permissible" value is three times the standard deviation or 3σ, where σ is the RMS value.

SECTION VI

METHODS FOR SIMPLIFYING THE COMPUTATION
OF TACLAND SYSTEM PERFORMANCE STATISTICS

A. SCOPE AND RESOLUTION OF THE DIFFICULTIES

The TACLAND system model which we have, at this point, assembled is, in general, nonlinear. The model includes two range-varying outer loop gains because of the angular nature of the terminal site measuring system. This range-variation in gain may be equivalently represented as a time-variation by using a distance-to-time coordinate transformation which is a function of approach velocity. For practically all vehicles, the trimmed approach velocity can be regarded as being piecewise constant for the purpose of developing this coordinate transformation. In this way, the range-varying TACLAND system model may be transformed into a linear dynamical model having, at worst, two time-dependent gains.

This linear, time-varying TACLAND system model applies for the interval of time between the end of the glide slope capture maneuver and the passage of the landing approach "window" at the 100 ft decision altitude. The duration of time for which this dynamical process is of interest is clearly finite. Because of this, we must regard the TACLAND system model as describing a finite duration process.

At the initiation of this process (the end of the glide slope capture maneuver), the glide slope deviation, airspeed deviation and localizer deviation from nominal values will each be characterized by a distribution. This feature imposes stochastic initial conditions on the dynamical TACLAND system model.

In the following subsections, we will first consider two alternative methods for computing the covariance matrix for key response variables at the approach window using the TACLAND system model discussed above. Following this, we will assess, in turn, the significance of the time-varying and finite time duration features of the process. These latter two topics lead, eventually, to the conclusion that system performance can be evaluated with sufficient accuracy using a time-invariant,

85

infinite time duration approximation to the linear time-varying, finite time duration, TACLAND system model. Furthermore, the effects of the stochastic initial conditions may be neglected.

This result represents a very considerable simplification which will, in turn, result in a considerable saving in time when performing computations. This is because variance computations for a time-invariant, infinite time duration system may be accomplished by the algebraic procedure given in Appendix E of Ref. 28. A modest extension of the technique presented there is given in Appendix C of this report so as to accommodate the computation of covariances as well.

B. COMPUTING VARIANCES AND COVARIANCES

When a linear systems analysis model is used and the distributions of the input variables are Gaussian, there are two relatively efficient methods for computing variances and covariances. These are the covariance propagation method (Ref. 29, 32) and the modified adjoint system method (Ref. 29 - 32). The modified adjoint system method, is the more appropriate when the variances and covariances are required only at one or two particular times, while the covariance propagation method is more appropriate when the variances and covariances are needed at several times or as continuous functions of time. Introduction of the landing approach window concept (introduced in Section I) means that the variances and covariances are of interest only at the time of window passage. Hence the modified adjoint system method will be more appropriate for landing approach system analysis when using the model discussed above.

The relative computational efficiency of the two methods is compared in Ref. 32 in terms of the number of integrations required. If the modified adjoint system method is to be used, each element of the covariance matrix for the key response variables may be computed by one simulation run involving 2n + 1 integrations in time, where n is the order of the linear system model differential equations. If p key response variables are required to describe system performance, then at

86

most only $p(p + 1)/2$ simulation runs are required to compute all elements of the covariance matrix for the key response variables. This is because the covariance matrix is symmetrical.

For the alternative covariance propagation method, all elements of the covariance matrix for the key response variables can be computed from a single simulation run. However, $n(n + 1)/2$ integrations in time are required, where n is again the order of the linear system model differential equations. Therefore, when $n \geq 4$, it is not only more appropriate but also more efficient to use the modified adjoint system method rather than the covariance propagation method for computing landing approach system performance at the approach window.

Even though the modified adjoint system method is the more efficient computational technique for the system model described above, it still may involve more computation and more complex programming than is necessary in order to arrive at accurate estimates of the TACLAND system performance statistics. For example, it would be very convenient if the variance computation procedure for linear, stationary, infinite duration processes could yield results which closely approximate those that would be obtained for the linear, time-varying, finite duration process model using the modified adjoint system method. This is because computation is much simpler and faster for the former case. Two matters must be carefully considered, however, before making this approximation:

- Significance of the time-varying character of the problem

- Significance of the fact that the process has a finite duration.

We shall consider each of these in turn in the following subsections.

C. THE TIME-VARYING CHARACTER OF THE SYSTEM MODEL IS NEGLIGIBLE

The number of time-varying parameters in the system model is at a minimum. The time-varying character of the gust-shaping filters has already been eliminated by assuming that the parameters for a particular altitude are representative of the essential effects upon system performance

at the window. The remaining time-varying effect arises because of the varying relation of linear and angular measures of the same variable through range, e.g., glide slope deviation. The beam bias, anomalies and fluctuation noise exhibit stationary angular measures, except when they are measured very near the transmitting antenna. Therefore the beam errors will be linearly decreasing with time when they are expressed in linear measures. However, since Ref. 41 shows that predicted microwave beam errors will contribute little to total system errors in the presence of severe atmospheric turbulence between the outer marker and the window of the Category IIB decision height, we shall neglect the time variation in linear measures of beam noise power in the examples here. Furthermore, since the outer loops of the TACLAND measuring system will normally incorporate some form of compensation which is a function of range to the terminal site, any time-variation in outer loop gain will be virtually eliminated except possibly when at very small ranges from the transmitting antenna. Time-varying effects may therefore be considered to be practically nil, and we may treat the TACLAND system model as a stationary (time-invariant) one.

D. FINITE-DURATION PROCESS EFFECTS ARE NEGLIGIBLE

The effect of assuming that the finite duration process can be approximated by an infinite duration process can best be appraised analytically by investigating the difference in the variances as computed by each approach for a very simple model of the problem. This matter might also be investigated empirically by a second approach which does not require any such simplifying approximation. This might be done by making several runs with the modified adjoint system model starting with the shortest run length of interest and gradually increasing the run length toward infinite time until no further significant changes in the variances are noted. The last results should equal the results from the first method of computation. Comparison of the results for shortest run length of interest with those for an infinite run length would enable evaluation of the approximation's validity.

88

The first approach, which can be pursued analytically, has been developed in detail in Ref. 32. The constituents of the very simple systems analysis model are: A stationary first order input shaping filter. This generates a stochastic input, $i(t)$, from unit white noise which is applied to the system starting at $t = 0$. This input has unity variance and a bandwidth of $\underline{a}$ rad/sec. The system is represented by a stationary first order lag $(\omega_c/s+\omega_c)$ with unity DC gain and bandwidth, or open-(outer) loop crossover frequency, of ω_c rad/sec.

The validity of approximating the finite duration process by the infinite duration process is assessed analytically in Ref. 32 by investigating the ratio of the variances computed for finite duration and for infinite duration using this simple model of the problem. If initial condition effects are neglected, the ratio of the finite duration variance in disturbance response, $\sigma_r^2(T)$, to the infinite duration variance, $\sigma_r^2(\infty)$, is

$$\frac{\sigma_r^2(T)}{\sigma_r^2(\infty)} = 1 + \frac{\omega_c + a}{\omega_c - a} e^{-2\omega_c T} - \frac{2\omega_c}{\omega_c - a} e^{-(\omega_c + a)T} \tag{VI-1}$$

where T represents the finite time duration of the landing approach. The ratio of variances can be computed for values of $\omega_c = 1/3$ rad/sec, $a = 2$ rad/sec, and $T = 115$ sec, which are characteristic of a conventional landing approach. Then:

$$\frac{\sigma_r^2(115)}{\sigma_r^2(\infty)} = 1 - \frac{7}{5} e^{-\frac{230}{3}} + \frac{2}{5} e^{-\frac{805}{3}} \tag{VI-2}$$

Since the second and third terms on the RHS of this equation are extraordinarily small in comparison with unity, the simpler infinite time duration approximation can be expected to be very accurate.

The difference between covariances computed for an infinite duration landing approach and the covariances for a finite duration approach which terminates at the time of passage of the approach window are

89

expected to be practically nil. Therefore we may indeed treat the TACLAND
system model as a linear, stationary, infinite time duration process,
provided the initial condition effects are negligible.

E. STOCHASTIC INITIAL CONDITION EFFECTS ARE NEGLIGIBLE

An approach similar to the one used above to show that finite duration
effects are negligible has been used in Ref. 32 to show that any reason-
able stochastic initial conditions on the system (at the end of the glide
slope capture maneuver) have only negligible effects on covariances at
the window. Again, take a very simplified view of the system. Represent
the system by a stationary first order lag with a bandwidth, or open-
(outer) loop crossover frequency of ω_c rad/sec. The mean square value,
or variance, $\sigma_{r_{ic}}^2(t)$, of the initial condition response of the system,
r, relative to its initial value, $\sigma_{r_{ic}}^2(0)$, can then be computed. This
ratio is:

$$\frac{\sigma_{r_{ic}}^2(t)}{\sigma_{r_{ic}}^2(0)} = e^{-2\omega_c t} \qquad (VI-3)$$

For the effect of stochastic initial conditions on covariances at the
window to be negligible, this ratio should be very small compared to one
for t = T. Again using the typical values of ω_c = 1/3 rad/sec and
T = 115.0 sec the ratio is:

$$\frac{\sigma_{r_{ic}}^2(T)}{\sigma_{r_{ic}}^2(0)} = e^{-\frac{230}{3}} \qquad (VI-4)$$

The ratio is indeed very small with respect to unity. Therefore any
likely stochastic initial conditions will have negligible effects on
performance at the window for the TACLAND systems analysis problem.
Notice that even if ω_c is as low as 0.1 rad/sec as is the case for

90

control of airspeed, the same conclusion holds true. This result is the
one we seek in order to justify use of the variance computation pro-
procedure (and its extension given in Appendix C). The procedure is,
strictly speaking, appropriate only for linear, stationary, infinite
duration processes.

F. THE SIMPLIFIED COMPUTATION OF THE COVARIANCE MATRIX

Approximation of the linear time-varying, finite duration process
model for the TACLAND measuring system by a linear, infinite duration,
stationary process model which is independent of initial conditions
has now been rationalized. This allows us to compute the covariance
matrix, by the purely algebraic procedure given in Appendix C. That is,
when numerical computations are performed, no numerical integration is
involved. Because of this, numerical computations are direct (i.e.,
do not involve iteration), are rapid, and do not require an error
analysis in order to validate integration step size, etc. The only
check required, is accomplished by inspecting the value of det $[C \mid D]$
(Refer to Eq 16 and 17 in Appendix C.) to determine that it is sufficiently
different from zero to assure that the matrix, $[C \mid D]$, is well conditioned
for inversion.

The key system response variables are glide slope deviation, airspeed
deviation and localizer deviation from nominal values. Because of the
symmetry about a vertical plane of the vehicle and guidance geometry,
the equations describing this system can be partitioned into two independent
sets. The two sets are the ones which involve in-plane coordinates, and
the ones which involve out-of-plane coordinates. Glide slope deviation
and airspeed deviation are in-plane coordinates. Localizer deviation is
an out-of-plane coordinate. Furthermore, the disturbances which force
the in-plane motions are statistically independent of the disturbances
which force the out-of-plane motions. Because of this, the covariance
of localizer deviation with either glide slope deviation or airspeed
deviation will be zero.

The covariance of glide slope deviation and airspeed deviation,
however, will not necessarily be zero, or for that matter even small.

In a well designed system, however, the covariance of glide slope deviation and airspeed deviation will either be very small or will be such that the particularly dangerous combinations (low and slow, high and fast) have a very low likelihood of occurring. This covariance, and the variances of glide slope deviation, airspeed deviation and localizer deviation may be computed using the equations and computer program given in Appendix C.

These computed covariances are then used in computing the key system centered probability, P_W. P_W is the probability of not attaining the window on any given approach. This probability, in turn, affects the measures of performance and safety in a sensitive way, and therefore its computation is the focal point of the systems analysis. Computation of this key probability is treated in the next following Section.

SECTION VII

CALCULATION OF APPROACH OUTCOME PROBABILITIES AND RELATED MEASURES OF PERFORMANCE AND SAFETY

In the last Section we pointed to the preferred methods for calculating the variances and covariances of the aircraft response variables in the presence of stochastic disturbances and noise. These depended on the approximately correct assumption that the closed loop systems might be represented (for the purpose intended) as linear with constant coefficients. When this is the case and when further, as we have already assumed, the gust intensities and radio noise signals are Gaussianly distributed, the distributions of the response variables will also be Gaussian. These distributions, however, will not, in general, have zero means. In particular the distributions of the lateral deviation from the beam, y, and the normal deviation from the beam, d, will tend to have non-zero mean values which may be functions of the beam bias errors, initial conditions, winds, and windshears.

A justification for neglecting the contributions to the mean values of the beam bias errors and the initial conditions has already been presented. This leaves only the winds and windshears, discussed in Section IV, as the disturbances which may contribute to the mean values of the responses which comprise the dimensions of the window.

The measures of performance and safety discussed in Section V depend on the evaluation of the probability of missing the window, P_W. The method of evaluating that probability is exposed in general terms in the next subsection. We then return to the calculation of numerical results for the two examples.

A. PARTITIONING THE PROBABILITY OF MISSING THE WINDOW

Contributions to the probability of missing the window, P_W, arise independently from the longitudinal and lateral deviations with respect

to the corresponding dimensions of the approach window. This is the case because the governing equations of motion are uncoupled.

By virtue of the independence of longitudinal and lateral deviations, P_W can be expressed as

$$P_W = P_{LONG} + P_{LAT} - P_{LONG}P_{LAT} \qquad \text{(VII-1)}$$

where P_{LONG} is the probability of exceeding the window boundary in d and/or u_{AS}, and P_{LAT} is the probability of exceeding the window boundary in y.

We might further concede that P_{LONG} or P_{LAT} may be conditioned upon the level of the deterministic disturbances (such as windshear level) and stochastic disturbances (such as the stochastic wind disturbance). This would result in

$$P_{LONG} = \int_{-\infty}^{\infty}\int_{-\infty}^{\infty}\int_{-\infty}^{\infty}\int_{-\infty}^{\infty} P_{LONG}(H,\dot{H},\sigma_{u_g}\sigma_{w_g})\rho(H)\rho(\dot{H})\rho(\sigma_{u_g})\rho(\sigma_{w_g})dH\ d\dot{H}\ d\sigma_{u_g}d\sigma_{w_g} \qquad \text{(VII-2)}$$

$$P_{LAT} = \int_{-\infty}^{\infty}\int_{-\infty}^{\infty}\int_{-\infty}^{\infty}\int_{-\infty}^{\infty} P_{LAT}(C,\dot{C},\sigma_{v_g}\sigma_{p_g})\rho(C)\rho(\dot{C})\rho(\sigma_{v_g})\rho(\sigma_{p_g})dC\ d\dot{C}\ d\sigma_{v_g}d\sigma_{p_g} \qquad \text{(VII-3)}$$

where H is headwind magnitude, C is crosswind magnitude, σ_{u_g} is the standard deviation of the longitudinal gust component and so forth, and $\rho(\cdot)$ is the probability of occurrence of the level $(\cdot)$ on a world-wide basis. This degree of refinement, however, is necessary only for examining system performance on an absolute basis. Because of the labor involved in finding reliable data on the $\rho(\cdot)$ and in computing the probabilities as a function of four variables, we shall investigate P_{LONG} and P_{LAT} only for the critical combinations of fixed H, $\dot{H}$, C, $\dot{C}$ and σ gust values given in Section IV. (Note that in the model the pitching gusts q_g are not independent of the normal gusts, nor are the yawing gusts r_g

94

independent of the side gusts, v_g. For this reason the effect of the
pitching and yawing gusts is included in the equations of motion and
the pitching and yawing gusts do not then need to be considered as
applied to the airplane.)

Consider P_{LAT} first because it is simpler. The mean and variance
of lateral deviation, y, are computed for the cases of the inputs of
Section IV applied to systems of Section III. These results define a
single dimensional Gaussian distribution which may be compared to the
lateral half-window dimension to compute P_{LAT}. The technique for this
is portrayed in Fig. 13, where $f_{LAT}(y-\overline{y}, D_{yy}(T))$ is the one-dimensional
Gaussian probability density function of lateral deviation. It is
characterized by the mean value, $\overline{y}$, and the variance or mean square,
$D_{yy}(T) = \sigma_y^2$. In Fig. 13, the sum of the shaded areas under the
probability density function is equal to P_{LAT}, the probability of not
attaining the window because of excessive lateral deviation. The
equation for P_{LAT} is:

$$P_{LAT} = \int_{-\infty}^{-(72+\overline{y})} \frac{e^{-\frac{y^2}{2\sigma_y^2}}}{\sqrt{2\pi}\sigma_y} \, dy + \int_{72-\overline{y}}^{-\infty} \frac{e^{-\frac{y^2}{2\sigma_y^2}}}{\sqrt{2\pi}\sigma_y} \, dy \qquad (VII-4)$$

Tables of the Gaussian (normal) probability distribution function
(e.g. Ref. 33) may be used to evaluate the two terms on the right hand
side of this equation.

Evaluation of P_{LONG} is somewhat more involved because the two-
dimensional probability density function for normal deviation from the
reference glidepath and airspeed deviation should be used. This is
because the covariance for these two variables will not necessarily be
zero. For fixed values of the deterministic input parameters, H and $\dot{H}$,
the mean normal and airspeed deviations at the window will have been
determined by solving the system equations with these deterministic
inputs up to the time of window passage. The covariance matrix, $\mathbf{D}(T)$,

95
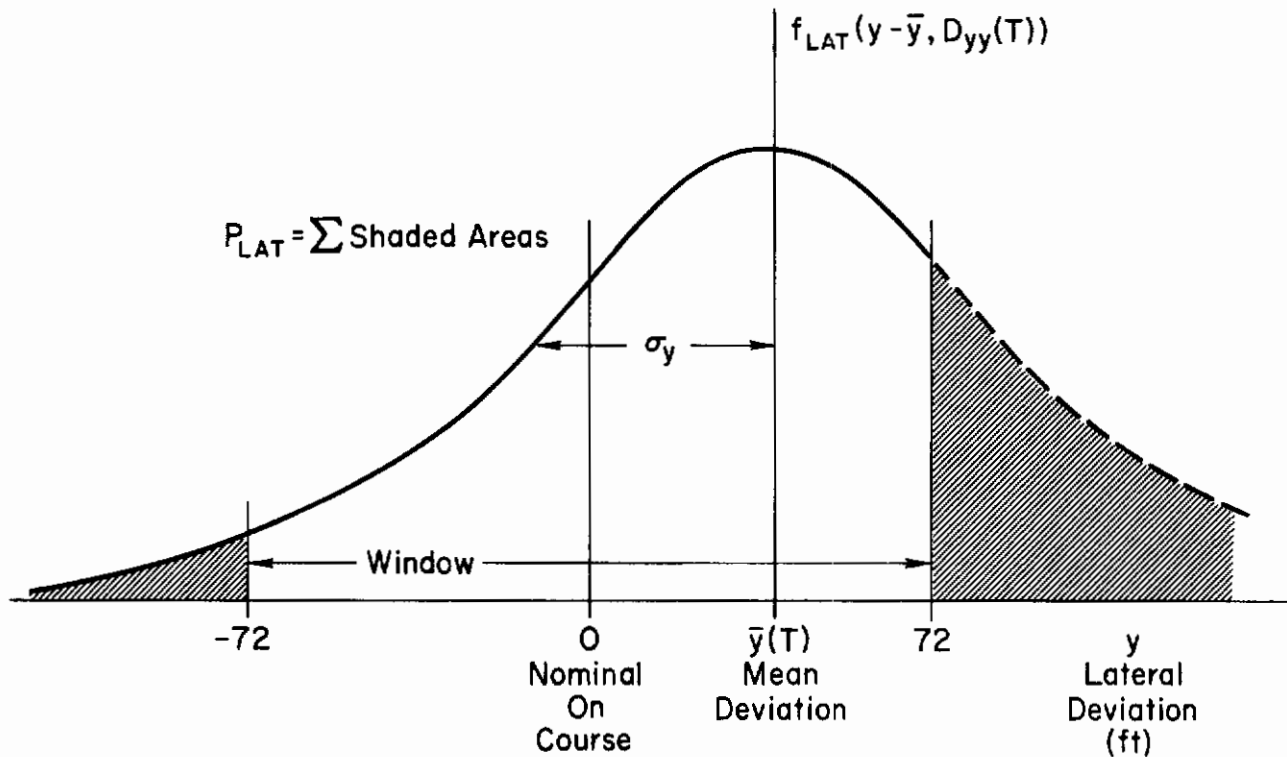
Figure 13. Relation of the Window and P_{LAT}
to the Probability Density Function

for normal and airspeed deviations can be calculated by any one of the three methods discussed in Section VI. in this case, $\overline{D}(T)$ is the 2 x 2 symmetric matrix:

$$\mathbf{D}(T) = \begin{bmatrix} D_{dd} & D_{du} \\ D_{du} & D_{uu} \end{bmatrix} \qquad (VII\text{-}5)$$

These quantities can be combined with the longitudinal window dimensions in order to compute P_{LONG}. The technique for this is portrayed pictorially in Fig. 14, where $f_{LONG}(d-\overline{d}, u_{AS}-\overline{u}_{AS}, \mathbf{D}(T))$ is the two-dimensional Gaussian probability density function of the longitudinal deviation. It is completely
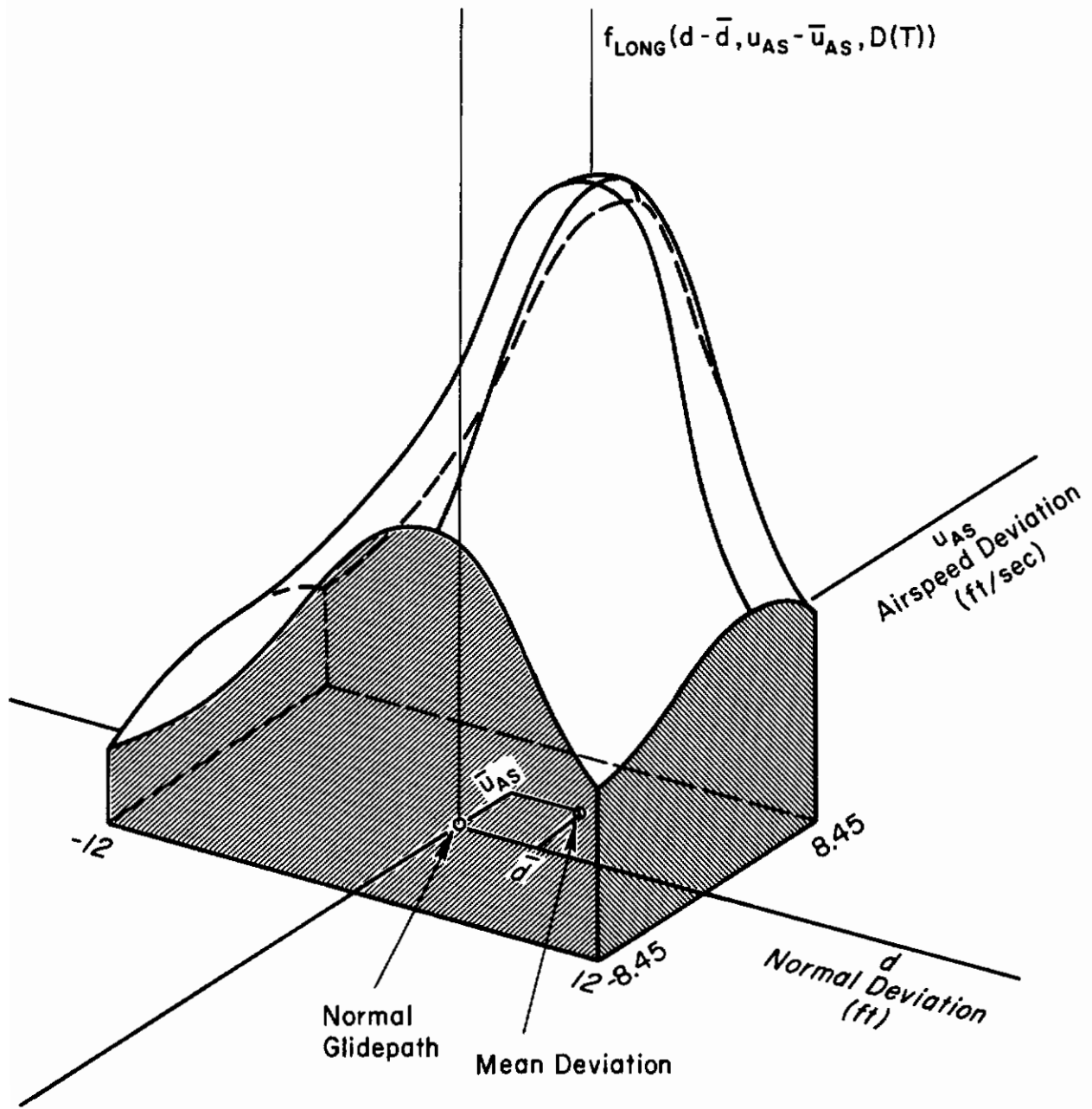
96

Figure 14. Relation of the Window and $(1 - P_{LONG})$
to the Probability Density Function

characterized by the mean values $\overline{d}$ and $\overline{u}_{AS}$ and by the 2 x 2 covariance matrix $\mathbf{D}(T)$. In this case, we have portrayed $(1-P_{LONG})$ as the volume under the two-dimensional probability density function and within the longitudinal window dimensions. To get P_{LONG}, merely subtract $(1-P_{LONG})$ from unity. The equation expressing P_{LONG} is:

$$P_{LONG} = 1 - \int_{-(12+\overline{d})}^{12-\overline{d}} \int_{-(8.45+\overline{u}_{AS})}^{8.45-\overline{u}_{AS}} \frac{e^{-\frac{1}{2}\{d, u_{AS}\}\mathbf{D}^{-1}(T)\begin{Bmatrix} d \\ u_{AS} \end{Bmatrix}}}{2\pi\sqrt{|\mathbf{D}(T)|}} \, dd \, du_{AS}$$

$$(VII-6)$$

P_{LONG} is best computed using the form given above, and using a digital computer program to evaluate the two-dimensional integral on the right hand side.

From this point, it is a relatively easy matter to compute P_W using Eq VII-1, and then to compute the probabilistic measure of performance and safety, $(1 - P_W P_D)^{-1}$, given in Section V. As explained there, a value of (for example) $P_D = 0.95$ is to be assumed for this computation where P_D is the probability of the pilot making the (correct) decision to discontinue an approach, given that he has not attained the window.

B. DETERMINISTIC WIND CONTRIBUTIONS TO THE MEAN VALUES

In evaluating the contributions of the winds and windshears to the normal and lateral deviations at the window two slightly different procedures have been used in the cases of the two examples.

Manual-flight director control of the A-7D is a system which does not provide for integration of either longitudinal or lateral deviation from the beam. The influence of steady wind components on the outcome of the approach will, therefore, be felt strongly in the absence of corrective action on the part of the pilot. On the other hand, the pilot may, indeed very likely does, provide a form of integral control with respect to what must be apparent steady errors in deviation from the glide slope. For this reason we will assume that the pilot can and

does compensate for the effect of steady headwinds or tailwinds. On the other hand, as will be shown, the effect of the assumed crosswind is minor and it perhaps would not be apparent. We therefore will assume that the pilot does not correct the error due to crosswind with any type of pseudo-integral control.

In the case of the "windproof" automatic pilot and approach coupler for the DC-8, integral control is provided in both deviation channels and there are no position errors at the window because of steady headwinds or crosswinds.

The effect of headwind and crosswind shears are felt by the systems for both the A-7D and DC-8, but the effects on the DC-8 system are much smaller than those produced by the A-7D system.

Table XXIV displays numerical results from calculations of the deterministic response of the manual-flight director control system for the A-7D to headwind, headwind shear, crosswind, and crosswind shear. The values tabulated are the deviations at the Cat II window. Note that since the system is linear, larger, or smaller, inputs will produce proportionately larger or smaller values of the deviations. It is remarkable that the mean glide slope deviation error solely in response to the headwind shear is more than half the permissible deviation for an acceptable approach, and that if the pilot did not trim out the effect of the headwind by means of psuedo-integral control, he would be far outside the window below the beam! Crosswind and crosswind shear, with their assumed directions, may be seen in the Table to cause nearly equal and opposite errors. This result might be considered to be artificial, but the contribution of either of these disturbance components to the mean lateral deviation at the window is small enough in comparison with the lateral dimension of the window so as to be very nearly insignificant.

Similar results are shown in Table XXV for the DC-8 and its assumed control system. Only the shears contribute to the mean values of longitudinal and lateral deviation at the window. For the assumed rather small values of shear, acting over only a small portion of the approach, the contributions to the mean values of longitudinal and lateral

TABLE XXIV

SYSTEM ERRORS IN THE PRESENCE OF DETERMINISTIC WINDS AND WINDSHEAR FOR
THE A-7D AIRCRAFT UNDER MANUAL APPROACH CONTROL WITH AN AN/CPU-80A FLIGHT DIRECTOR

Coordinates of Cat II Approach "Window"	Total Contribution to Mean Error at "Window"	Source of Mean Error			
		Headwind $-16.9 \leq H \leq 42.2$ ft/sec throughout entire approach	Headwind shear $\dot{H}=0.855$ ft/sec^2 (4 kts/100 ft between 200 ft and 100 ft altitude)	Crosswind $C=25.4$ ft/sec throughout entire approach	Crosswind shear $\dot{C}=-0.855$ ft/sec^2 (-4 kts/100 ft between 200 ft and 100 ft altitude)
Glide Slope Deviation (ft)	6.41	* −23.4(headwind) 9.4(tailwind)	6.41	–	–
Lateral Deviation (ft)	0.41	–	–	4.09	-3.68
Lateral Deviation (ft)	-3.68	–	–	0**	-3.68
Airspeed Error (ft/sec)	-5.77	0	-5.77	–	–

* These results of the linearized perturbation analysis do not assume an integral control supplied by the pilot manually to trim out the steady-state component of headwind-induced error normal to the 1:20 glide slope. Their influence is to be neglected.

** C = 0. This situation leads to a greater mean error at the window.

TABLE XXV

SYSTEM ERRORS IN THE PRESENCE OF WINDSHEAR FOR THE DC-8-60
AIRCRAFT UNDER AUTOMATIC APPROACH CONTROL WITH AN ADVANCED AUTOMATIC PILOT

Coordinates of Cat II Approach "Window"	Total Contribution to Mean Error at "Window"	Source of Mean Error*	
		Headwind shear $\dot{H}=0.771$ ft/sec^2 (4 kts/100 ft between 200 ft and 100 ft altitude)	Crosswind shear $\dot{C}=-0.771$ ft/sec^2 (-4 kts/100 ft between 200 ft and 100 ft altitude)
Glide Slope Deviation (ft)	1.49	1.49	-
Lateral Deviation (ft)	-1.57	-	-1.57
Airspeed Error (ft/sec)	-7.94	-7.94	-

* There is no mean error because of steady headwind or crosswind.

deviation at the window because of the windshears are here seen to be very small in comparison with the dimensions of the window itself.

C. RESPONSE TO STOCHASTIC DISTURBANCES

The individual root mean square (RMS) responses of the closed loop systems of Section III to the several components of the stochastic disturbances described in Section IV are next calculated by the preferred methods outlined in Section VI. The RMS responses to the several inputs are then combined into a root sum squared (RSS) response for all the inputs acting simultaneously.

(In the case of manual-flight director control of the A-7D, the pilot's remnant, in part, scales with the mean squared value of the displayed signals and it can only be determined at this point in the analysis. The responses to the remnant input may then be calculated, and their contribution is then, in turn, incorporated into the total RSS response for each motion variable of interest.)

For convenience, the RSS motion in each variable of interest may be converted into a marginal probability that certain events will occur considering the stochastic inputs alone. The acceptable events of interest are: 1) being inside the window, and 2) not exceeding the "limits" for pilot acceptance.

Estimation of the marginal probabilities is actually based on a multivariate Gaussian probability distribution with zero means and covariances. $\overline{yu_{AS}}$ and $\overline{yd}$ are zero by virtue of the independence of the longitudinal and lateral motions. We shall also shortly see that, in a typical case, the covariance $\overline{du_{AS}}$ is negligible in comparison with the autocovariances σ_d^2 and $\sigma_{u_{AS}}^2$. The reader should recall that the dimensions of the "window" are:

(u_{AS}) airspeed: ± 5.0 kts $= \pm 8.45$ ft/sec

(d) glide slope deviation: ± 12.0 ft $\quad\Big\}$

(y) lateral deviation: ± 72.0 ft $\quad\Big\}$ FAA Category IIB

and the "limits" for pilot acceptance are:

$(a_{z_{cg}})$ normal acceleration: ±0.5 g = ±16.1 ft/sec^2

(θ) pitch attitude: ±6.0 deg = $\pm$ 0.105 rad

(φ) bank attitude: ±6.0 deg = ±0.105 rad

(p) roll rate: ±10.0 deg/sec = ±0.175 rad/sec

(ψ) heading: ±5.0 deg = ±0.087 rad

$\left.\rule{0pt}{2.5cm}\right\}$ (recommended by RTCA SC-79)

Results of the calculations of the response to stochastic disturbances of the A-7D airplane with manual-flight director control are presented in Tables XXVI(A) and (B).

Table XXVI(A) is for the longitudinal motion variables. Here it may be observed that the dominant contributions to deviations in both airspeed and deviation normal to the beam arise from the action of the longitudinal gusts. The contributions of the vertical gusts and the beam fluctuation noise are comparatively small. Note that the marginal probabilities of being inside the window are not very high. Fluctuations in normal acceleration are so small by comparison to the acceptable limit that it is uninteresting to tabulate them. Otherwise, somewhat surprisingly, the correlation between deviations normal to the beam and in airspeed turns out to be very small by comparison with the (autoco-) variances in normal deviation and in airspeed. The marginal probabilities are therefore very close to being independent and we shall not give any further consideration to the possibility of a correlation between the variables which determine size of the window.

Data for the random responses in the lateral motion variables for the A-7D system are summarized in Table XXVI(B). Both side and rolling gusts contribute significantly to the standard deviation in lateral displacement from the beam and to the standard deviations in roll rate and bank angle. Other responses are effectively uninteresting.

In a fashion almost exactly parallel to the results for the A-7D, Tables XXVII(A) and (B) display the results of calculating the response to stochastic disturbances for the DC-8 with an advanced

TABLE XXVI

STANDARD DEVIATIONS OF SYSTEM RESPONSE TO STOCHASTIC DISTURBANCES
FOR THE A-7D AIRCRAFT UNDER MANUAL APPROACH CONTROL WITH AN AN/CPU-80A FLIGHT DIRECTOR

(A) Longitudinal Motion Variables

Contribution To Standard Deviation in Error	Disturbance Source			Root-Sum-Squared Disturbance Correlated Error	Total RSS Error Including Pilot's Remnant Contribution	Marginal Probability of Being Inside Cat II "Window" or Pilot Acceptance Limits on Each Approach P_M
	u_g σ_{u_g}=10 ft/sec Longitudinal Gusts	w_g σ_{w_g}=6.5 ft/sec Normal Gusts	Microwave Scanning Glide Slope Fluctuation σ_{GS}=1.32 ft T_o=0.2 sec			
$\sigma_{u_{AS}}$(ft/sec)	9.11	0.162	0.0202	9.11	9.13	0.644
σ_u (ft/sec)	3.99	0.162	0.0202	3.99	-	-
$\sigma_{\dot{d}_{cg}}$(ft/sec)	4.16	1.92	0.0420	4.58	-	-
$\sigma_{d_{cg}}$ (ft)	17.2	7.55	0.162	18.8	19.1	0.514
σ_θ (rad)	0.0120	0.00235	0.000207	0.0122	0.0352	0.9972
$\sigma_{\delta_{THROTTLE}}$ (rad)	0.00712	0.00141	0.0000194	0.00726	-	-
σ_{δ_i}(PILOT) (rad)	0.00926	0.00813	0.000202	0.0123	0.0127	-
Covariance $\overline{\partial u_{AS}}$	-2.98	0.000959	0.00286			
sgn(cov)$\sqrt{|cov|}$	-1.73	0.0300	0.0535			

TABLE XXVI

STANDARD DEVIATIONS OF SYSTEM RESPONSE TO STOCHASTIC DISTURBANCES

FOR THE A-7D AIRCRAFT UNDER MANUAL APPROACH CONTROL WITH AN AN/CPU-80A FLIGHT DIRECTOR

(B) Lateral Motion Variables

Contribution To Standard Deviation in Error	Disturbance Source			Root-Sum-Squared Disturbance Correlated Error	Total RSS Error Including Pilot's Remnant Contribution	Marginal Probability of Being Inside "Window" or Acceptance Limits on Each Approach
	v_g σ_{v_g}=10 ft/sec Lateral Gusts	P_g σ_{p_g}=.0438 $\frac{rad}{sec}$ Rolling Gusts	Microwave Scanning ₵ Azimuth Fluctuation σ_{y_c}=7 ft T_o=0.2 sec			
$\sigma_{\ddot{y}_{cg}}$ (ft/sec)	6.67	1.69	0.214	6.88	7.58	-
$\sigma_{y_{cg}}$ (ft)	30.6	10.4	1.10	32.4	38.2	0.9736
σ_p (rad/sec)	0.0485	0.0135	0.00252	0.0504	0.0545	0.9986
σ_φ (rad)	0.0546	0.0180	0.00279	0.0576	0.0666	0.884
σ_r (rad/sec)	0.0336	0.00256	0.00388	0.0339	0.0342	-
σ_ψ (rad)	0.0411	0.00738	0.000946	0.0418	0.0440	0.9526
$\sigma_{\delta_a(PILOT)}$ (rad)	0.0483	0.00689	0.00191	0.0488	0.0507	-

105

TABLE XXVII

STANDARD DEVIATIONS OF SYSTEM RESPONSE TO STOCHASTIC DISTURBANCES
FOR THE DC-8-60 AIRCRAFT UNDER AUTOMATIC APPROACH CONTROL WITH AN ADVANCED AUTOMATIC PILOT

(A) Longitudinal Motion Variables

| Contribution To | Disturbance Source | | | Root-Sum-Squared Disturbance Correlated Error (Standard Deviation) | Marginal Probability of Being Inside Cat II "Window" or Pilot Acceptance Limits on Each Approach P_M |
	u_g $\sigma_{ug}=10$ ft/sec	w_g $\sigma_{wg}=6.5$ ft/sec	Microwave Scanning Glide Slope Fluctuation $\sigma_{GS}=1.32$ ft $T_o=0.2$ sec		
$\sigma_{u_{AS}}$(ft/sec)	11.4	2.32	0.0431	11.7	0.531*
σ_u (ft/sec)	3.05	2.32	0.0431	3.83	-
$\sigma_{\dot{h}_{cg}}$(ft/sec)	2.54	3.39	0.171	4.24	-
$\sigma_{d_{cg}}$(ft)	4.41	3.68	0.314	5.75	0.963
σ_θ (rad)	0.0183	0.0215	0.00519	0.0287	0.99974
σ_{δ_e} (rad)	0.0269	0.0315	0.00827	0.0422	-

* There is no autothrottle.

TABLE XXVII

STANDARD DEVIATIONS OF SYSTEM RESPONSE TO STOCHASTIC DISTURBANCES
FOR THE DC-8-60 AIRCRAFT UNDER AUTOMATIC APPROACH CONTROL WITH AN ADVANCED AUTOMATIC PILOT

(B) Lateral Motion Variables

Contribution To	Disturbance Source			Root-Sum-Squared Disturbance Correlated Error (Standard Deviation)	Marginal Probability of Being Inside Cat II "Window" or Pilot Acceptance Limits on Each Approach P_M
	v_g $\sigma_{v_g}=10.0$ ft/sec	p_g $\sigma_{p_g}=0.0165$ rad/sec	Microwave Scanning $\mathbf{L}$ Azimuth Fluctuation $\sigma_{y_c}=7.0$ ft $T_O=0.2$ sec		
$\sigma_{\dot{y}_{cg}}$ (ft/sec)	1.79	1.22	0.418	2.20	-
$\sigma_{y_{cg}}$ (ft)	3.70	9.56	1.31	10.3	$(1 - 2\times10^{-11.86})$
σ_p (rad/sec)	0.0265	0.00445	0.0249	0.0366	0.9999813
σ_ϕ (rad)	0.0234	0.0915	0.0130	0.0954	0.728
σ_r (rad/sec)	-	(Not Computed)	(Computed)	-	-
σ_ψ (rad)	0.0421	0.00615	0.00224	0.0426	0.9594
σ_{δ_a} (rad)	0.0440	0.0165	0.0753	0.0888	-
σ_{δ_r} (rad)	0.0989	0.00140	0.00330	0.0989	-

automatic pilot and approach coupler. Note, however, that in both Tables that there is, in this case, no need to take the pilot's remnant into account.

Table XXVII(A) shows again that the principal contributions to the standard deviations in airspeed and in normal displacement from the beam centerline are caused by the longitudinal gusts. In this case, however, in part because the deviations in normal displacement are smaller with the advanced automatic flight control system, the normal gusts are also a very appreciable factor in the total RSS error in normal displacement. Otherwise note that in the complete absence of a throttle control, the deviations in airspeed exceed the root mean square longitudinal gust velocity. This in turn leads to a low marginal probability of being inside the airspeed dimension of the window at the Cat II decision height.

In point of fact, it may be unrealistic to evaluate the probability that the airplane will be inside the airspeed dimension of the window at the instant it reaches the decision height. What probably happens during an approach in gusty air is that the pilot "averages" the indicated fluctuations in airspeed. In the model which we have considered the actual average of the perturbations in airspeed because of the stochastic disturbances will be zero. On the other hand a pseudo-average obtained by passing u_{AS} through a low pass filter with (say) a time constant of five seconds would yield a short-term average which might be more representative of a pilot's judgment, at the decision height, as to whether the airplane was at an airspeed so significantly different from the trim speed as to justify a go-around.

Again the deviations in normal acceleration are so small as not to be worth tabulating.

Deviations in the lateral motion variables of the DC-8 in response to the stochastic disturbance inputs are presented in Table XXVII(B). Because of the very high performance sideslip stability augmenter, and the high bandwidth lateral deviation loop, we find there that the contributions of the wind disturbances to the lateral deviation from the beam are very small indeed. On the contrary side, the deviations in

bank angle and heading cannot be so favorably compared to the limits proposed by RTCA SC-79. This, however, is a nearly inevitable consequence of the levels of gust disturbance.

For the rather large RMS side and rolling gust velocities which have been assumed, the standard deviations in rudder and aileron deflections are each a little less than 6 deg. This represents about one-third of the available authority for each control. A higher gain in the rudder and aileron control loops would permit better gust effect suppression but at the cost of more control activity. In the absence of specific guidelines on acceptable control activity, one-third authority on an RMS basis was taken to be an upper limit, but this is only a guess. If lower limits should be imposed, loop gains would have to be lowered throughout the system. In particular, the crossover frequency of the lateral displacement control loop would have to be lowered and the probability of exceeding the lateral dimension of the window would be increased.

If desired, the independent marginal probabilities of being inside the window and/or within the limits for pilot acceptance can be very simply combined to yield a number which is the probability that the stochastic disturbances, by themselves, will produce an outcome which is not a success. The probability of an unsuccessful outcome is:

$$P_{\overline{S}} = 1 - \prod_{i=1}^{n} (P_{M_i})$$

where P_{M_i} = ith marginal probability

   n = number of limits (including window dimensions)

For example, the probability of being <u>outside</u> the purely geometric dimensions of the window because of the stochastic disturbances alone is:

$$P_{\overline{S}} = 1 - \prod_{i=1}^{2} (P_{M_i})$$

where, in this case, the two marginal probabilities are the probabilities
listed in Tables XXVI(A), XXVI(B), XXVII(A) and XXVII(B) corresponding
to the variances in normal deviation, d, and lateral deviation, y.
Considering the variances of d and y, the probabilities of an unsuccessful
outcome because of the stochastic disturbances alone are 0.50 for the
A-7D and 0.037 for the DC-8. This very great difference in performance
begins to point up the advantage of the advanced automatic system.

D. MEASURES OF PERFORMANCE AND SAFETY

System errors at the window because of deterministic inputs have been
summarized in Tables XXIV and XXV, and the RSS responses to the stochastic
disturbances have been presented in Tables XXVI and XXVII. These results
can now be combined in the fashion described in Section VI to calculate
the marginal probability of being inside the window on any given approach
and further the probability of a missed approach, P_{MA}. Finally the
measure of performance and safety $(1 - P_{MA})^{-1}$ can be calculated for the
two example systems.

Table XXVIII displays the intermediate results for the A-7D with
manual flight director control. Note here particularly that both the
mean error because of the deterministic inputs and the standard deviation
of the stochastic response to disturbances combine to produce a low
marginal probability of being inside the limiting dimension of the window
in glide slope deviation. Otherwise the marginal probability of being
inside the window is determined almost entirely by the response to
the random inputs.

Similar data for the case of the DC-8 with an advanced automatic
pilot are presented in Table XXIX. The marginal probabilities of being
inside the window are much higher in this case with the exception of the
probability being within the prescribed limits on airspeed. This last
probability could be made higher with the installation of an autothrottle.

Table XXX summarizes the results for the two examples and carries
the calculations through to the accident exposure multiplier. Actually
four cases are shown. Since, as has already been explained, it may be

TABLE XXVIII

MARGINAL PROBABILITY OF BEING INSIDE THE WINDOW FOR THE
A-7D AIRCRAFT UNDER MANUAL APPROACH CONTROL WITH AN
AN/CPU-80A FLIGHT DIRECTOR

Coordinates of Cat II Approach "Window"	Total Contribution to Mean Error at "Window" $\left(\text{from Table} \atop \text{XXIV}\right)$	Total RSS Error Including Pilot's Remnant Contribution $\left(\text{from Table} \atop \text{XXVI}\right)$	Marginal Probability of Being Inside Cat II "Window" on Each Approach P_M
Glide Slope Deviation (ft)	6.41	19.1	0.446
Lateral Deviation (ft)	0.41	38.2	0.9405
Lateral Deviation (ft)	-3.68 (no crosswind)	38.2	0.9394
Airspeed Error (ft/sec)	-5.77	9.13	0.556

111

TABLE XXIX

MARGINAL PROBABILITY OF BEING INSIDE THE WINDOW FOR THE
DC-8-60 AIRCRAFT UNDER AUTOMATIC APPROACH CONTROL WITH
AN ADVANCED AUTOMATIC PILOT

Coordinates of Cat II Approach "Window"	Total Contribution to Mean Error at "Window" $\left(\text{from Table } XXV\right)$	RSS Disturbance Correlated Error $\left(\text{from Table } XXVII\right)$	Marginal Probability of Being Inside Cat II "Window" on Each Approach P_M
Glide Slope Deviation (ft)	1.49	5.75	0.9567
Lateral Deviation	-1.57	10.3	$(1 - 10^{-11.425} - 10^{-12.366})$
Airspeed Error (ft/sec)	-7.94	11.7*	0.437

* There is no autothrottle.

TABLE XXX

MISSED APPROACH PREDICTIONS IN A SEVERE ENVIRONMENT

	Prob. of being outside window P_W	Prob. of Missed Approach (If $P_D = .95*$) P_{MA}	Accident Exposure Multiplier $(1 - P_{MA})^{-1}$
A-7D Manual Approach			
(d, y, u_{AS})	0.77	0.73	3.7
$(d, y \text{ only})$	0.58	0.55	2.2
DC-8 Automatic Approach			
$(d, y, u_{AS}\text{-no auto throttle})$	0.58	0.55	2.2
$(d, y \text{ only})$	0.043	0.041	1.04
Recommended requirement based on $P_{MA/ARR} = \dfrac{P_{MA}}{1 - P_{MA}} \leq 0.05$	-	0.0476	1.05

* P_D is the conditional probability that the pilot will make the correct decision, given that he is outside the window.

113

somewhat unrealistic to assume that the pilot will execute a missed approach if his airspeed is off at the instant of window passage, we have shown the probabilities of being outside the dimensions of the window with and without considering the airspeed dimension. Performance and safety for the A-7D in low visibility approaches is severely limited by the lag filters in the pitch and roll axes of the flight control system for the purpose of command rate attenuation. On the other hand, neglecting the influence of turbulence induced errors in airspeed, performance and safety for the DC-8 are good. The probability of being outside the geometric dimensions of the window is small and the accident exposure multiplier is acceptably low.

SECTION VIII

SUMMARY OF IMPLICATIONS FOR THE MEASURING SYSTEM

One of the purposes of the investigation reported here has been to develop a method of determining requirements for the measuring system. Subject to a large number of fixed assumptions, the method has been demonstrated in connection with two examples, and we are in a position to trace the influence of changes in the design of the system on performance and safety. To actually do so, however, has not been within the scope of this study. Nevertheless, the understanding gained from analysis of the system can be used in such a way as to be able to make some statements concerning requirements on the measuring system. In particular we can point out some of the areas in which tradeoffs can be made.

In connection with the example of the DC-8, we have <u>assumed</u> zero boresight errors, low fluctuation noise, the availability of high quality beam rate information, and an advanced automatic flight control system. We have further assumed moderate windshear and a severe turbulence environment, and have shown that, neglecting airspeed errors, the accident exposure multiplier is just barely less than the recommended maximum value. Clearly no concession can be made in the quality of the measuring system without decreasing safety. Perhaps, however, the requirement has been set too stringently in view of the assumed level of turbulence, and a somewhat degraded performance would, in fact, be acceptable especially under more nearly normal conditions. On the other hand, since the dominant contribution to the probability of being outside the geometric limits of the window arises from the glidepath error response to turbulence, some degradation of the measuring system could be tolerated if the control system were further improved with, for example, direct lift control.

There is, however, a keen desire to keep complexity on the ground, at least for many categories of users, and that brings us to the question of tradeoffs between the characteristics of the ground equipment and the airborne portion of the measuring system.

115

The principal measuring system candidate for TACLAND is a scanning beam system, and in such a system, one of the central issues with respect to requirements is what the scan rate should be. We cannot answer that question with finality, but we can again point to advantages and disadvantages of a degree of complexity in the airborne equipment.

A. SCANNING BEAM TECHNIQUES

The intermittent reception of guidance data, rather than continuous reception as is provided by the conventional instrument landing system (ILS), is an inherent characteristic of scanning beam instrument landing systems. The considerable advantages of scanning beam systems in other respects than data rate, as recognized in recent recommendations of Special Committee SC-117 of the Radio Technical Commission for Aeronautics, make them a strong candidate for automatic, as well as manually controlled, approach and landing. However, concern has arisen about possible deficiencies in data rate, especially for automatic path control, unless the beam scanning rate is quite high. Higher data rates have two disadvantages: (1) complexity in the ground-based equipment resulting from the scanning system and (2) reduction of the dwell time of the beam on the receiver antenna. The second disadvantage reduces the position accuracy that can be derived in the air on each scan.

Significantly greater costs and complications in ground-based equipment are entailed in high scanning rates than in low ones; therefore, it is well to specify the lowest rate that will ensure adequate accuracy and stability in approach, flare and alignment path-following. This minimum rate can be determined by performance analysis and computer simulation of the guidance process for various types of aircraft that will use the system. Before we present some results, we shall summarize key tradeoffs which affect the techniques of scanning beam transmission and reception.

The ground equipment may transmit a synchronized stepped beam or may transmit on the scanning beam encoded precision glide slope and azimuth angles as functions of the scanning angles. The airborne equipment determines angular position by counting steps or by decoding the angle data contained in the peak amplitude of the received beams

116

and then determines distance by interrogating and receiving a reply from a transponder at the site of the azimuth transmitting antenna. This last is termed distance measuring equipment (DME). (See Ref. 34.)

Whether the beam moves continuously or is stepped, the information derived at the receiver has a granularity. For a continuously moving beam, the granularity is a result of the signal modulation. It is small in magnitude in relation to the desired system accuracy. The desired system accuracy has been stated to be between 0.05 and 0.1 deg. (Ref. 35)

It would require an extremely large number of individual steps to cover incrementally the scanned sector. Stepped systems, therefore, usually employ interpolation techniques in order to achieve a higher accuracy than is represented by the sector angle of each step. (Ref. 35)

The angular information, conveyed by the scanning beam, can be derived by comparing beam passage to a reference time, or it can be directly transmitted as a beam modulation. The choice is between simplicity and accuracy. (Ref. 35)

Derivation of the instant of beam passage with a precision and linearity suitable for landing requires a consistently high signal gradient as the beam passes the aircraft antenna. Although simple in principle, and successful at low-to-moderate elevation angles, this is difficult to guarantee in practice at the very low angles for flare and roll out guidance. A more dependably precise method at very shallow angles is to transmit a beam which is modulated or encoded in such a way that it conveys the angle of its center regardless of its half-power beam width.

Most of the practical forms of beam modulation for the landing guidance measuring system can be classified as either frequency modulation-continuous wave (FM-CW) or pulse modulation, of which variable pulse repetition period (PRP) is a common example. FM-CW systems are limited in coverage by the bandwidth required for the modulation, while PRP systems are limited by the reduction of available samples at extremes where the repetition period is long (Ref. 35).

With this diversity of candidates for encoding the transmission in mind, we have nevertheless prepared a generic block diagram of the airborne portion of the measuring system in Fig. 15. A common airborne antenna, receiver and decoder (or demodulator or converter, depending on the type of beam modulation) are time-shared for two angles and DME, for which the interrogator is not shown. Since the elapsed time between receipt of angle pairs is compatible with the DME round-trip time, the decoder may also include the computation of transverse displacement errors (independent of range) in a linear dimension by scaling operations which are equivalent to dividing each angle by the distance to its corresponding apex. This computation also implies subtraction of a standard glide slope origin offset distance from the result of colocated azimuth-site DME, unless the glide slope course-softening should be timed from an initial point or based on altitude or DME at the glide path intercept point. Thus, the output of the decoder is a sample of each of two displacement errors.

B. SIGNAL RECOVERY AND RECONSTRUCTION

In a scanning beam system, no information is supplied to an aircraft except during the brief dwell of a radio beam on the airborne antenna. The "impulse" of guidance data derived from the beam must be held, as a continuous reference for path control, until updated by the next beam passage. Since the beam width is generally small, the dwell time is much less than the interval between beam passages. Thus, the first step in signal processing following encoding may be closely represented by a classical impulsive sampler and zero order hold. Some advantages and disadvantages associated with this simplest form of continuous signal extrapolation are listed in Table XXXI.

One complication of the greatest practical significance is the existence of sample damping, which is not normally encountered in "hard-wired" sampled-data systems. In a scanning beam guidance system, the technique of data recovery involves dependence of the magnitude of detected path error on signal strength, or on the information-bit content (e.g., pulse count) of the intercepted beam. Moreover, the guidance equipment designer can deliberately reduce the output response
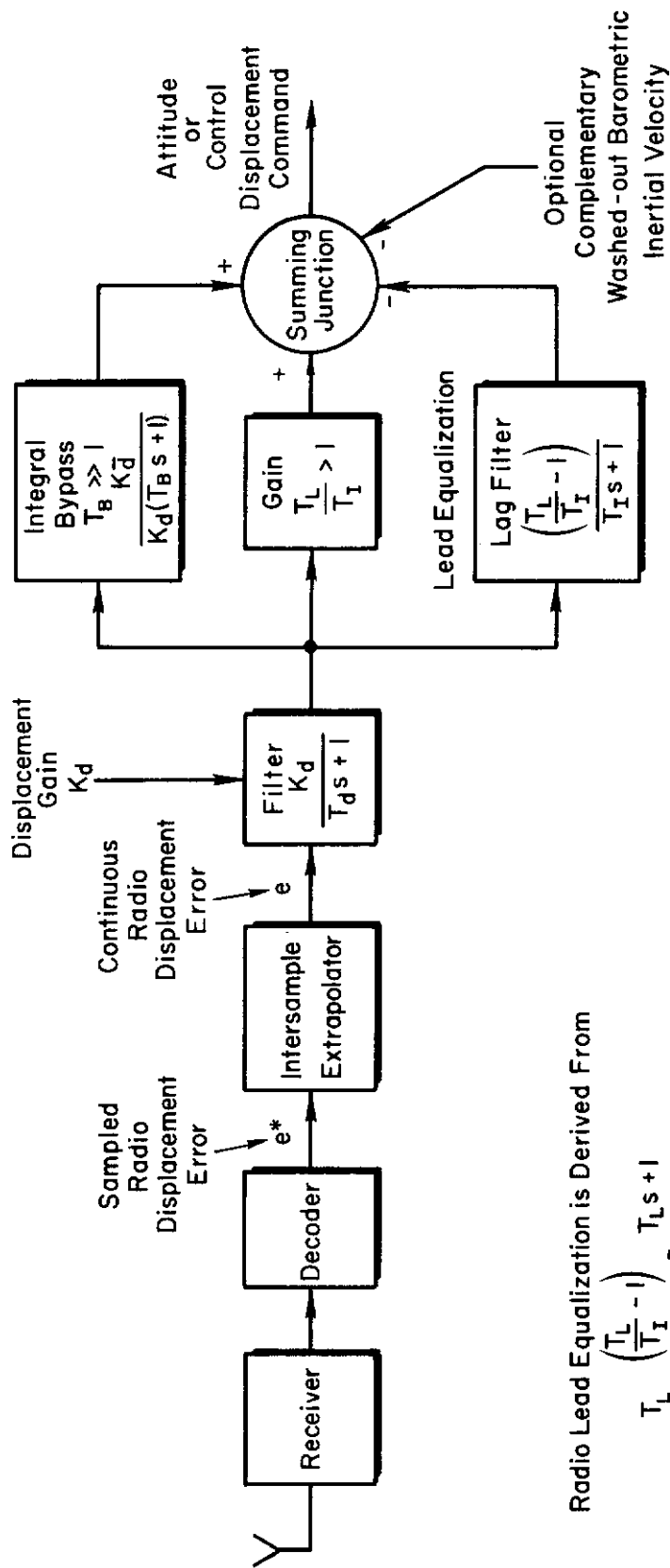
118

Figure 15. Airborne Portion of the Position Measuring System

Radio Lead Equalization is Derived From

$$\frac{\left(\dfrac{T_L}{T_I}-1\right)}{\dfrac{T_L}{T_I}-1} \cdot \frac{1}{T_I s+1} = \frac{T_L s+1}{T_I s+1}$$
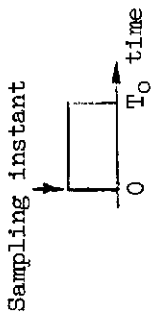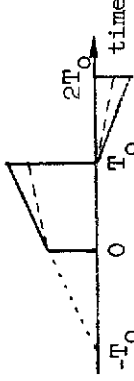
per sample to some fraction of the remaining error between his output
and the detected position -- knowing that this tends to reduce guidance
noise at the expense of time lag. The effect of such damping, in the
form of "partial boxcar sampling," on the response of the decoder to a
step change in aircraft position causes the boxcar output signal to follow
an exponential envelope. Thus a first order time lag may be introduced,
in the intersample extrapolator. This lag can be evaluated for any
given damping fraction in terms of the effects on gain and phase angle
as a function of input signal frequency.

The "extrapolator" block shown in Figure 15 allows also for first
order extrapolation of guidance data during the sampling intervals with
partial velocity weighting. Table XXXI shows that first order extrapolation
can reduce scanning rate requirements by a factor of nearly two-fifths.
A very small price in complexity need be paid for this advantage,
because, in practice, this is most conveniently done physically within
the decoder. In addition, these decoder and extrapolator blocks may
include other internal signal processing which would affect frequency
response, such as a built-in noise filter. On the other hand, it may be
preferrable to do all noise filtering in external circuits as shown in
Fig. 15. Noise promotes control actuator wear and unreliability as well
as unacceptability to pilots. One way to reduce the power spectral density
of fluctuation noise in control activity is to increase scanning rate.
The other way is to apply noise filters without compromising the system's
closed-loop frequency response so essential to approach success.

The remaining blocks in Fig. 15 illustrate the various noise filters,
the radio displacement gain signal path, the integral bypass for
automatic crosswind and headwind trim, and the radio lead equalization
network, which, in practice, may be provided by subtracting a suitably
scaled lagged radio displacement signal from the scaled displacement
signal itself. These continuous variable networks have, in the past,
usually been entirely in the province of the flight control subsystem.
However, some of these elements, or their functional equivalents, may be
more effectively, more economically, or perhaps unavoidably, included
in the guidance receiver and decoder. In any event, a clear understanding

TABLE XXXI

CANDIDATES FOR CONTINUOUS INTERSAMPLE EXTRAPOLATION

WITH A SAMPLED-DATA POSITION MEASURING SYSTEM

	ADVANTAGES	DISADVANTAGES
ZERO ORDER HOLD (Boxcar Hold) Sampling instant 	● Simplest for airborne equipment ● Requires only harmonic noise rejection filter	✗ Reduces position-loop phase margin unless updating frequency is over 180 times crossover frequency ✗ Requires highest updating frequency from ground-based equipment
FIRST ORDER HOLD Adjustable Constants: rate-weighting* damping†	● Maintains continuous position-loop phase margin with updating frequency as low as 75 times crossover frequency ● Offers rate-weighting and damping adjustments adaptable to any vehicle-control system ● Requires lower updating frequency from ground-based equipment	✗ More complex for airborne equipment ✗ May reduce position-loop gain margin significantly unless a low pass noise rejection filter is used

* Rate-weighting coefficient controls rate of linear extrapolation.

† Damping coefficient controls the relative share of the previous sampled derivative and the first back difference used in computing the present sampled derivative.

121

of their functions is necessary to a proper system and equipment design.

C. MINIMUM SCANNING RATES

The results of performance analysis in Ref. 41 have shown that the contributions of moderate windshear and severe atmospheric turbulence to approach tracking error predominate over the contributions of microwave scanning beam fluctuation noise, reflection anomalies and static bias errors as long as the updating frequency of the scanning beam measuring system is at least 2 Hz. The gust- and shear-upset errors, as well as the anomaly-following errors, will decrease approximately as the inverse square of the tracking loop crossover frequency. This is why it will now be necessary more than ever before to achieve the highest possible crossover frequency so as to suppress the errors induced by the atmospheric environment during approach and landing.

Nevertheless, it is pointless to try to establish a lower bound on scanning frequency by minimizing the total error power from gust-upset, anomaly-following and fluctuation noise contributions. This is because the crossover frequency required to minimize total tracking error power in severe turbulence will exceed vehicle aerodynamic stability and control limitations as long as the updating frequency is at least 2 Hz. The interactions of these factors are depicted graphically in Fig. 16. Notice that the crossover frequency required for least total error power will increase even more beyond vehicle limitations as the broad-band fluctuation noise contribution is reduced by increasing the scanning frequency above 2 Hz.

Since noise contribution reduction cannot realistically be employed to determine a suitable scan rate, the lower bound on the scanning frequency will instead be governed by the least acceptable margin of stability associated with the maximum possible crossover frequency (if this is limited by vehicle aerodynamic stability and control) or by the margin of stability associated with the largest crossover frequency required to satisfy approach tracking performance standards. Since a
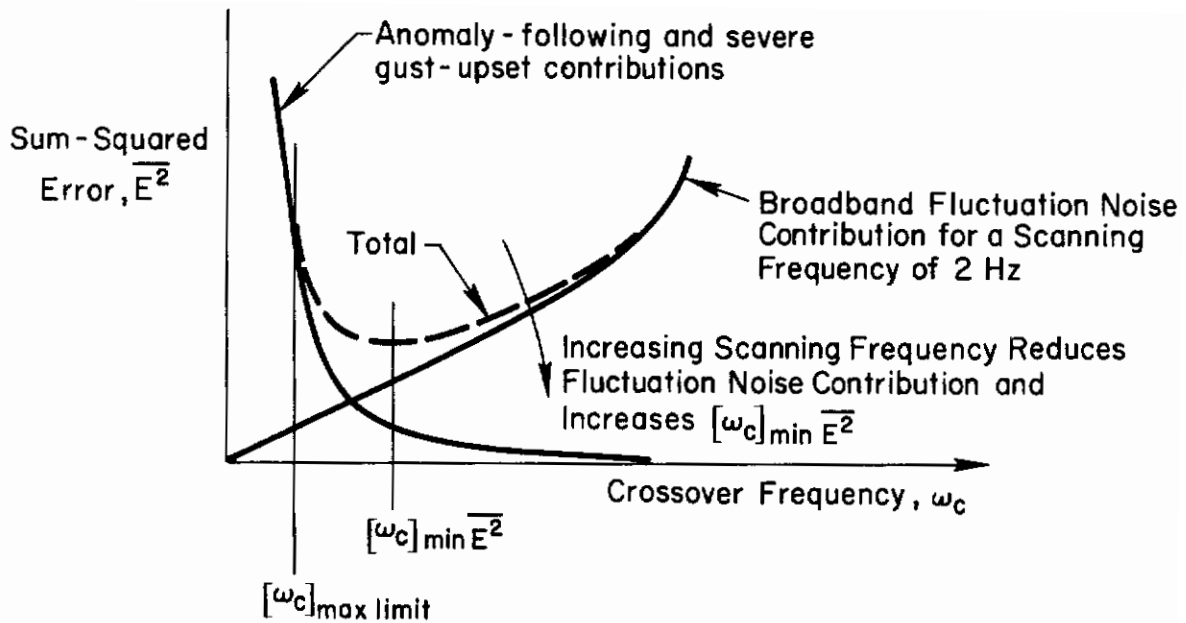
Figure 16. Illustration of the Crossover Frequency Which
Minimizes Sum-Squared Tracking Error and the
Maximum Crossover Frequency Subject to Vehicle
Aerodynamic Stability and Control Limitations

high crossover frequency achieved at the expense of a low margin of
stability will itself result in poor approach performance, the system
designer is not at liberty to trade stability margin for reducing
scanning frequency while at the same time trying to maintain an
adequately high crossover frequency.

It is now possible to illustrate a procedure for selecting a
reasonable scanning frequency. Our choice will be bounded from below
by an allowable reduction in stability margin for continuous transmission
of data which translates into an allowable decrease in crossover
frequency to recover the continuous margin. For example the sampling
frequency must exceed the crossover frequency by the ratio 180:1, if a
zero order (boxcar) intersample "hold" or extrapolator is to introduce
not more than 1 deg of additional phase lag at the crossover frequency.
If the crossover frequency is equal to, say, 1/3 rad/sec with continuous
measurement of error, this will require an updating frequency in excess
of 10 Hz. However, since the ground-based microwave scanning beam

measuring subsystem may tend to become more complex and more costly or less reliable as the required updating frequency exceeds 8 Hz, some reduction in a required updating frequency of 10 Hz or more may be desirable. Figure 17 shows that substantial reduction in the minimum required updating frequency will accompany use of a first order inter-sample extrapolator and noise rejection filter in the airborne portion of the measuring subsystem. Now the sampling frequency must exceed the half-power attentuation frequency of the noise reflection filter by at least the ratio 2 π in order to permit a first order smoothing filter to reduce the peak oscillatory output of the first order extrapolator which is at one-half the sampling frequency. The smoothing filter will then introduce a portion of the phase lag at crossover. For example, a sampling frequency of 4 Hz will permit the break frequency of the data hold noise rejection filter to be 12 times the crossover frequency. A first order smoothing filter will introduce less than 5 deg of phase lag at crossover for a break frequency ratio of 12 times crossover. Alternatively, for a sampling frequency of 4 Hz, the crossover frequency will be about 90 percent of the value possible with continuous transmission of error, if one attempts to preserve the phase margin of stability.

On the other hand, a sampling frequency of 8 Hz will permit the break frequency of the data hold noise rejection filter to be almost 23 times the crossover frequency. A first order smoothing filter will then introduce only 2.5 deg of phase lag at crossover. The crossover frequency will be about 95 percent of the value possible with continuous transmission of error if one attempts to preserve the phase margin of stability. Thus a sampling frequency of 8 Hz appears ample to allow for some increase in crossover frequency.

We can apply the rationale depicted in Fig. 17 to the A-7D and DC-8 examples, and, because we wish to preserve at least the measures of approach performance which have been illustrated, we adopt a stringent criterion for trading off margins in stability in exchange for crossover frequency. The predicted lower bound on updating frequency is based on accepting not more than 1 deg loss in phase margin nor more than 0.3 dB loss in gain margin in comparison with a continuous measuring system.
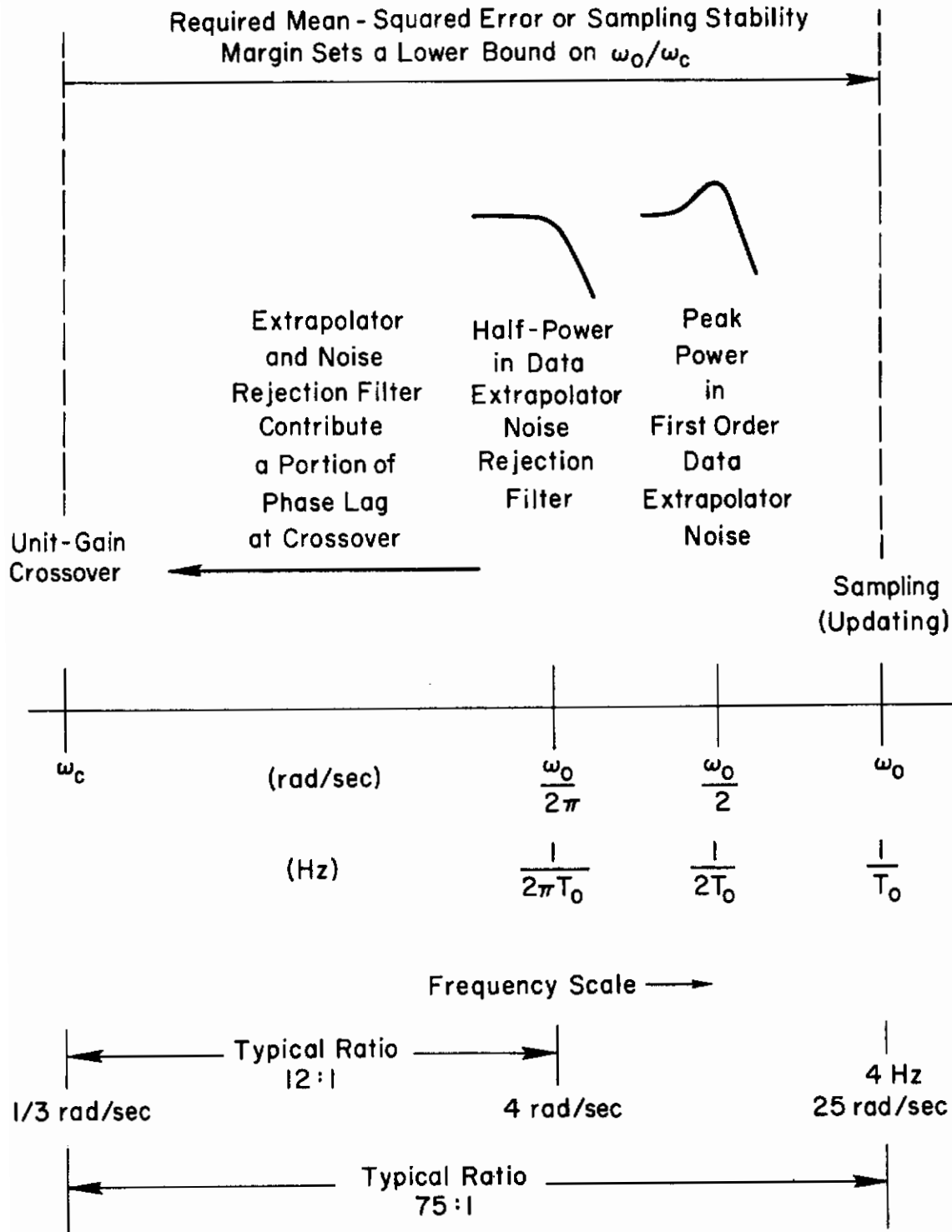
Figure 17. Frequency Scale Illustrating the Relationships Which
Govern the Lower Bound on Sampling Frequency
Associated with a Unit-Gain Crossover Frequency

125

TABLE XXXII

PREDICTED LOWER BOUND ON SAMPLING (UPDATING) FREQUENCY

FOR THE A-7D AND DC-8 EXAMPLES WITH A MICROWAVE SCANNING MEASURING SYSTEM

	Order of Data Extrapolator	Number of First Order lag Noise Rejection Filters	Unit-Gain Crossover Frequency ω_c (rad/sec)	Half-Power Frequency in Noise Rejection Filter(s) (rad/sec)	Peak Power Frequency in Data Extrapolator (rad/sec)	Sampling (Updating) Frequency (rad/sec)
A-7D Manual Approach						
Glide slope	First	One	0.17	4	6.3	12.5 (2 Hz)
℄ Azimuth	First	Two	0.15	0.1, 4	6.3	12.5 (2 Hz)
DC-8 Automatic Approach						
Glide slope	First	One	0.75	4*	28.3	56.5 (9 Hz)
℄ Azimuth	First	Two	0.23	2, 4	9.4	18.8 (3 Hz)

* This applies only to the samples derived from the microwave measurements. A complementary instanteous (inertial) vertical speed measurement of higher bandwidth is required to achieve the stated crossover frequency.

The sampling frequencies required by this criterion are displayed in Table XXXII. The results in Table XXXII can be obtained with a simple hybrid first order intersample data extrapolator which augments the first back difference with a measure of the sampled time derivative. A lower bound of 2 or 3 Hz will accommodate all cases in Table XXXII except the one for DC-8 glide slope regulation which has the highest crossover frequency, 0.75 rad/sec. In this case the sampling frequency must be at least 9 Hz even with a first order data extrapolator.

Similar predictions for a zero order (boxcar) data hold are presented in Table XXXIII for comparison. The lower bound on sampling frequency is more than doubled because of the increased open-loop phase lag of the zero order hold at lower sampling frequencies. Notice that the DC-8 glide slope regulation now demands a sampling frequency of at least 24 Hz. Therefore a significant tradeoff must be made between the additional complexity of even the simplest first order data extrapolator in all airborne equipment or the increased complexity required in the ground-based equipment by an increase in the updating frequency. The possible choice would seem to favor the airborne first order data extrapolator.

TABLE XXXIII

PREDICTED LOWER BOUND ON SAMPLING (UPDATING) FREQUENCY FOR THE A-7D AND DC-8 EXAMPLES WITH A MICROWAVE SCANNING MEASURING SYSTEM AND A ZERO ORDER HOLD

	Sampling (Updating) Frequency (rad/sec)
A-7D Manual Approach	
Glide slope	37.7 (6 Hz)
$\mathcal{L}$ Azimuth	31.4 (5 Hz)
DC-8 Automatic Approach	
Glide Slope	150.0 (24 Hz)
$\mathcal{L}$ Azimuth	50.0 (8 Hz)

D. SUMMARY

In the presence of severe atmospheric wind conditions, a low accident exposure multiplier requires as high an approach (and flare and ground roll) tracking loop crossover frequency as possible to suppress upset errors, which dominate over scanning beam fluctuation errors. Table XXXI showed previously that the sampling frequency, in turn, should exceed the crossover frequency by at least a ratio of 75:1, if the first order intersample extrapolator and its noise rejection filter were not to compromise the tracking loop phase margin by more than 1 deg nor gain margin by more than 0.3 dB with respect to that for a continuous measuring system. Loss in stability margin translates directly into a loss in crossover frequency to recover stability and an increase in the accident exposure multiplier in severe windshear and turbulence. Each user should, in seeking certification of his automatic landing system, be entitled to some tolerance in making this tradeoff. However, if the lower bound on the measuring system updating rate is already too low, the user's tolerance will have vanished.

The predicted lower bound on sampling frequency presented in summary Table XXXIV for the A-7D example and in summary Table XXXV for the DC-8 example is therefore based on the stringent requirements cited previously for very little compromise in stability margin from that for a continuous measuring system. Tables XXXIV and XXXV also present for comparison the corresponding (higher) lower bound on sampling frequency, if the airborne equipment were, instead, to employ a zero order (boxcar) extrapolator.

TABLE XXXIV

PREDICTED LOWER BOUND ON SAMPLING (UPDATING) FREQUENCY
FOR THE A-7D EXAMPLE WITH A MICROWAVE SCANNING MEASURING SYSTEM

	Unit-Gain Crossover Frequency (rad/sec)	Continuous Outer-loop Phase Margin (deg) Gain Margin (db)	Order of Data Extrapolator Rate Coef. k Damping Coef. z	Sampled Outer-loop Phase Margin (deg) Gain Margin (db)	Lower Bound on Sampling (Updating) Frequency (Hz)*	Ratio of Sampling Frequency to Crossover Frequency $\dfrac{2\pi}{\omega_c T_o}$
Glide slope	0.17	60° 9.2 db at .39 rad/sec	Zero k = 0 z = 1	59° 8.9 db	6	210
			First k = .8 z = .5	59° 8.9 db	2	74
Centerline Azimuth	0.15	37° 8.8 db at .35 rad/sec	Zero k = 0 z = 1	36° 8.5 db	5	210
			First k = .8 z = .5	37° 8.5 db	2	84

*Based on not more than 1° loss in phase margin nor more than .3 db loss in gain margin from that for a continuous measuring system

TABLE XXXV

PREDICTED LOWER BOUND ON SAMPLING (UPDATING) FREQUENCY
FOR THE DC-8 EXAMPLE WITH A MICROWAVE SCANNING MEASURING SYSTEM

	Unit-Gain Crossover Frequency (rad/sec)	Continuous Outer-loop Phase Margin (deg) Gain Margin (db)	Order of Data Extrapolator Rate Coef. k Damping Coef. z	Sampled Outer-loop Phase Margin (deg) Gain Margin (db)	Lower Bound on Sampling (Updating) Frequency* (Hz)	Ratio of Sampling Frequency to Crossover Frequency $\frac{2\pi}{\omega_c T_o}$
Glide slope	0.75	$32°$ 8 db at 1.83 rad/sec	Zero k = 0 z = 1	$31°$ 7.7 db	24	200
			First k = .8 z = .8	$32°$ 7.8 db	9	75
Centerline Azimuth	0.23	$41°$ 16.3 db at .92 rad/sec	Zero k = 0 z = 1	$40°$ 15.6 db	8	219
			First k = .8 z = .8	$41°$ 15.5 db	3	82

*Based on not more than $1°$ loss in phase margin nor more than .3 db loss in gain margin from that for a continuous measuring system, except for ℄ Azimuth, which has an extraordinarily large gain margin.

SECTION IX

CONCLUSIONS

The investigation, reported here, of TACLAND measuring system requirements for low-visibility landing approach had the two-fold purpose of evolving a practical systems analysis procedure for evaluation of the characteristics of the measuring system and of illustrating the application of that procedure.

A. MEASURING SYSTEM EVALUATION PROCEDURE

A linear dynamic system model is practical for evaluating low-visibility approach tracking performance. The approach task itself is one of regulating against disturbances which upset the aircraft from following a desired rectilinear path in space, and the changes in altitude do not importantly change the flight condition. Hence, aircraft motions can be adequately represented in the trimmed landing approach by ordinary linear differential equations with constant coefficients.

Linear feedback arrangements are likewise adequate for describing approach control systems. The feedback control arrangements for the dynamic system model are based on receiving nominally periodic samples of position solely from a terminal site measuring subsystem in conformity with signal format recommendations by Radio Technical Commission for Aeronautics Special Committee 117. Provisions are included in the dynamic system model for deriving time integrals and rates of change of sampled position in airborne equipment and for deriving otherwise continuous measurements of aircraft state variables by airborne sensors such as rate gyros, attitude and directional gyros, strapped-down accelerometers and air data sensors.

The dynamic system model includes two range-varying outer loop gains, because the terminal site measuring system provides angular position in two coordinates. This range-variation in gain may be equivalently represented as a time-variation by using a distance-to-time coordinate transformation which is a function of average approach velocity. In this way the range-varying system model may be transformed into a linear dynamical model having, at worst, two time-dependent gains.

131

Approach system performance can be evaluated using a stationary infinite time duration approximation to the linear time-varying, finite time duration TACLAND system model provided distance-measuring equipment or its equivalent is available to compensate for the range-dependent outer loop gain of a terminal site measuring system. Nevertheless, the apparent terminal site measurement errors such as beam bias, anomalies and fluctuation noise will decrease linearly with increasing time when the control system outer loop gain is compensated for range-variation. However, the predicted microwave scanning beam errors will contribute so little to total system errors in the presence of severe atmospheric turbulence between the outer marker and the present Cat IIB decision height of 100 feet that we may neglect the time variation in linear measures of beam noise when applying the evaluation procedure in severe turbulence. Stochastic initial conditions associated with the acquisition of the approach guidance reference may be neglected without affecting the evaluation of candidate systems. Since the distributions of the inputs and disturbances acting throughout the approach are Gaussian, the calculation of the variances of and covariances among measures of system performance may be simply done by closed form integrals in terms of algebraic equations rather than by time domain simulation.

Introduction of the concept of a landing approach window at the decision altitude means that the average tracking errors are of interest only at the time of window passage. This greatly simplifies the definition of a unified, sensitive system-centered probabilistic measure of approach success, the probability of attaining the window on any given approach. This probability is used in the system performance and safety measure, the accident exposure multiplier because of missed approaches or the average number of approaches which must be made to achieve one successful approach (within the window) for each arrival at the terminal.

The present state of models for microwave scanning beam measuring system aberrations, atmospheric windshear, and stochastic turbulence probably does not allow the calculation of an absolute probabilistic measure of approach success on a world-wide basis. Instead candidate measuring systems may be compared by conditioning the probability of

132

attaining the window on critical combinations of inputs and disturbances which are <u>representative</u> of local conditions at a specific terminal site.

B. APPLICATION OF THE EVALUATION PROCEDURE

Severe atmospheric turbulence and moderate windshears contribute the predominant approach tracking errors which can lead to a rather low probability of approach success. Contemporary flight control systems provide a lower flight control system response bandwidth and more low frequency rigidity in pitch attitude and heading than are desirable for suppressing approach course-following and glide slope tracking errors induced by turbulence and shears. Consequently an advanced automatic flight control system with superior short-period windproofing qualities was synthesized by relaxing rigidity in pitch attitude and heading to illustrate that a high probability of approach success can be achieved with a properly designed flight control system even in the presence of severe atmospheric disturbances. It was shown that with proper windproofing an average of only 105 approaches would be required to achieve 100 successful approaches through the present Cat II window for each 100 arrivals in the terminal area. In a contrasting example, under IFR manual control without windproofing, 220 approaches would be required to produce 100 successful ones.

The expected anomalies and fluctuation noise in a microwave scanning beam measuring system will not limit performance at the Cat II window, if the updating frequency is at least 2 Hz. Instead, the practical lower bound on updating frequency for a sampled approach measuring system will be limited by the highest position-loop crossover frequency required to assure the desired measure of approach success at the window.

The use of first order intersample extrapolation in the airborne receiving portion of the measuring system to provide a continuous reconstructed displacement signal for use by the flight control system appears to be a practical means of reducing scan rate requirements. This will permit a lower updating frequency on the order of only 80 times the position-loop crossover frequency. Two hundred times the position-loop crossover frequency would otherwise be required if only a zero order (boxcar) hold were employed to extrapolate the received position samples.

133

The probability of a missed sample has been estimated on the order of 0.001. However, the influence of a missed sample on the approach success probability is negligible, even for a missed sample probability as high as 0.2. The effect of missed samples, therefore, has been neglected in the application of the evaluation procedure.

The pilot's scanning remnant has been predicted in the application to a manually-controlled approach under IFR using a flight director with monitored situation information. The scanning remnant contributes little incoherent power to the total error variance and, therefore, little to the accident exposure multiplier. This is perhaps as one would expect, if the flight director is so designed that it can be properly used for manual approach control while the pilot monitors the confidence-inspiring situation information.

In applying the procedure to an automatically controlled approach we have assumed zero boresight bias errors, low fluctuation noise, the availability of high quality beam rate information, and an advanced automatic flight control system to cope with severe turbulence. We have further assumed moderate windshear and a severe turbulence environment, and have shown that, neglecting airspeed errors, the accident exposure multiplier is just barely less than the recommended maximum value of 1.05. Clearly no concession can be made in the quality of the measuring system without decreasing safety. Perhaps, however, the requirement has been set too stringently in view of the assumed level of turbulence, and a somewhat degraded performance would, in fact, be acceptable especially under more nearly normal conditions. On the other hand, since the dominant contribution to the probability of being outside the geometric limits of the window arises from the glidepath error response to turbulence, some degradation of the measuring system could be tolerated if the control system were further improved with, for example, direct lift control. In any event the applications strive to make it clear that the results are not necessarily the "sacred wisdom of an oracle" but depend on ground rules adopted by the user. To this end we have tried to provide a flexible procedure which will accept a variety of practical system disturbances and which will permit the user some latitude in selecting system stability, performance, safety and pilot acceptance criteria for evaluating the salient characteristics of scanning beam measuring systems.

REFERENCES

1. Litchford, G. B., _Synthesis of a Multifunctional Tactical Landing System_, AFFDL-TR-67-188, January 1968

2. Beneke, J., and C. W. Wightman, _Guidance Concepts for the Tactical Instrument Landing System (TACLAND)_, AFFDL-TR-67-189, January 1968

3. Dax, P. R., H. C. Hiscox, and W. J. Palmer, _Tactical Instrument Landing System Study_, AFFDL-TR-68-12, March 1968

4. Cafarelli, N. J., Jr., and M. A. Meyer, _TACLAND Studies (Tactical Instrument Landing)_, AFFDL-TR-68-42, April 1968

5. Sullivan, N., and J. K. Taylor, _Tactical Instrument Landing (TACLAND) System Study_, AFFDL-TR-68-22, May 1968

6. Litchford, G. B., _New Developments in Scanning Beam Landing Guidance Systems_, AFFDL-TR-69-107, December 1969

7. Johnson, W. A., and D. T. McRuer, _Development of a Category II Approach System Model_, STI TR-182-1, December 1969

8. McRuer, D., I. Ashkenas, and D. Graham, _Aircraft Dynamics and Automatic Control_, Systems Technology, Inc., Hawthorne, 1968

9. Teper, G. L., _Preliminary Users Manual for Tymshare Aircraft Equations of Motion Exact Factors Program_, STI WP-700-2, August 1969

10. McRuer, D. T., I. L. Ashkenas, and H. R. Pass, _Analysis of Multiloop Vehicular Control Systems_, ASD-TDR-62-1014, March 1964

11. Anonymous, _Computer, Flight Director CPU-80/A_, Military Specification MIL-C-83014(USAF), 14 June 1967

12. McRuer, D. T., D. Graham, E. S. Krendel, and W. Reisener, Jr., _Human Pilot Dynamics in Compensatory Systems_, AFFDL-TR-65-15, July 1965

13. McRuer, D., H. R. Jex, W. F. Clement, and D. Graham, _Development of a Systems Analysis Theory of Manual Control Displays_, STI TR-163-1, October 1967

14. Anonymous, _Standard Performance Criteria for Autopilot/Coupler Equipment_, Paper 31-63/DO-118, Radio Technical Commission for Aeronautics SC-79, Washington, D. C., March 14, 1963

15. Anonymous, _Automatic Flight Control Systems for Piloted Aircraft_, Bureau of Aeronautics Report AE-61-4 VI, April 1956

16. Anonymous, _Compilation of Data on the NASA Ames Landing Simulator_, STI TR-170-12, February 1968

17. Anonymous, _Flying Qualities of Piloted Airplanes_, Military Specification MIL-F-008785A(USAF), 31 October 1968

18. Chalk, C. R., T. P. Neal, and T. M. Harris, _Background Information and User Guide for MIL-F-008785A(USAF), "Military Specification-Flying Qualities of Piloted Airplanes,"_ Cornell Aeronautical Laboratory, Inc., 10 June 1968

19. Chalk, C. R., T. P. Neal, T. M. Harris, F. E. Pritchard, and R. J. Woodcock, _Background Information and User Guide for MIL-F-8785B(ASG), "Military Specification - Flying Qualities of Piloted Airplanes,"_ AFFDL-TR-69-72, August 1969

20. Anonymous, Supplemental Data on Scanning Beam Guidance System for Approach and Landing, Prepared for RTCA SC-117, by AIL Division of Cutler-Hammer, Inc., August 1969

21. Anonymous, Unpublished communications between STI and AIL Division of Cutler-Hammer, Inc., 13 November 1969, 20 February 1970

22. Clement, W. F., _Random Sampling Remnant Theory Applied to Manual Control_, STI TM-183-A, March 1969

23. Allen, R. W., W. F. Clement, and H. R. Jex, _Research on Display Scanning, Sampling, and Reconstruction Using Separate Main and Secondary Tracking Tasks_, STI TR-170-2, July 1969

24. Jex, H. R., and R. E. Magdaleno, "Corroborative Data on Normalization of Human Operator Remnant," _IEEE Trans._, Vol. MMS-10, No. 4, December 1969, pp. 137-140

25. Weir, D. H., and F. R. Alex, _Estimation of Pilot Remnant for Flight Director Control Tasks During Landing Approach_, STI WP-170-26, 20 January 1970

26. Weir, D. H., and R. H. Klein, _The Measurement and Analysis of Pilot Scanning and Control Behavior During Simulated Instrument Approaches_, NASA CR-1535, June 1970

27. Hofmann, L. G., _Measures of Performance and Safety_, STI WP-192-4, 31 October 1969

28. Newton, G. C., Jr., L. A. Gould, and J. F. Kaiser, Analytical Design of Linear Feedback Controls, John Wiley and Sons, New York, 1957, Appendix E

29. Laning, J. H., Jr., and R. H. Battin, Random Processes in Automatic Control, McGraw-Hill Book Company, Inc., New York, 1956, Chapter 6

30. DeRusso, P. M., R. J. Roy, and G. M. Close, State Variables for Engineers, John Wiley and Sons, New York, 1965, Chapter 5

31. McRuer, D., I. Ashkenas, and D. Graham, Aircraft Dynamics and Automatic Control, Systems Technology, Inc., Hawthorne, 1968, Chapter 10

32. Hofmann, L. G., Several Considerations in Estimating TACLAND Performance Statistics Using Systems Analysis, STI WP-192-5, 14 November 1969

33. Abramowitz, M., and J. A. Stegun, eds., Handbook of Mathematical Functions, National Bureau of Standards, Applied Mathematics Series, 55, June 1964, pp. 966-973

34. Woodward, J. E., Post-1970 Scanning Beam Approach and Landing, presented at Eighth AGARD Guidance and Control Panel on Aircraft Landing Systems, May 1969

35. Pogust, F. B., Status of Microwave Scanning Beam Landing System Developments, presented at IEEE EASCON 1969, Washington, D. C., October 1969

36. McRuer, D. T., Unified Analysis of Linear Feedback Systems, ASD-TR-61-118, July 1961

37. Ashkenas, I. L., and D. T. McRuer, Approximate Airframe Transfer Functions and Application to Single Sensor Control Systems, WADC-TR-58-82, June 1958

38. Aseltine, J. A., Transform Method in Linear System Analysis, McGraw-Hill Book Company, Inc., New York, 1958

39. Shipley, P. P., "A Unified Approach to Synthesis of Linear Systems," IEEE Trans. on Automatic Control, Vol. AC-8, No. 2, April 1963, pp. 114-120

40. Anonymous, Super Basic, Tymshare Manuals Reference Series, April 1969

41. Clement, W. F., <u>Analysis of Landing Guidance and Control with a</u>
     <u>Periodically Sampled Data Measuring System</u>, STI WP-192-1,
     September 1969

42. Clement, W. F., and L. G. Hofmann, <u>A Systems Analysis of Manual</u>
     <u>Control Techniques and Display Arrangements for Instrument</u>
     <u>Landing Approaches in Helicopters</u>, Vol. I: <u>Speed and Height</u>
     <u>Regulation</u>, JANAIR Report 690718, (STI TR-183-1), July 1969

APPENDIX A

A SIMPLIFIED EQUIVALENT REPRESENTATION OF THE A-7D PITCH AXIS MANUAL CONTROL SYSTEM WITH "CONTROL AUGMENTATION"

Refer to Fig. 18. All inputs and feedbacks are referenced to the electrical summing junction at the input of the AFCS Dual Series Actuators.

$$
\delta_{iT} = \frac{1}{0.55\,s + 1}\left\{ \frac{.6}{57.3}\left[F_{sp} - \frac{2.75}{32.2}\,a_{z_{cg}} - 9.6\,s\,\dot{\theta} \right] \right.
$$

$$
+ \frac{2}{(32.2)(57.3)}\left[-a_{z_{cg}} + 15\,s\,\dot{\theta} \right] + 0.5\,\dot{\theta}
$$

$$
\left. + \frac{7(0.55\,s + 1)}{72(57.3)}\left[F_{sp} - \frac{2.75}{32.2}\,a_{z_{cg}} - 9.6\,s\,\dot{\theta} \right] \right\}
$$

$$
\delta_{iT} = \left[\frac{0.0105}{0.55\,s + 1} + 0.0017 \right] F_{sp}
$$

$$
- \left[\frac{1.98 \times 10^{-3}}{0.55\,s + 1} + 0.145 \times 10^{-3} \right] a_{z_{cg}}
$$

$$
- \left[\frac{0.0837\,s}{0.55\,s + 1} + 0.0163\,s - 0.5 \right] \dot{\theta}
$$

$$
\delta_{iT} = \left[\frac{12.2 + 0.935\,s}{0.55\,s + 1} \right] \times 10^{-3}\,F_{sp}
$$

$$
- \left[\frac{2.12 + 0.08\,s}{0.55\,s + 1} \right] \times 10^{-3}\,a_{z_{cg}}
$$

$$
- \left[\frac{0.00897\,s^2 - 0.175\,s - 0.5}{0.55\,s + 1} \right] \dot{\theta}
$$

$$
\delta_{iT} = \left[\frac{s + 13}{s + 1.82} \right] \frac{0.935}{0.55} \times 10^{-3}\,F_{sp}
$$

$$
- \left[\frac{s + 26.5}{s + 1.82} \right] \frac{0.08}{0.55} \times 10^{-3}\,a_{z_{cg}}
$$

$$
- \left[\frac{(s + 2.54)(s + 22.0)}{s + 1.82} \right] \frac{0.00897}{0.55}\,\dot{\theta}
$$

Figure 18. A-7D Pitch Axis Manual Control System
with "Control Augmentation"

Neglect the dynamic contribution from each high frequency zero relative to the pole at s = -1.82.

$$\delta_{iT} = \frac{1}{0.55\,s + 1}\left\{12.2 \times 10^{-3}\,F_{sp} - 2.12 \times 10^{-3}\,a_{z_{cg}}\right\}$$

$$- 0.358 \frac{(s + 2.54)}{(s + 1.82)}\,\theta$$

Define $\delta_{ip} = 12.2 \times 10^{-3}\,F_{sp}$ and $\frac{1}{T_f} = 1.82$, then:

$$\delta_{iT} = \frac{1}{0.55\,s + 1}\left\{\delta_{ip} - 2.12 \times 10^{-3}\,a_{z_{cg}}\right\} - 0.358 \frac{(s + 2.54)}{(s + 1/T_f)}\,\dot{\theta}$$

This is the simplified equivalent form represented in Fig. 6 of the text.

APPENDIX B

SYSTEM SURVEYS FOR MANUAL AND AUTOMATIC CONTROL

A. PROCEDURE FOR MULTILOOP SYSTEM SYNTHESIS

The key to multiloop synthesis lies in the adroit selection of loop closure possibilities on the first trial. This is followed by subsequent analysis with the method presented in Ref. 10. In such a procedure, a trial set of closure possibilities is analyzed to determine the closed-loop system's dynamic characteristics. These are then compared with dynamic performance objectives. Deficiencies revealed by the comparison are, hopefully, eliminated, or at least reduced, by subsequent modifications. The modifications result in a new system for trial which is analyzed and assessed, etc., in its turn. The iterations continue until the trial system characteristics are consonant with the dynamic performance objectives. The number of iterations required to achieve the ultimate system depends on the designer's knowledge of single-loop servo-analysis techniques, understanding of vehicle dynamics, and appreciation of the changes in effective-vehicle dynamics caused by idealized single-loop controllers. The multiloop analysis procedure has been developed so as to enhance insight and preserve a direct connection with the problem at each step.

The analysis of a system characterized by linear constant-coefficient differential equations proceeds in six essential steps:

1. Delineation of nominal open-loop system characteristics in terms of transfer functions, $G(s)$.

2. Selection of loops and their compensation, and determination of a loop-closure sequence.

3. Determination of nominal closed-loop transfer functions from the open-loop transfer functions.

4. Determination of the changes in $G(s)$ resulting from the expected variations in the controller and controlled element characteristics.

5. Consideration of the effects of open-loop system variations on closed-loop behavior.

6. Calculation of nominal and off-nominal closed-loop system responses for pertinent inputs.

The first step above -- delineation of the open-loop characteristics in terms of a transfer function, $G(s)$ -- can be accomplished by transformation of the system differential equations to algebraic equations. Tables III and IV in Section II summarize the results for the two aircraft used in the illustrative examples.

It is difficult to succinctly and persuasively describe all the considerations which may enter into a designer's choice of loops to close and compensation to be applied in each loop in the second step above. An understanding of the problem is best developed by considering illustrative examples. The process of loop selection does not involve unique operations in compliance with a straightforward routine. Selection of a particular block diagram, or sequence of closures, from among the several possible ones is subject to choices. The rationale for the choices in the examples presented here has been described in Section III. From the point of view of analysis, the closure sequence is immaterial. In synthesis, however, the closure sequence can be all-important. For instance, certain loops are necessarily closed before others for which they provide parallel equalization; and the necessary use of incomplete loop closure criteria causes some loop closure sequences to result in extreme variations in loop adjustments during successive iterations, whereas for other sequences there is practically no change from one iteration to the next. Because of considerations such as these, there are preferred loop closure sequences. For vehicular control systems a set of factors which will ordinarily provide the insight needed to construct a unique closure sequence is presented in Ref. 10.

The third, fourth and fifth steps in the sequence of analysis form the core of feedback system analysis. This requires the solution for the roots of

$$1 + G(s) = 0 \qquad\qquad (B-1)$$

subject to the off-nominal variations expected in G(s). Although it may seem very simple, a great deal of effort has been devoted to finding effective methods for performing these steps which are simple to perform and at the same time promote insight.

The factor $1/[1 + G(s)]$ is the classical sensitivity function which expresses the relative change in closed-loop characteristics in response to a causative relative change in open-loop characteristics. Thus the measure $1/[1 + G(s)]$ indicates directly the reduction in the "sensitivity" of the system to many of the influences which would otherwise tend to corrupt its performance.

It has further been both necessary and desirable to expand the scope of the concept of sensitivity to measures which explicitly relate the roots of $1 + G(s) = 0$ to the complex singularities of the open-loop function G(s). Such measures are called "gain", "(open-loop) pole", "(open-loop) zero" and "(open-loop) parameter" sensitivities. Sensitivities among these measures explicitly relate the closed-loop differential variations to the open-loop differential variations with respect to the nominal values of parameters. The pre-eminent and most widely used of these sensitivities is the gain sensitivity.

B. INTRODUCTION TO THE SYSTEM SURVEYS

In the illustrative examples of analytical steps three, four and five as applied here, the open-loop transfer function G(s) is a ratio of rational polynomials in the complex variable, s, of the Laplace transform.* The analytical function G(s) can be represented graphically as a function of particular values of s, such as real values, $\pm\sigma$, and imaginary values, $\pm j\omega$, in a way which reveals some of the closed-loop sensitivities as well as the nominal closed-loop roots of $1 + G(s) = 0$

---

* Although the restriction to a rational form of G(s) does result in loss of generality, G(s) can include such terms as $e^{-\tau s}$ by using rational Padé approximations of essential singularities, for example.

themselves. This graphical representation of G(s) is called a "system survey." It is based, in general, on a unification (Ref. 36) of two artificially separated graphical views of the linear feedback analysis problem, the complex "root locus" and the generalized Bode diagram which includes the "frequency response" plotted on logarithmic coordinates. The system surveys presented here are, however, founded on the asymptotic logarithmic Bode diagram of G(s). The two special functions $|G(\pm\sigma)|$ and $|G(j\omega)|$ are then added to their common asymptote to form a σ-Bode and a $j\omega$-Bode graph. The polar angles $\underline{/G(\pm\sigma)}$ and $\underline{/G(j\omega)}$ are plotted on an accompanying graph having a log frequency scale common with that of the amplitude functions. It often happens that only the branch of the σ-Bode corresponding to the negative real values of s is important so that only $|G(-\sigma)|$ need be calculated and only in the intervals where $\underline{/G(-\sigma)}$ corresponds to the criterion for closed loop roots, -180 deg. Because the coefficients of the transfer functions are real, the poles and zeros of G(s) are always either real or complex conjugate pairs, hence the $j\omega$-Bode diagram is symmetrical about the origin and need be represented only for positive frequencies to establish gain and phase margins of stability and their sensitivities.

The σ-Bode diagram is, in fact, a locus of negative real roots as a function of gain. This is the simplest example of the "Bode root locus." Its branches are represented in the system surveys presented here by bold loci. The complex root locus is then added to the Bode diagram to complete the Bode root locus. Dotted loci represent the complex branches in the system surveys presented here. Since the complex branches of the Bode root locus require three variables (i.e., damping ratio, as well as frequency and gain) for their functional description, whereas the logarithmic coordinates of the Bode diagram represent only frequency and gain, the closed loop damping ratio is customarily identified at several discrete points on the complex Bode root locus in the neighborhood of unit gain crossover. From this identification, the sensitivity of closed loop damping ratio to gain variation can be estimated directly on the Bode root locus.

The multiloop system surveys have been prepared and are presented here in a sequence which corresponds to the closure sequence. The

control loops are divided into groups of "inner" and "outer" loops, reflecting the closure sequence. The command loops, dictated by the landing approach or other tracking task, ordinarily form the outer loops. Feedbacks intended to provide equalization for subsequent loops, or to suppress subsidiary degrees of freedom which have undesirable effects on subsequent loops, form a group of inner loops.

The innermost loop is closed first with tentatively selected equalization and gain; and the closed inner loop roots are found. These roots become the system's (open loop) poles for the next loop closure in the sequence.

If there is more than one control point among the loops in the closure sequence there will be "coupling loops." Using the same gain and equalization which has been selected for an inner loop, one must close any corresponding coupling loops. The closed loop roots resulting from this coupling closure become the system's (open loop) zeros for the next loop closure in the sequence.

After some repetition of this procedure as required by the closure sequence, the outermost loop is closed in a conventional manner as if it were the only loop around the modified system transfer function appropriate to the outer loop. If the result of the outer loop closure is not satisfactory as measured, for example, by the calculation of nominal and off-nominal closed loop system responses for pertinent inputs in the sixth step of the system analysis, the analyst may have to repeat portions or all of the closure sequence with different equalizations and gains.

Each of the system surveys lists the control law for the feedback loop which it represents. The moduli of the open loop factors of $G(s)$ are labelled with a symbolic, shorthand notation at the discontinuities in the asymptote of $G(s)$. The moduli of the closed loop factors of $1 + G(s) = 0$ are labelled by small squares along the Bode root locus at unit values (0 dB) of amplitude corresponding to the selected gain. In the case of inner loops these closed loop roots are also labelled with a symbolic, shorthand notation to assist the reader in transferring

corresponding factors to subsequent outer loops in the closure sequence.

The symbolic, shorthand notation is based on the one introduced in Ref. 37. It consists of a sequence of inverse time "constants," $1/T_i$, undamped natural frequencies, ω_j, and damping ratios, ζ_j, representing the open loop vehicle, control system, and equalization transfer function factors. The ith and jth subscripts are appropriate abbreviations of the corresponding dynamic modes of the vehicle and control system in the case of pole factors. In other cases the subscripts denote the motion variable described by a transfer function numerator or on which the loop equalization operates.

The notation for a closed loop factor is the same as that for the open loop factor with the addition of a prime superscript when the closed loop and open loop transfer function factors have the same form (i.e., both are real or both are complex). The number of primes present indicates the number of loops closed previously which affect the factor considered. In this case the origin of the closed loop factor is always clear (e.g., $\omega_d \rightarrow \omega_d'$, $\omega_p \rightarrow \omega_p'$, $\omega_\varphi \rightarrow \omega_\varphi'$, $T_R \rightarrow T_R'$, $T_{\varphi_1} \rightarrow T_{\varphi_1}'$, $T_{d_1} \rightarrow T_{d_1}'$, etc.).

When the closed loop factors differ in form from their open loop origins several possibilities exist:

a. For closed loop factors which have the same form as, and are approaching, open loop zeros, the closed loop factor notation is that of the open loop zeros (plus a prime). For example, open loop quantities $(s + 1/T_s)$ and $(s + 1/T_{d_2})$, which couple to form a quadratic approaching the open loop zeros of $(s^2 + 2\zeta_r\omega_r s + \omega_r^2)$, would give rise to a closed loop factor ordinarily denoted as $(s^2 + 2\zeta_r'\omega_r's + \omega_r'^2)$.

b. For closed loop factors which differ in form from both the open loop pole factors from which they depart and the open loop zero factors which they ultimately approach, a special notation is coined which ordinarily reflects the origin of the factor. For example, closed loop poles which start from $s = 0$ and $s = -1/T_R$, then couple to form a quadratic factor, and subsequently decouple to end finally at two real zeros, would be denoted as $s^2 + 2\zeta_R'\omega_R's + \omega_R'^2$ in the quadratic region.

c. Closed loop factors which have no readily identified origin or end point, such as one starting at s = 0 and approaching s = ∞ as gain increases, are given a specially coined notation, e.g., $1/T_c'$.

When the application of these rules by rote would result in confusion in the local context, a new form is substituted for the closed loop factor involved. Primes, however, are always retained.

With this introduction to the rationale for and the content of a system survey, we are ready to examine some examples for manual and automatic approach control. We shall begin with some of the surveys corresponding to the A-7D flight director system block diagram for manual speed and glide slope displacement control in Fig. 6, Section III. (The block diagram of the lateral-directional system for the A-7D is presented in Fig. 10, Section III.) This is followed by the example of the automatic approach control system for the DC-8. (See Fig. 7 and Fig. 11, Section III, for the block diagrams.)

C. MANUAL LONGITUDINAL APPROACH CONTROL IN THE A-7D

Figure 19 illustrates a survey of the manual washed-out pitch attitude loop closure through stabilator control with a low gain manual airspeed-to-throttle loop already closed. (A survey of the airspeed-to-throttle closure is not shown, because the low loop gain hardly alters either the phugoid characteristics or the pitch attitude response characteristics to stabilator control.) The significant point to notice in Fig. 19 is the low crossover frequency which is limited by the first order lag $1/T_f'$ in the A-7D primary manual stabilator flight control system with control augmentation. This lag, in turn, will cause a very low short period damping ratio, if the loop gain were increased to improve phugoid damping and increase phugoid bandwidth so as to improve glide slope tracking precision. Consequently pitch attitude lead equalization has been incorporated in the flight director control law to improve short period damping, although it is not required by Ref. 11. A low crossover frequency has been selected so as to provide a generous nominal margin of short period stability in this inner loop, for the
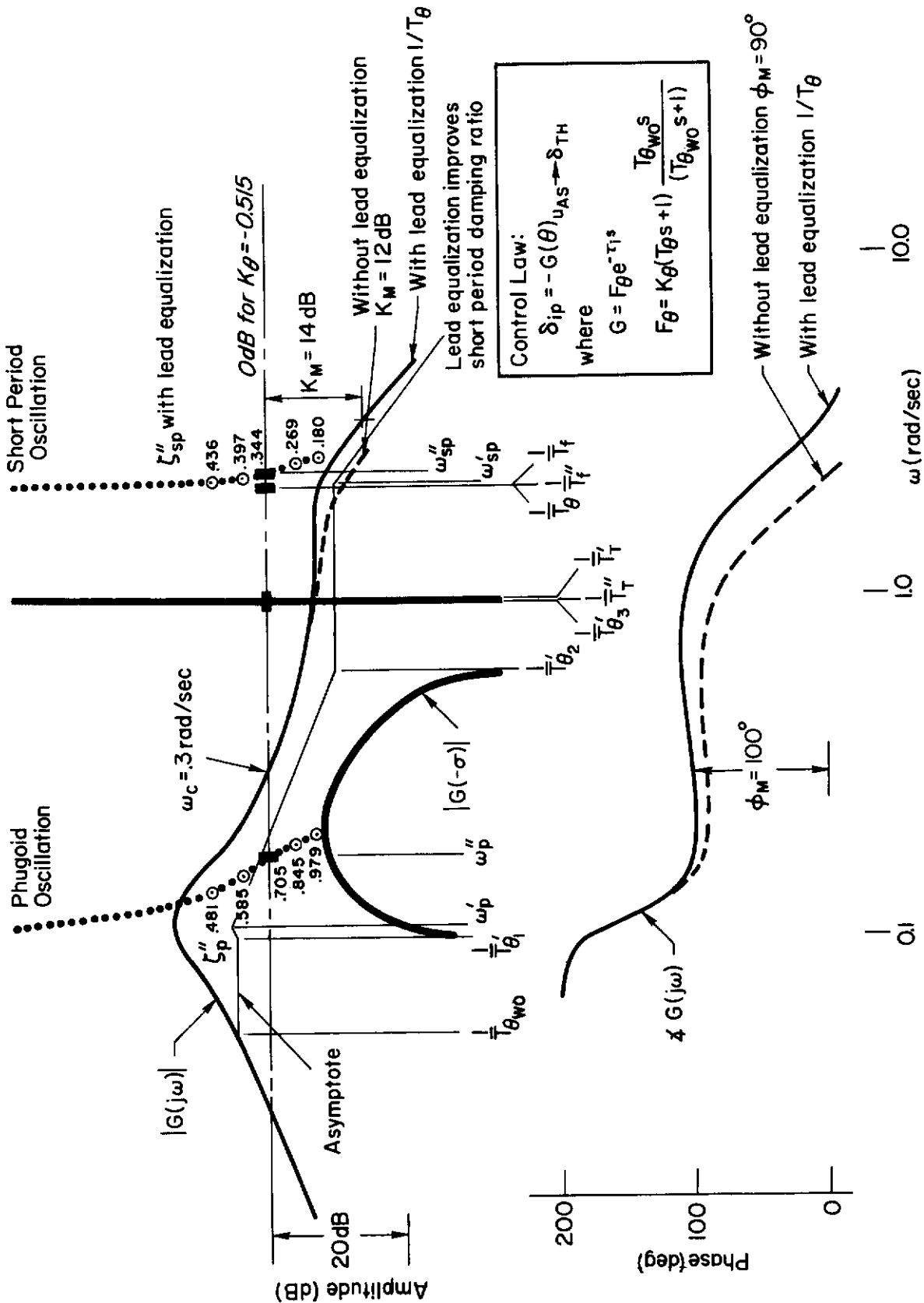
Figure 19. System Survey of Pitch Attitude Closure ($\theta \longrightarrow \delta_{ip}$) with a Manual Airspeed-to-Throttle Loop Closed for the A-7D Aircraft

149

reason that subsequent loop closures will have no beneficial effect on the short period damping ratio and all loops will be subject to variations in the pilot's gain and time delay.

A survey of the intermediate washed-out barometric vertical velocity loop closure to pitch command is shown in Fig. 20. The purpose of this feedback is to provide phugoid damping. The survey shows, however, that the inverse washout time constant $1/T_h^*$ must be on the order of $1/T_{h_1}^{\prime}$, the smallest zero in the vertical velocity response to a pitch command. This is about an order of magnitude smaller than the recommended value in Ref. 11. Since the vehicle pitch axis control system already has a command rate attentuation filter, $1/T_f$, the inclusion of another filter, $1/T_{\theta_c}$, in the flight director is actually redundant. The survey in Fig. 20 shows that $1/T_{\theta_c}$ cannot be much less than 1 rad/sec without negating the value of the vertical velocity feedback. A more desirable choice for $1/T_{\theta_c}$ would be 2 rad/sec (T_{θ_c} = 0.5 sec). The survey shows that such a choice would remove the real closed loop pole at 0.607 rad/sec, which will decrease in magnitude with increasing gain $-K_h$ and will further serve to depress the glide slope (outer) loop crossover frequency in the subsequent closure. However, we have selected $1/T_{\theta_c}$ = 1 rad/sec (T_{θ_c} = 1 sec) in Fig. 20 so as to illustrate how it compromises glide slope crossover frequency.

A survey of the outer glide slope displacement loop closure to vertical speed command is presented in Fig. 21. This shows that the cost of an adequate closed loop path-following (phugoid) damping ratio (0.353) must be paid for with a low crossover frequency, ω_c = 0.17 rad/sec, in the A-7D AN/CPU-80A flight director system.

D. MANUAL LATERAL APPROACH CONTROL IN THE A-7D

The next three surveys correspond to the A-7D flight director system block diagram for manual lateral displacement control in Fig. 10, Section III, with yaw rate and roll rate damping loops closed.

The survey of roll attitude feedback to manual aileron control is depicted in Fig. 22. Although the purpose of this closure is to regulate against upsets in roll attitude and to increase roll control

150

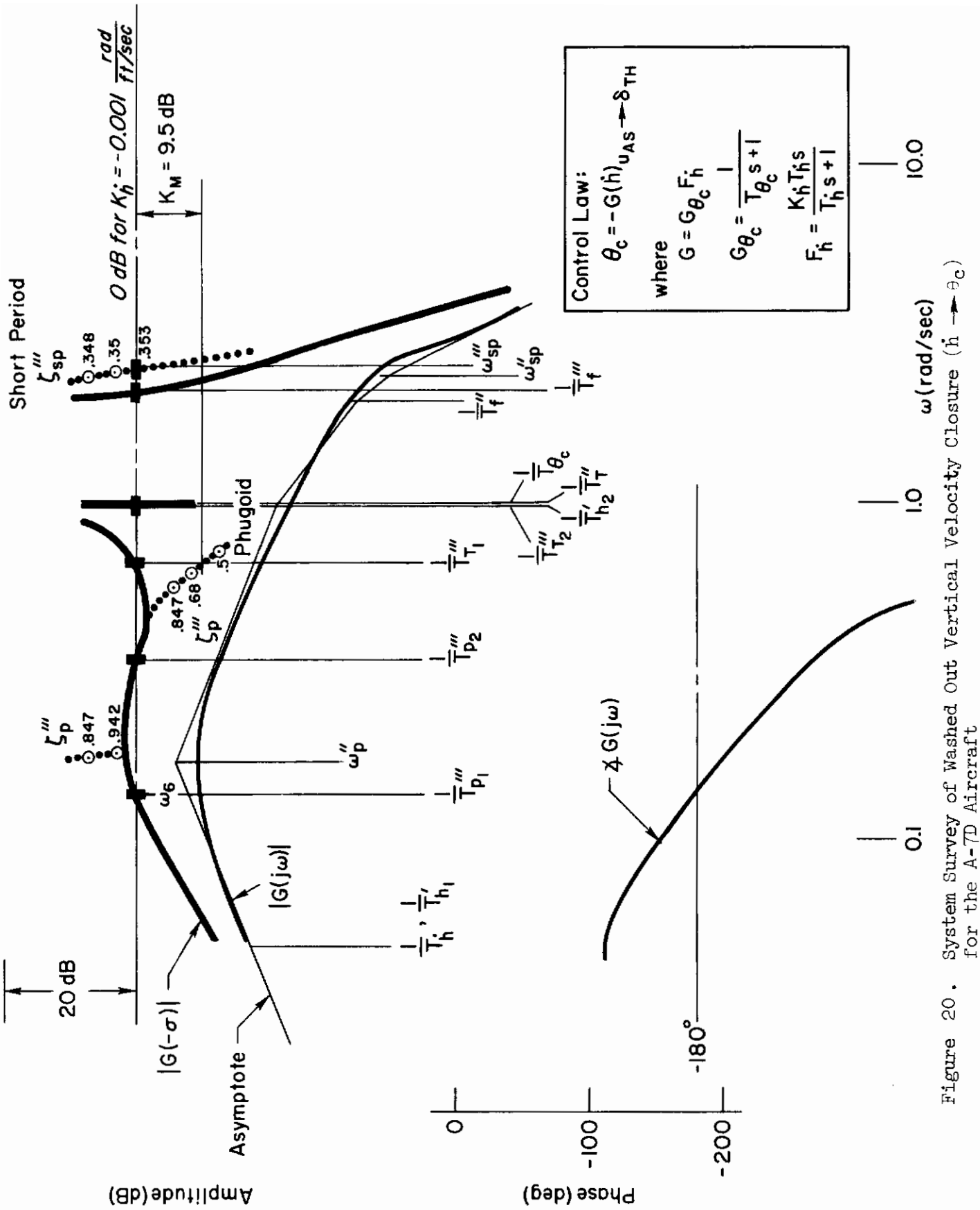Figure 20. System Survey of Washed Out Vertical Velocity Closure ($\dot{h} \longrightarrow \theta_c$) for the A-7D Aircraft

151

Figure 21. System Survey of Glide Slope Displacement Closure ($d \longrightarrow \dot{h}_c$) for the A-7D Aircraft

152

Control Law:

$$\delta_{a_p} = -G(\phi)_r \rightarrow \delta_r$$
$$p \rightarrow \delta_a$$

where

$$G = F_\phi e^{-\tau_a s}$$

$$F_\phi = K_\phi (T_\phi s + 1) \frac{T_{\phi_{wo}} s}{(T_{\phi_{wo}} s + 1)}$$

Figure 22. System Survey of Roll Attitude Closure ($\phi \rightarrow \delta_{ap}$) with Yaw and Roll Rate Dampers for the A-7D Aircraft

153

bandwidth so as to improve turning control bandwidth, neither purpose is fulfilled very well. This is because the A-7D primary lateral control system incorporates a first order lag $1/T_a$ of almost the same value as the rolling subsidence $1/T_R''$. Consequently, although it is not required by Ref. 11, roll attitude lead equalization has been incorporated in the flight director control law to salvage a well-damped roll control bandwidth of 1 rad/sec ($\omega_c = 0.6$ rad/sec).

The gain (or crossover frequency) of the washed-out heading closure to roll command is limited by the allowable decrease in damping of the roll oscillation, which also decreases in bandwidth to about 0.6 rad/sec (Fig. 23). The low roll and heading loop crossover frequencies augur a low lateral displacement loop crossover frequency ($\omega_c = 0.15$ rad/sec) in the survey of Fig. 24, with low frequency radio lead equalization supplied at one-half of the inverse heading washout time constant.

E. AUTOMATIC LONGITUDINAL APPROACH CONTROL IN THE DC-8

The next two system surveys correspond to an advanced windproof system for automatic pitch attitude and glide slope displacement control in the DC-8. This is illustrated in the block diagram, Fig. 7, Section III. Figure 25 shows a survey of the automatic washed-out pitch attitude loop closure through elevator control. The reciprocal washout time constant, $1/T_{wo}$, is selected in the neighborhood of $1/T_{\theta_2}$, the larger zero in the numerator of the pitch attitude-to-elevator transfer function. This assures nearly pure gain attitude feedback at the open loop short-period frequency so as to increase the closed loop short-period frequency. The addition of the attitude rate feedback signal to the washed-out attitude signal establishes the inverse lead equalization time constant $1/T_E$ somewhat above the open loop short-period frequency so as to assure a very good short-period damping ratio at unit gain crossover.

Although the phugoid frequency decreases in Fig. 25, the automatic glide slope displacement loop survey in Fig. 26 shows that a high closed loop path-following (modified phugoid) frequency can be recovered through second-order radio lead equalization in the outer loop closure. At very low frequencies in Fig. 26, the open loop system behaves as a

Figure 23. System Survey of Heading Closure ($\psi \longrightarrow \psi_c$) for the A-7D Aircraft
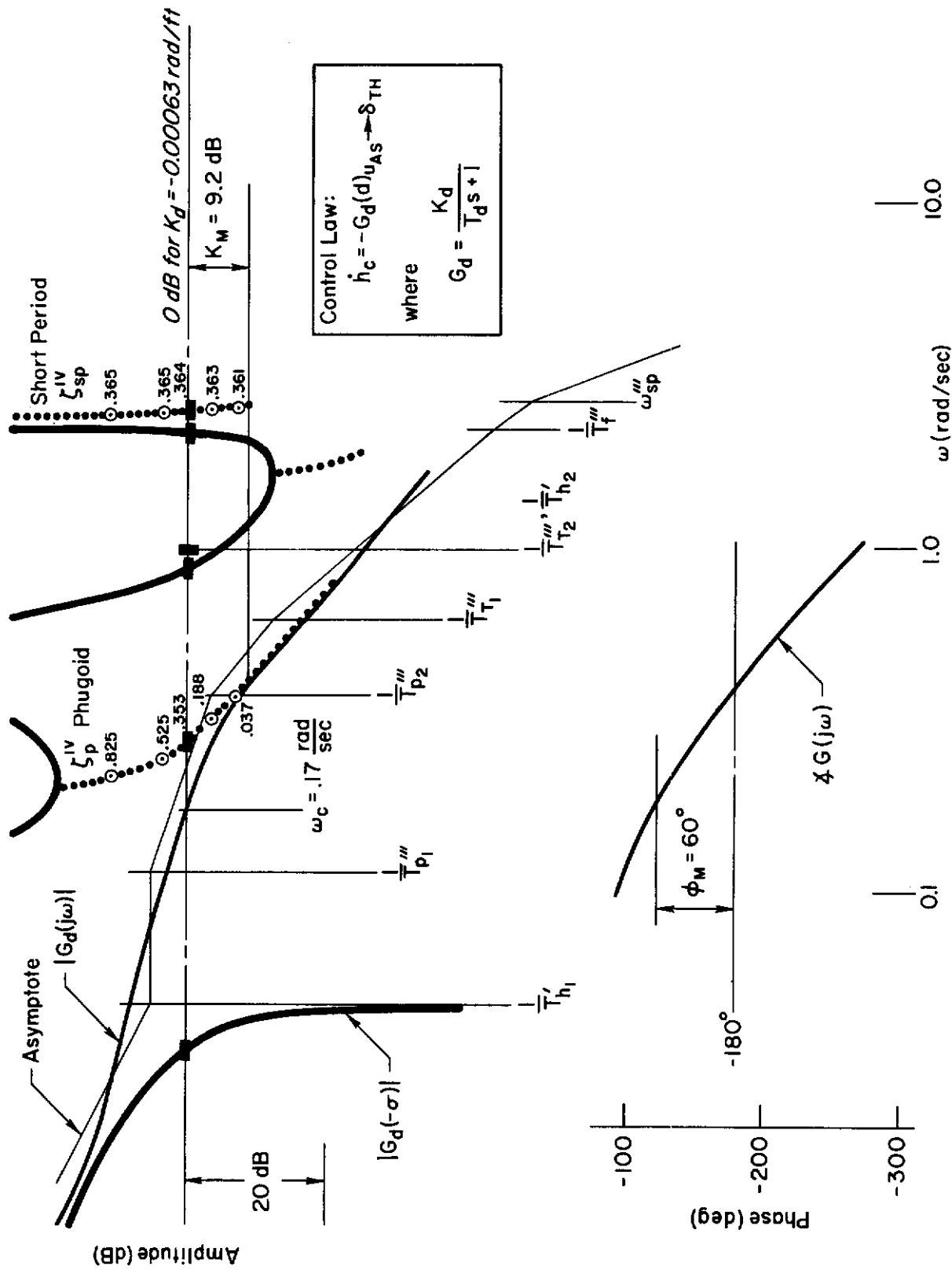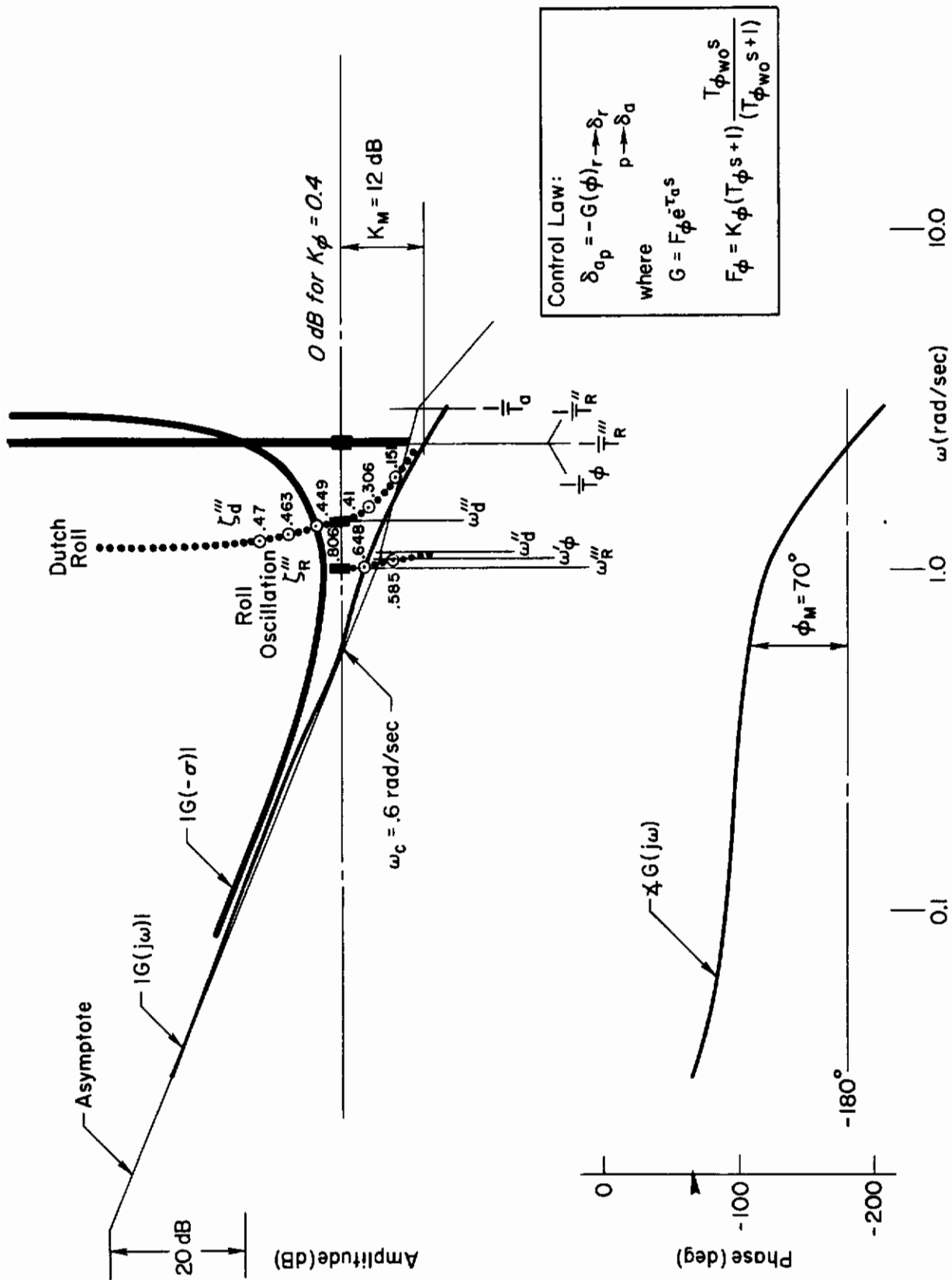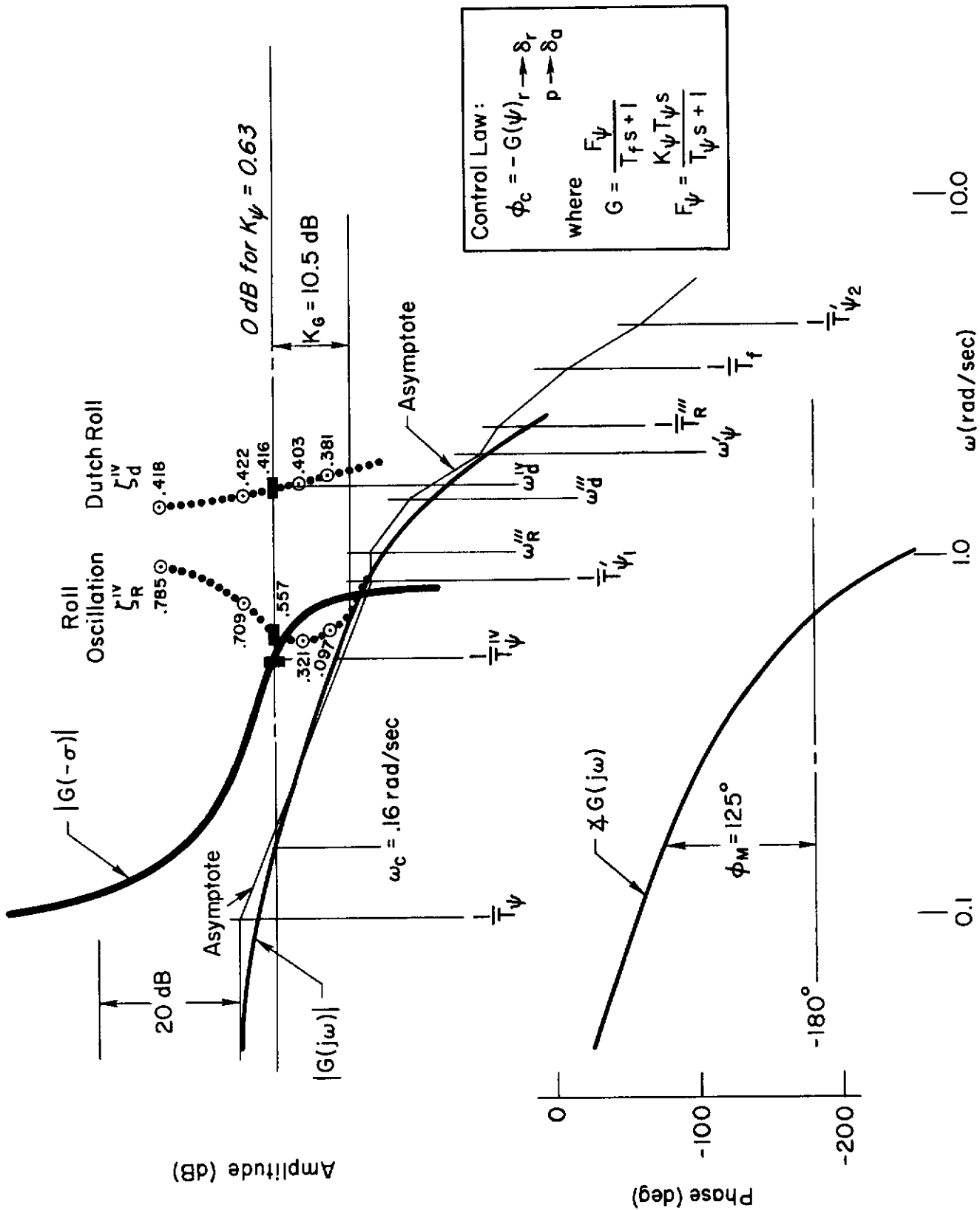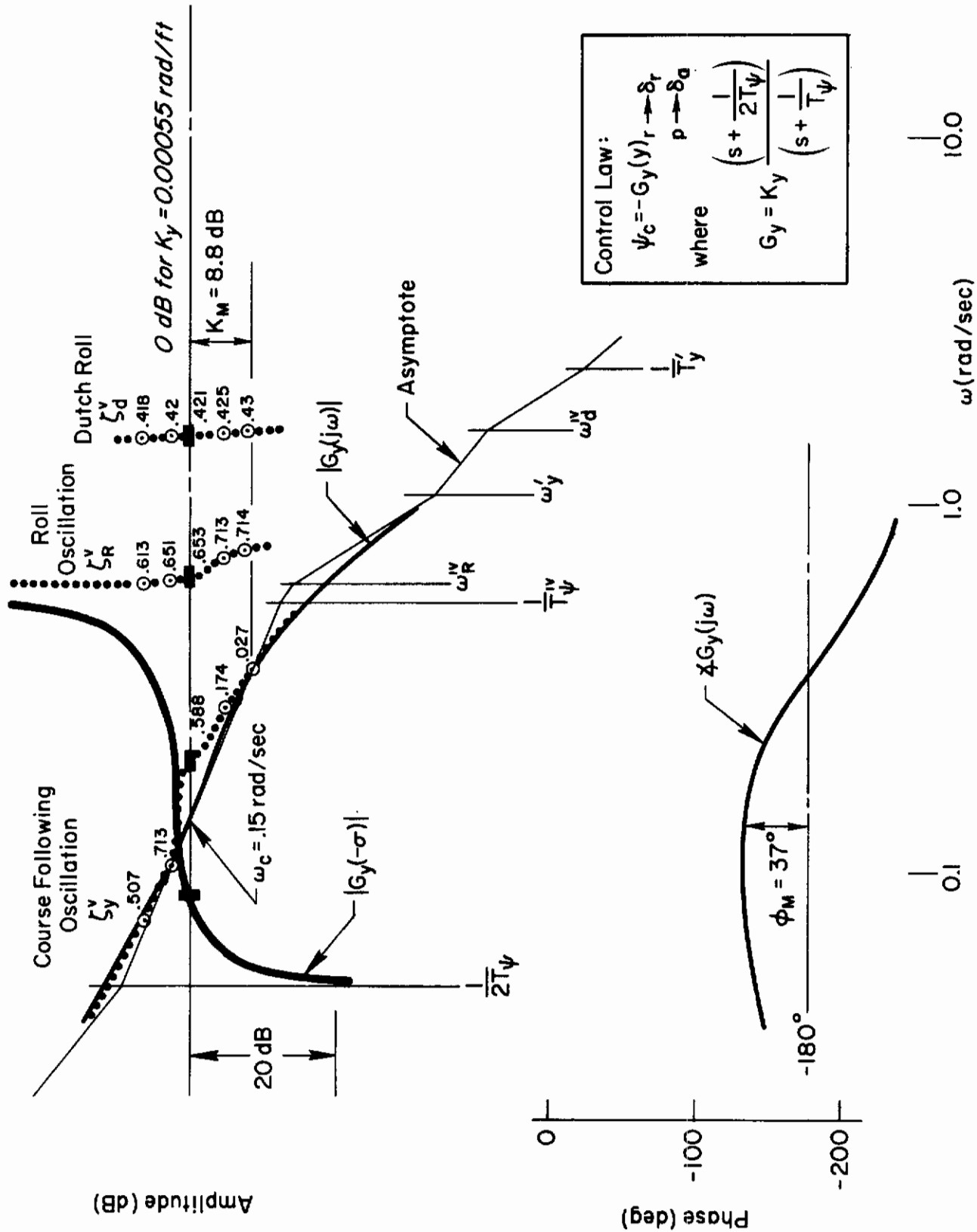
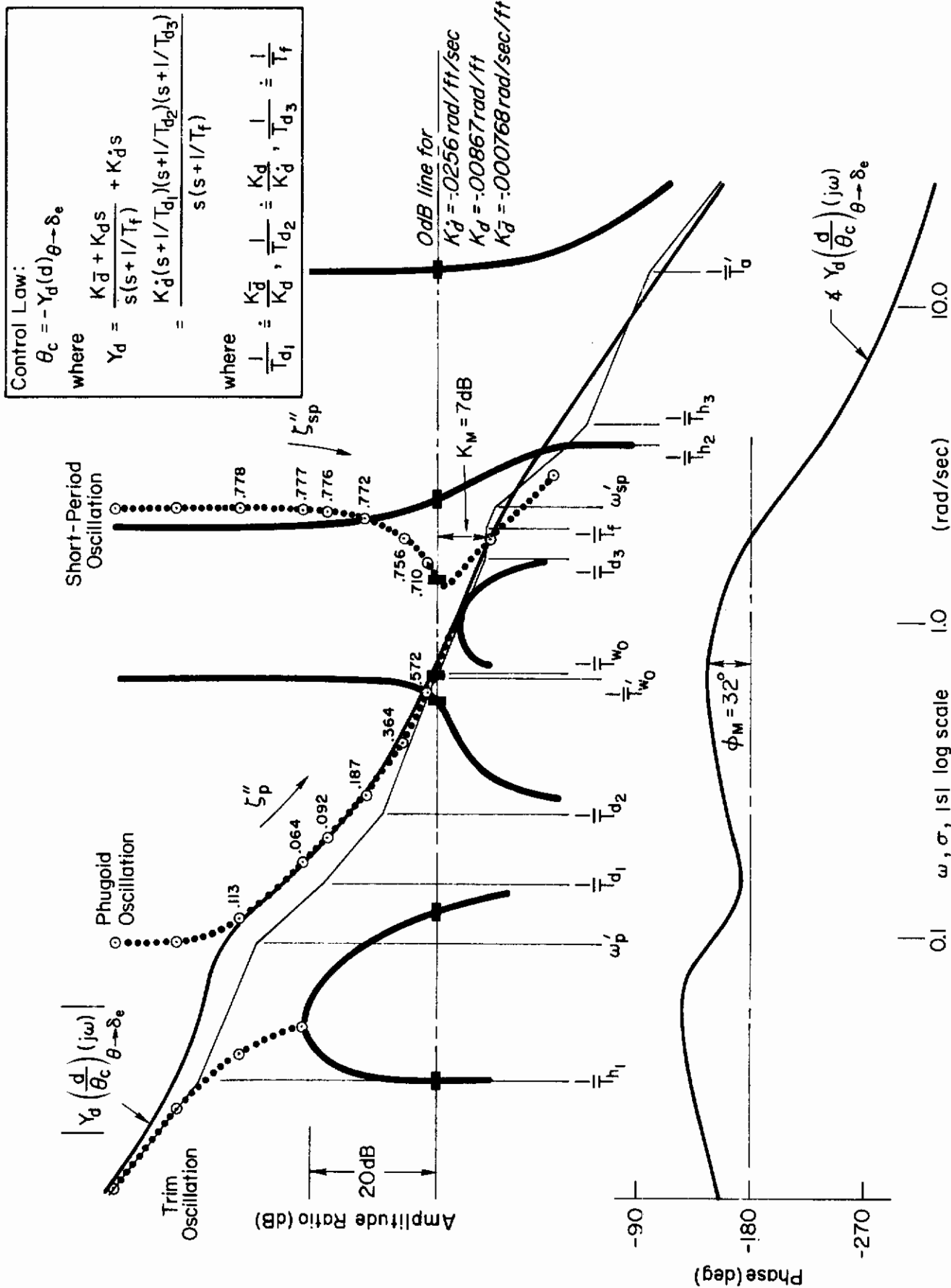Figure 24. System Survey of Lateral Displacement Closure ($y \rightarrow \psi_c$) for the A-7D Aircraft

Figure 25. System Survey for Pitch Attitude Loop Closure for DC-8 Automatic Approach

Figure 26. System Survey for Glide Slope Deviation Loop Closure for DC-8 Automatic Approach

158

double integrator (K/s^2) because of the integral bypass in the glide slope deviation controller. The path-following lead equalization adjustments are provided by $1/T_{d_1}$ and $1/T_{d_2}$. A crossover frequency corresponding to a maximum phase margin of about 32 deg is achieved at 0.75 rad/sec with a closed loop phugoid damping ratio of 0.66.

F. AUTOMATIC LATERAL APPROACH CONTROL IN THE DC-8

The remaining system surveys correspond to an advanced windproof system for automatic lateral-directional approach control in the DC-8. This is illustrated in the block diagram, Fig. 11, Section III. The survey of lateral acceleration feedback to the rudder in Fig. 27 shows why this loop closure is termed a "sideslip stability augmentor." Modest increases in both Dutch roll damping and frequency accompany the suitably chosen accelerometer location with a lead-lag frequency ratio of 1:10. The practical results are akin to those results which are theoretically possible with lead-lag equalization of sideslip angle feedback. Generous phase and gain margins have been adopted to avoid demanding excessive rudder authority.

The survey in Fig. 28 shows the loci of roll attitude response numerator <u>zeros</u> for aileron control with the sideslip augmentor coupling loop closed. This survey is included to illustrate its virtual identity to the one for the system <u>poles</u> in Fig. 27. This fact will insure the suppression of both the Dutch roll amplitude and the contribution of the actuator and accelerometer lag filter subsidences, in the rolling response to aileron inputs regardless of the accelerometer feedback gain chosen.

The survey of the roll attitude-to-aileron loop closure in Fig. 29 shows that a nearly ideal K/s controlled element can be created with a lead-lag equalization having a frequency ratio of about 1:4 from the rolling subsidence, $1/T_R'$, to the lag break frequency, $1/T_{L_\phi}$, at 5 rad/sec. A high roll crossover frequency ($\omega_c = 1.8$ rad/sec) with ample phase margin (60 deg) can be achieved to provide a well-damped roll control oscillation and good disturbance suppression bandwidth without requiring excessive aileron authority.

159
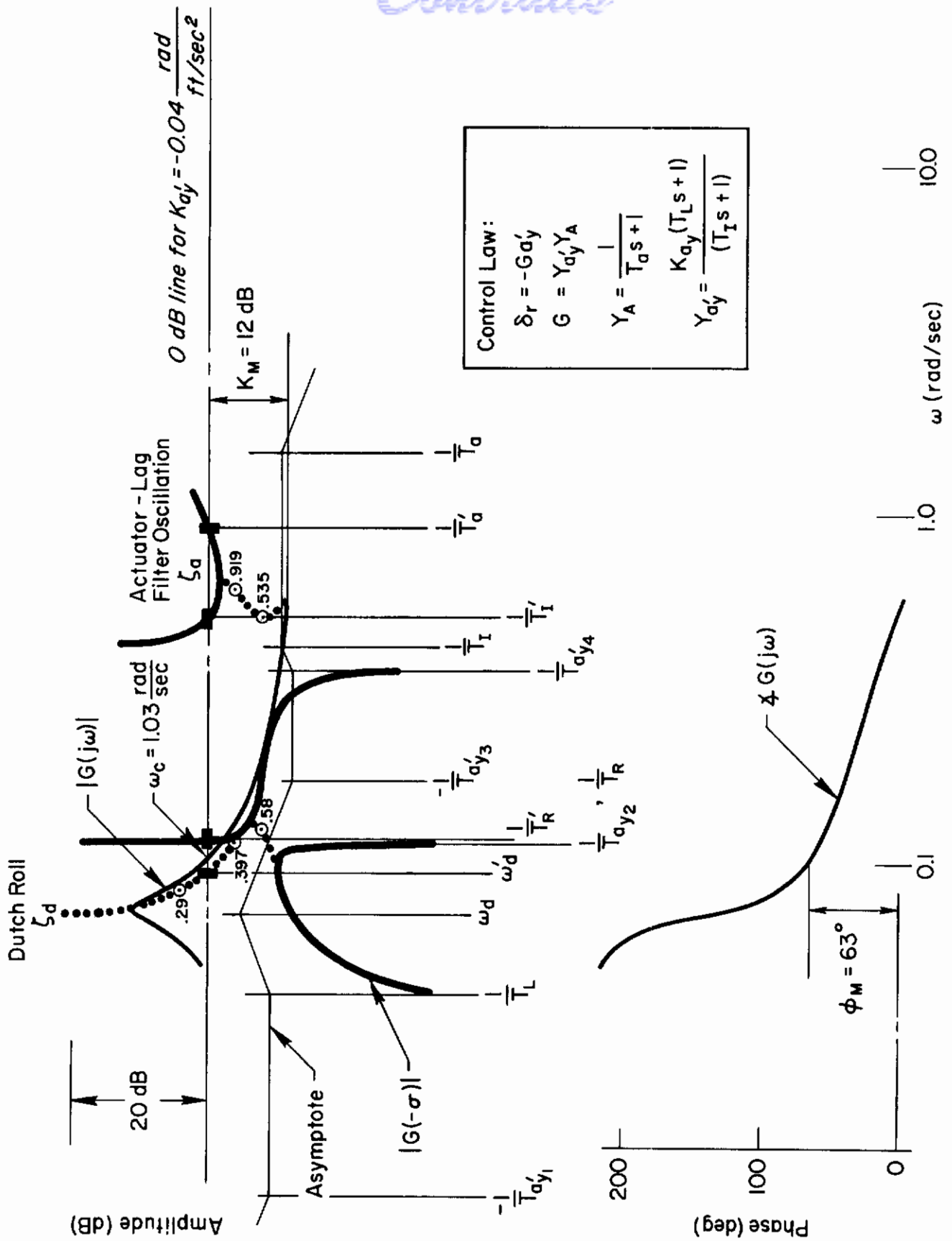
Figure 27. System Survey of DC-8 Sideslip Stability Augmentation $a_y' \longrightarrow \delta_r$ in Approach for Dutch Roll Damping and Lateral Windproofing

160

Figure 28. System Survey of the Closed-Loop Aileron-to-Roll Attitude Response
Numerator Zeros as a Function of the Sideslip Stability Augmentation
Feedback Gain for the DC-8 Automatic Lateral Approach Control

161
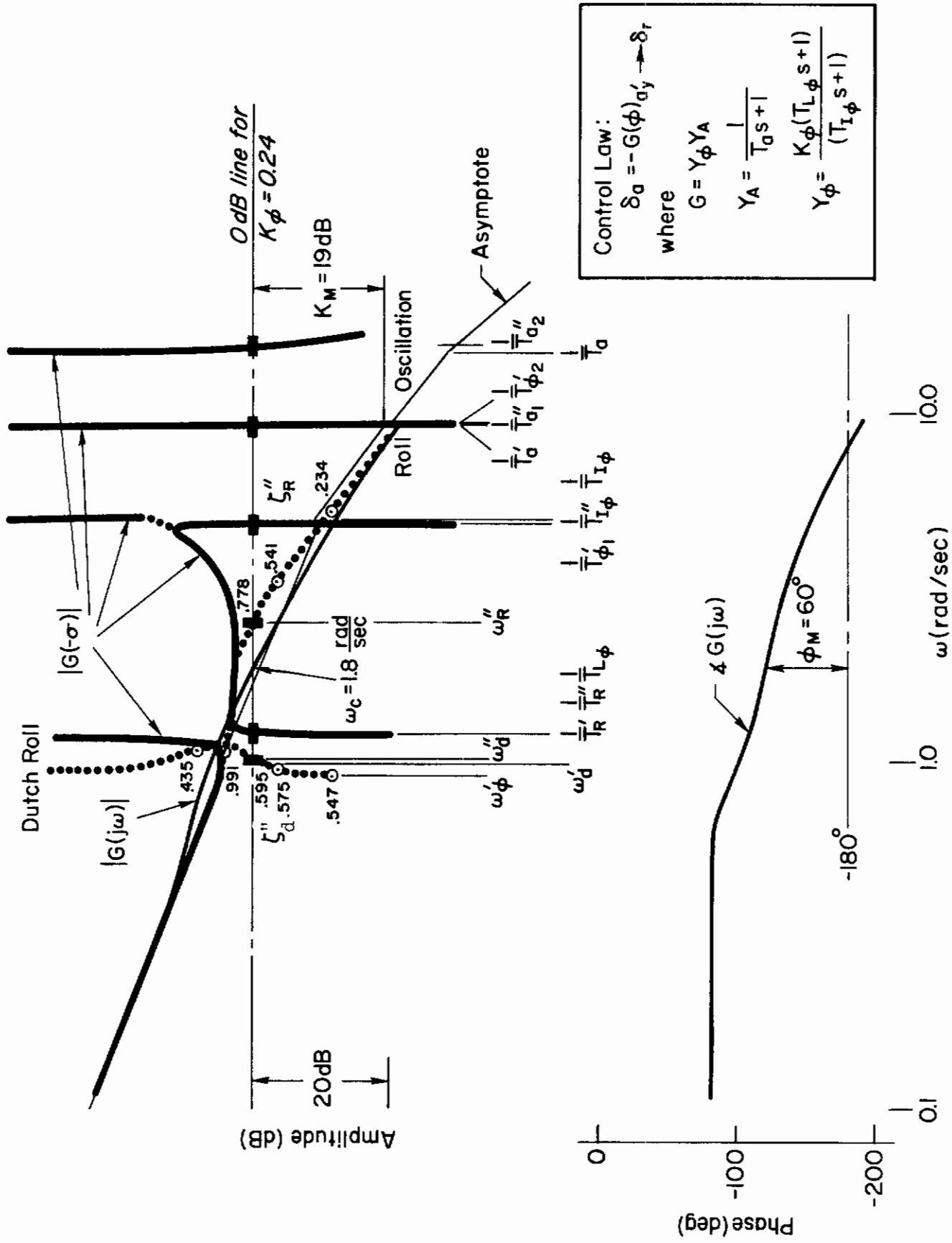
Figure 29 . System Survey of DC-8 Automatic Roll Attitude Control Loop in Approach

162

The concluding survey of the lateral displacement-to-roll command outer loop closure in Fig. 30 shows that an adequate crossover frequency of 0.235 rad/sec can be achieved corresponding to a maximum phase margin of 41 deg. At very low frequencies in Fig. 30, the open loop system behaves as a triple integrator (K/s^3) because of the integral bypass in the lateral displacement controller. The second-order course-following lead equalization adjustment is provided at the frequency ω_{L_y}. Both the very low frequency crosswind trim oscillation and the course-following oscillation are very well-damped with damping ratios of about 0.7.

OdB line for
$K_y = .0084 \, rad/ft$

$K_M = 16.34 \, dB$

Roll
Oscillation

$.77 \; \zeta_R'''$

.761

.754

.749

Course–
Following
Oscillation

Asymptote

$\dfrac{1}{T_f}$

ω_R''

ω (rad/sec)

$\dfrac{1}{T_{\dot y}}$
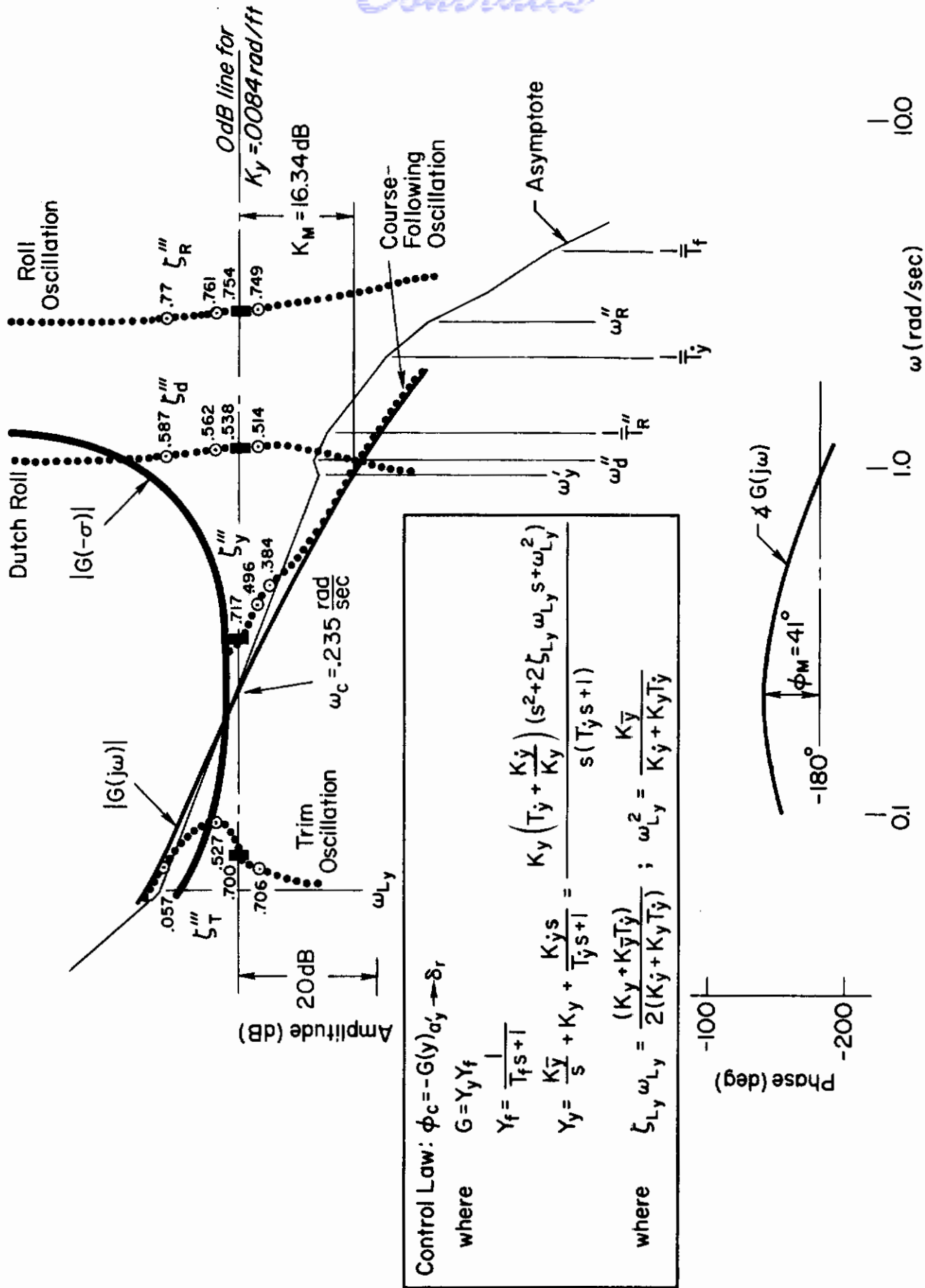
Dutch Roll

$.587 \; \zeta_d'''$

.562

.538

.514

$-\dfrac{1}{T_R''}$

$|G(-\sigma)|$

ω_y'

ω_d''

ζ_y'''

.717

.496

.384

$|G(j\omega)|$

$\omega_c = .235 \; \dfrac{rad}{sec}$

$\not< G(j\omega)$

$\phi_M = 41°$

$-180°$

.057 $\; \zeta_T'''$

.527

.700

.706

Trim
Oscillation

ω_{L_y}

20dB

Amplitude (dB)

Phase (deg)

-100

-200

Control Law: $\phi_c = -G(y)_{d_y} \longrightarrow \delta_r$

where $G = Y_y Y_f$

$Y_f = \dfrac{1}{T_f s + 1}$

$Y_y = \dfrac{K_{\bar y}}{s} + K_y + \dfrac{K_{\dot y} s}{T_{\dot y} s + 1} = \dfrac{K_y \left(T_{\dot y} + \dfrac{K_{\dot y}}{K_y} \right)(s^2 + 2\zeta_{L_y}\omega_{L_y}s + \omega_{L_y}^2)}{s(T_{\dot y}s + 1)}$

$\omega_{L_y}^2 = \dfrac{K_{\bar y}}{K_{\dot y} + K_y T_{\dot y}}$

where $\zeta_{L_y}\omega_{L_y} = \dfrac{(K_y + K_{\bar y}T_{\dot y})}{2(K_{\dot y} + K_y T_{\dot y})}$

Figure 30. System Survey of DC-8 Automatic Lateral Deviation Control Loop in Approach

164

APPENDIX C

EVALUATION OF THE COVARIANCE MATRIX
FOR STATIONARY PROCESSES

Efficient computation of the covariance matrix elements for stationary processes is required for the evaluation of TACLAND measuring system performance. This Appendix develops the necessary theory and the related computer program.

The development proceeds in several steps. First, the evaluation of a single element of the covariance matrix is expressed as the infinite time integral of the product of two deterministic time functions. These two deterministic time functions are simply the two impulse responses of the stationary process for the response variables of interest. Next, two different, algebraic methods for evaluating the infinite time integral of the product of the two time functions are given. The second method is then developed in detail in terms of the stationary process transfer function polynomial coefficients. Finally a computer program based on the second method, instructions for its use, and an example are given.

A. DETERMINISTIC EQUIVALENT OF COVARIANCE

Consider the ith and jth outputs of a stationary process forced by a single independent stochastic input, i. Furthermore, let the stochastic input be represented by filtered (shaped) unit white noise. The block diagram of Figure 31 depicts the system producing the ith and jth outputs, x_i and x_j, in response to a single independent stochastic input, i.

The impulse response of x_i at time t to a unit impulse in u applied τ seconds earlier is $f_i(\tau)$ where $f_i(\tau)$ is simply the inverse Laplace transform of $F_1(s) F_0(s)$. Similarly, the impulse response of x_j is $f_j(\tau)$.

The covariance of the ith and jth outputs is given by the expectation of the product, $x_i(t)x_j(t)$, or $E\left[x_i(t)x_j(t)\right]$. Since the process is stationary, $E\left[x_i(t)x_j(t)\right]$ is invariant with time and may be expressed in terms of the impulse response functions, $f_i(\tau)$ and $f_j(\tau)$ and the unit white noise input, u, by using the convolution integral. The result is:
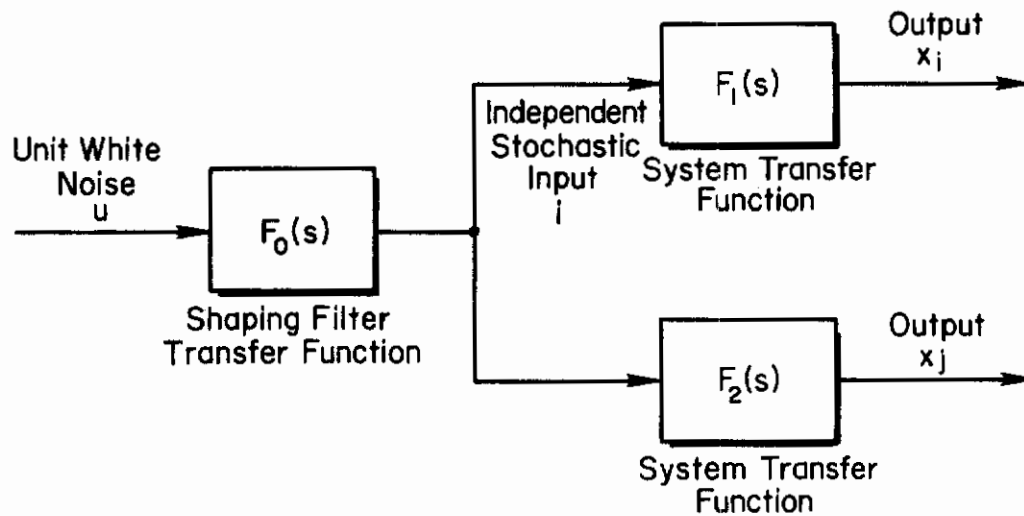
165

Figure 31. Block Diagram of Stationary Process
Having Outputs x_i and x_j in Response to Input i

$$E\left[x_i(t)x_j(t)\right] = E\left[\int_0^\infty d\tau_1 f_i(\tau_1)u(t-\tau_1)\int_0^\infty d\tau_2 f_j(\tau_2)u(t-\tau_2)\right] \quad (C-1)$$

Because $u(t-\tau_1)$ is not a function of τ_2, it may be moved under the second integral. Then the first integral is a function of the second integral. Also, since $f_i(\tau)$ and $f_j(\tau)$ are deterministic functions, the expectation may be taken within the integrals. That is, the right hand side of Eq C-1 becomes:

$$\int_0^\infty d\tau_1 f_i(\tau_1)\int_0^\infty d\tau_2 f_j(\tau_2)E\left[u(t-\tau_1)u(t-\tau_2)\right]$$

166

However, $E\left[u(t-\tau_1)u(t-\tau_2)\right]$ is an expression for the autocorrelation function for unit white noise. This autocorrelation function is a unit impulse which occurs for $\tau_2 = \tau_1$. It is denoted by $\delta(\tau_2-\tau_1)$. (Recall that the autocorrelation function for unit white noise is a unit impulse because, by definition, the unit white noise signal at any time, t_1, is uncorrelated with the unit white noise signal at every other instant of time, $t \neq t_1$.) The second integral can then be evaluated:

$$\int_0^\infty d\tau_2 f_j(\tau_2)\delta(\tau_2-\tau_1) = f_j(\tau_1) \qquad\qquad \text{(C-2)}$$

Equation C-1 can then be expressed as

$$E\left[x_i(t)x_j(t)\right] = \int_0^\infty f_i(\tau_1)f_j(\tau_1)d\tau_1 = I_{ij} \qquad\qquad \text{(C-3)}$$

where, for brevity, we denote $E\left[x_i(t)x_j(t)\right]$ by I_{ij}. The final step is to make the change of variable, $\tau_1 = t$. Then

$$I_{ij} = \int_0^\infty f_i(t)\ f_j(t)\ dt \qquad\qquad \text{(C-4)}$$

where $f_i(t)$ is now interpreted to be the impulse response at time, t, to a unit impulse applied at time, $t = 0$, and similarly for $f_j(t)$.

Consequently I_{ij} is the infinite time integral of the product of two deterministic functions of time. This, of course, is the result sought at the outset in this subsection. The next subsection will consider two ways to evaluate this integral by purely algebraic means.

B. ANALYTICAL EVALUATION OF THE INTEGRAL OF THE PRODUCT OF TWO TIME FUNCTIONS

Consider two stable functions of positive time, $f_i(t)$ and $f_j(t)$, and their Laplace transforms, $F_i(s)$ and $F_j(s)$, respectively, and the integral of interest:

$$I_{ij} = \int_0^\infty f_i(t)\, f_j(t)\, dt \qquad (C\text{-}5)$$

If $F_i(s)$ and $F_j(s)$ are proper rational fractions, it is well known (Appendix A of Ref. 38) that

$$\mathcal{L}\left[f_i(t)\, f_j(t)\right] = \sum \begin{bmatrix} \text{residues of } F_i(w)\, F_j(s\text{-}w) \\ \text{at the poles of } F_i(w) \end{bmatrix} \qquad (C\text{-}6)$$

Using the final value theorem, Eq C-5 can be written

$$I_{ij} = \sum \begin{bmatrix} \text{residues of } F_i(w)\, F_j(\text{-}w) \\ \text{at the poles of } F_i(w) \end{bmatrix} \qquad (C\text{-}7)$$

or alternately in the notation used in solving the Weiner-Hopf equation in the frequency domain:

$$I_{ij} = \sum \text{ of residues of } \left[F_i(s)\, F_j(\text{-}s)\right]_+ \qquad (C\text{-}8)$$

Equation C-8 is, however, not necessarily the most efficient way to proceed in view of existing algorithms when numerical computations are involved. It is shown in Newton, Gould and Kaiser (Ref. 28, Appendix E) that a change in variable and the properties of the inverse Laplace transform at $t = 0$ and of the limit of the inverse Laplace transform as $t \to 0$ reduce the expression for the integral to simple forms.

Let $F_i(s)$ have the denominator polynomial $d(s)$ of order n and $F_j(s)$ the denominator $c(s)$ of order m. Now from Ref. 28

$$I_{ij} = \frac{1}{2\pi j} \int_{-j\infty}^{j\infty} F_i(s)\, F_j(\text{-}s)\, ds \qquad (C\text{-}9)$$

168

$$I_{ij} = \frac{1}{2\pi j} \int_{-j\infty}^{j\infty} \left[\frac{a(s)}{d(s)} + \frac{b(-s)}{c(-s)} \right] ds \qquad \text{(C-10)}$$

where the quantity in the square brackets is an alternative expression for $F_i(s)\, F_j(-s)$. Continuing, using a change of variable in the second term:

$$I_{ij} = \frac{1}{2\pi j} \int_{-j\infty}^{j\infty} \frac{a(s)}{d(s)}\, ds + \frac{1}{2\pi j} \int_{-j\infty}^{j\infty} \frac{b(s)}{c(s)}\, ds \qquad \text{(C-11)}$$

Equation C-11 expresses the inverse Laplace transforms of $a(s)/d(s)$ and $b(s)/c(s)$ evaluated at $t = 0$. Because at $t = 0$ the inverse Laplace transform is one-half of the limit of the inverse Laplace transform as $t \to 0$ the value of the integral, I_{ij}, is given by the initial-value theorem as

$$I_{ij} = \mathcal{L}^{-1}\left[\frac{a(s)}{d(s)} \right]_{t=0} + \mathcal{L}^{-1}\left[\frac{b(s)}{c(s)} \right]_{t=0} \qquad \text{(C-12)}$$

$$I_{ij} = \frac{1}{2} \lim_{t \to 0} \mathcal{L}^{-1}\left[\frac{a(s)}{d(s)} \right] + \frac{1}{2} \lim_{t \to 0} \mathcal{L}^{-1}\left[\frac{b(s)}{c(s)} \right] \qquad \text{(C-13)}$$

$$I_{ij} = \frac{1}{2} \lim_{s \to \infty} \left[\frac{s\, a(s)}{d(s)} \right] + \frac{1}{2} \lim_{s \to \infty} \left[\frac{s\, b(s)}{c(s)} \right] \qquad \text{(C-14)}$$

$$I_{ij} = \frac{a_{n-1}\, c_m + b_{m-1}\, d_n}{2\, d_n\, c_m} \qquad \text{(C-15)}$$

where d_n is the coefficient of s^n in $d(s)$, etc. If the numerator polynomials of $F_i(s)$ and $F_j(s)$ are $g(s)$ of order p and $h(s)$ is of order q, then

$$a(s)\, c(-s) + b(-s)\, d(s) = g(s)\, h(-s) \qquad \text{(C-16)}$$

169

and the objective is to solve for a_{n-1} and b_{m-1} given $c(s)$, $d(s)$, $g(s)$ and $h(s)$. Following Shipley's approach for solving problems of this type (Ref. 39):

$$
\begin{bmatrix}
c_0 & 0 & \cdots & 0 \\
\cdot & c_0 & & \cdot \\
\cdot & \cdot & & \cdot \\
\cdot & \cdot & & 0 \\
(-1)^m c_m & \cdot & & c_0 \\
0 & (-1)^m c_m & & \cdot \\
\cdot & \cdot & 0 & \cdot \\
\cdot & \cdot & & (-1)^m c_m
\end{bmatrix}
\begin{Bmatrix}
a_0 \\ \cdot \\ \cdot \\ \cdot \\ \cdot \\ \cdot \\ \cdot \\ a_{n-1}
\end{Bmatrix}
$$

$$(m+n) \times n$$

$$
+ \begin{bmatrix}
d_0 & 0 & \cdots & 0 \\
\cdot & d_0 & & \cdot \\
\cdot & \cdot & & \cdot \\
\cdot & \cdot & & 0 \\
d_n & \cdot & & d_0 \\
0 & d_n & & \cdot \\
\cdot & 0 & & \cdot \\
\cdot & \cdot & & \cdot \\
\cdot & \cdot & & d_n
\end{bmatrix}
\begin{Bmatrix}
b_0 \\ \cdot \\ \cdot \\ \cdot \\ \cdot \\ \cdot \\ \cdot \\ (-1)^{m-1} b_{m-1}
\end{Bmatrix}
\qquad \text{(C-17)}
$$

$$(m+n) \times m$$

$$
= \begin{bmatrix}
g_0 & 0 & \cdots & 0 \\
\cdot & g_0 & & \cdot \\
\cdot & \cdot & & \cdot \\
\cdot & \cdot & & 0 \\
g_p & \cdot & & g_0 \\
0 & g_p & & \cdot \\
\cdot & 0 & & \cdot \\
\cdot & \cdot & & \cdot \\
0 & 0 & & g_p \\
0 & 0 & \cdots & 0 \\
\cdot & \cdot & & \cdot \\
0 & 0 & \cdots & 0
\end{bmatrix}
\begin{Bmatrix}
h_0 \\ \cdot \\ \cdot \\ \cdot \\ \cdot \\ \cdot \\ \cdot \\ \cdot \\ \cdot \\ (-1)^q h_q
\end{Bmatrix}
= \begin{Bmatrix}
g_0^* \\ \cdot \\ \cdot \\ \cdot \\ \cdot \\ g_p^* \\ 0 \\ \cdot \\ 0
\end{Bmatrix}
$$

$$(m+n) \times (q+1)$$

170

The matrix or vector on the right hand side of Eq C-17 must be augmented with $(m+n-p-q-1)$ rows of zeros so that the orders of the alternate expressions for the numerator of $F_i(s)$ $F_j(-s)$ are comparable (i.e., when Eq C-17 is pre-multiplied through by $s^0 \ldots s^{m+n-1}$). Equation C-17 can be rewritten in vector-matrix form as

$$C\,a + D\,b = G\,h = g^* \qquad (C\text{-}18)$$

using the obvious definitions for the symbols. Consequently,

$$\underset{(m+n)\times(m+n)}{\begin{bmatrix} C & \vdots & D \end{bmatrix}} \; \underset{(m+n)\times 1}{\left\{ \frac{a}{b} \right\}} = \underset{(m+n)\times(q+1)}{G} \; \underset{(q+1)\times 1}{h} = \underset{(m+n)\times 1}{g^*} \qquad (C\text{-}19)$$

and Cramer's rule gives

$$a_{n-1} = \frac{\det\begin{bmatrix} C_a & \vdots & D \end{bmatrix}}{\det\begin{bmatrix} C & \vdots & D \end{bmatrix}} \qquad (C\text{-}20)$$

$$b_{m-1} = \frac{\det\begin{bmatrix} C & \vdots & D_b \end{bmatrix}}{\det\begin{bmatrix} C & \vdots & D \end{bmatrix}} \qquad (C\text{-}21)$$

where

$$C_a = \begin{bmatrix} c_0 & 0 & \cdots & 0 & g_0^* \\ \cdot & & c_0 & & \cdot \\ \cdot & & \cdot & & \cdot \\ \cdot & & \cdot & & \cdot \\ (-1)^m c_m & & \cdot & & g_p^* \\ 0 & & (-1)^m c_m & & 0 \\ \cdot & & 0 & & \cdot \\ \cdot & & \cdot \; \cdot & & \cdot \\ \cdot & & \cdot & & \cdot \end{bmatrix} \qquad (C\text{-}22)$$

$$(m+n)\times n$$

and

$$D_o = \begin{bmatrix} d_o & 0 & \cdots & 0 & g_o^* \\ \cdot & d_o & & & \cdot \\ \cdot & \cdot & & & \cdot \\ \cdot & \cdot & & & \cdot \\ d_n & \cdot & & & \cdot \\ 0 & d_n & & & g_p^* \\ \cdot & 0 & & & 0 \\ \cdot & \cdot & & & \cdot \\ \cdot & \cdot & & & \cdot \\ \cdot & \cdot & & & \cdot \end{bmatrix}_{(m+n) \times n}$$

(C-23)

Since this is the algorithm used for numerical calculation via the Phillips' integrals (see Eq E.1-19, p. 370, Ref. 28), creation of a program for evaluation if I_{ij} via Eq C-15 and C-20 through C-23 should be reasonably straightforward.

This would be the traditional way, and indeed, it was the way we chose to proceed.

When the overall systems analysis problem is considered, however, one must take into account the fact that the eigenvalues of $d(s)$ and $c(s)$ will often have been calculated for other purposes. This fact would make evaluation if I_{ij} via the sum of residues method (Eq C-8) quite appealing since a modal response coefficient calculation subroutine could doubtless be made a part of the systems analysis package. The best approach would probably include both methods. The evaluation could then be branched to one technique or the other depending upon whether or not the required eigenvalues were available from previous calculations.

C. PROGRAM FOR EVALUATING COVARIANCE

Evaluation of a single element of the covariance matrix is to be accomplished using Eq C-15 and C-20 through C-23 of the previous subsection. The program implementing these equations is written in Super Basic language for use on the Tymshare computer system (Ref. 40).

172

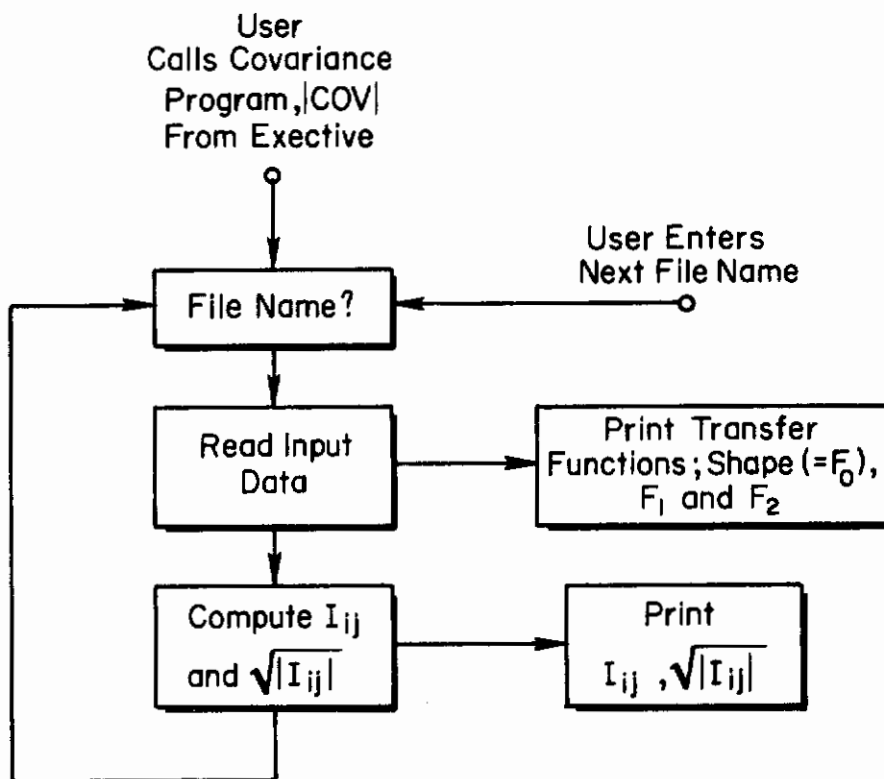A flow diagram for this program is given in Fig. 32. The program

Figure 32. Covariance Program Flow Diagram

listing is displayed in Table XXXVI. (The binary version of this program is here assumed to be stored in the file named /COV/.)

1. Program Use

Prepare one input data field for the three transfer functions necessary for computation of each covariance desired. The format for this data field is given below.

Each of the three transfer functions must be of the form,

TABLE XXXVI

LISTING FOR COVARIANCE PROGRAM

```
5    PRINT

10 PRINT "FILE NAME"

15   DIM Z(15),P(15),Z$(15,2),P$(15,2),A(-2:35)

20   BASE 0

25 INPUT  F

30 DIM T(35),B(35),F(35),F$(35),C(35),C$(35),H(35),
H$(35),G(35),G$(35)

35   K=0

40 OPEN F,INPUT,1

45   INPUT FROM 1:K1,Z1,Z2,P1,P2

50   FOR I=1 TO 15

55   Z(I),P(I),Z$(I,1),Z$(I,2),P$(I,1),P$(I,2)=0

60   NEXT I

65 IF Z1=0 THEN 85

70FOR I=1 TO Z1

75INPUT FROM 1: Z(I)

80NEXT I

85IF Z2=0 THEN 105

90FOR I=1 TO Z2

95INPUT FROM 1: Z$(I,1),Z$(I,2)

100NEXT I

105IF P1=0 THEN 125

110FOR I=1 TO P1

115INPUT FROM 1: P(I)

120NEXT I

125IF P2=0 THEN 145

130FOR I=1 TO P2

135INPUT FROM 1: P$(I,1),P$(I,2)
```

(cont'd)

TABLE XXXVI (cont'd)

```
140 NEXT I

145 K=K+1

150 GOSUB 595

155 GOSUB 735

160 IF K=1 THEN 175

165 IF K=2 THEN 225

170 IF K=3 THEN 275

175 N2=N1,D2=D1

180 FOR I=0 TO N2

185 F(I)=T(I)

190 T(I)=0

195 NEXT I

200 FOR I=0 TO D2

205 F$(I)=B(I)

210 B(I)=0

215 NEXT I

220 GO TO 45

225 N3=N1,D3=D1

230 FOR I=0 TO N3

235 C(I)=T(I)

240 T(I)=0

245 NEXT I

250 FOR I=0 TO D3

255 C$(I)=B(I)

260 B(I)=0

265 NEXT I

270 GO TO 45

275 FOR I=0 TO N2+N3
```

TABLE XXXVI (cont'd)

```
280H(I)=0

285IF I-N3>=0 THEN J1=I-N3 ELSE J1=0

290IF N2<=I THEN J2=N2 ELSE J2=I

295FOR J=J1 TOJ2

300H(I)=H(I)+F(J)*C(I-J)

305NEXT J,I

310FOR I=0 TO D2+D3

315H$(I)=0

320IF I-D3>=0 THEN J1=I-D3 ELSE J1=0

325IF D2<=I THEN J2=D2 ELSE J2=I

330FOR J=J1 TO J2

335H$(I)=H$(I)+F$(J)*C$(I-J)

340NEXT J,I

345N3=N3+N2

350D3=D3+D2

355FOR I=0 TO N2+N1

360G(I)=0

365IF I-N1>=0 THEN J1=I-N1 ELSE J1=0

370IF N2<=I THEN J2=N2 ELSE J2=I

375FOR J=J1 TO J2

380G(I)=G(I)+F(J)*T(I-J)

385NEXT J,I

390FOR I=0 TO D2+D1

395G$(I)=0

400IF I-D1>=0 THEN J1=I-D1 ELSE J1=0

405IF D2<=I THEN J2=D2 ELSE J2=I

410FOR J=J1 TO J2

415G$(I)=G$(I)+F$(J)*B(I-J)
```

TABLE XXXVI (cont'd)

```
420 NEXT J,I

425 N1=N1+N2,D1=D1+D2

430 IF N1>D1 THEN GO TO 585

435 IF N3>D3 THEN GO TO 585

440 BASE 1

445 VAR =ZERO

450 DIM A$(D1+D3,D1+D3),B$(D1+D3,N3+1),D(N3+1,1),E$(D1+D3,1
),S$(D1+D3,1)

455 FOR J=1 TO D1

460 FOR I=J TO D3+J

465 A$(I,J)=(-1)↑(I-J)*H$(I-J)

470 NEXT I,J

475 FOR J=D1+1 TO D1+D3

480 FOR I=J-D1 TO J

485 A$(I,J)=G$(I-J+D1)

490 NEXT I,J

495 FOR J=1 TO N3+1

500 D(J,1)=(-1)↑(J+1)*H(J-1)

505 FOR I=J TO N1+J

510 B$(I,J)=G(I-J)

515 NEXT I,J

520 MATE$=B$*D

525 MAT A$=INV(A$)

530 MAT S$=A$*E$

535 I=.5*(S$(D1,1)/G$(D1)+(-1)↑(D3-1)*S$(D1+D3,1)/H$(D3))

540 PRINT

545 PRINT

550 PRINT "COVARIANCE      =";I                    (cont'd)
```

TABLE XXXVI (cont'd)

```
555 PRINT

560 PRINT

565 PRINT "ABSV SQ RT COV =";SQR(ABS(I))

570 PRINT

575 CLOSE 1

580 GO TO 5

585 PRINT"NUMERATOR GREATER THEN DENOMINATOR"

590 GO TO 5

595PRINT

600PRINT

605IF K=1 THEN PRINT " TRANSFER FUNCTION SHAPE"

610IF K=2 THEN PRINT"TRANSFER FUNCTION F1"

615IF K=3 THEN PRINT "TRANSFER FUNCTION  F2"

620PRINT

625PRINT "  GAIN = ";K1

630IF Z1=0 THEN 655

635FOR I=1 TO Z1

640PRINT

645PRINT " Z(";I;") = ";Z(I)

650NEXT I

655IF Z2=0 THEN 680

660FOR I=1 TO Z2

665PRINT

670PRINT " ZDR(";I;") =";Z$(I,1);"ZNF(";I;") =";Z$(I,2)

675NEXT I

680IF P1=0 THEN 705

685FOR I=1 TO P1

690PRINT
```

(cont'd)

TABLE XXXVI (cont'd)

```
695PRINT "P(";I;") = ";P(I)

700NEXT I

705IF P2=0 THEN 730

710FOR I=1 TO P2

715PRINT

720PRINT " PDR(";I;") = ";P$(I,1);" PNF(";I;") = ";P$(I,2)

725NEXT I

730RETURN

735FOR I=-2 TO 35

740A(I)=0

745NEXT I

750A(0)=K1

755IF Z1=0 THEN 780

760FOR I=1 TO Z1

765FOR J=I TO 0 STEP -1

770A(J)=Z(I)*A(J)+A(J-1)

775NEXT J,I

780IF Z2=0THEN 805

785FOR I=1 TOZ2

790FOR J=Z1+2*Z2 TO 0 STEP -1

795A(J)=Z$(I,2)*(Z$(I,2)*A(J)+2*Z$(I,1)*A(J-1))+A(J-2)

800NEXT J,I

805FOR I=0 TO Z1+2*Z2

810T(I)=A(I)

815A(I)=0

820NEXT I

825A(0)=1

830 IF P1=0 THEN 855
```

(cont'd)

TABLE XXXVI (concluded)

```
835 FOR I=1 TO P1

840FOR J=I TO 0 STEP -1

845A(J)=A(J)*P(I)+A(J-1)

850NEXT J,I

855IF P2=0 THEN 880

860FOR I=1 TO P2

865FOR J=P1+2*I TO 0 STEP -1

870A(J)=P$(I,2)*(P$(I,2)*A(J)+2*P$(I,1)*A(J-1))+A(J-2)

875NEXT J,I

880FOR I=0 TO P1+2*P2

885B(I)=A(I)

890 NEXT I

895N1=Z1+2*Z2,D1=P1+2*P2

900RETURN
```

$$G(s) = \frac{K \prod (s + z_i) \prod (s^2 + 2\zeta_j \omega_j s + \omega_j^2)}{\prod (s + p_k) \prod (s^2 + 2\zeta_\ell \omega_\ell s + \omega_\ell^2)}$$

where,
$i = 1,2,..,NZ1$
$j = 1,2,..,NZ2$
$k = 1,2,..,NP1$
$\ell = 1,2,..,NP2$

Put into the shorthand notation this becomes,

$$G(s) = K \frac{\prod\limits^{NZ1} (z_i) \prod\limits^{NZ2} (\zeta_j, \omega_j)}{\prod\limits^{NP1} (p_k) \prod\limits^{NP2} (\zeta_\ell, \omega_\ell)}$$

$G(s)$, of course, represents $F_0(s)$, $F_1(s)$ or $F_2(s)$ as the case may be. The data field consists of the following array of numerical values.

parameters
for TRANSFER
FUNCTION SHAPE
= $F_0(s)$

$\left\{ \begin{array}{l} K, NZ1, NZ2, NP1, NP2, z_1, .., z_{NZ1}, \zeta_1, \omega_1, .. \\ .., \zeta_{NZ2}, \omega_{NZ2}, p_1, .., p_{NP1}, \zeta_1, \omega_1, .., \zeta_{NP2}, \omega_{NP2} \end{array} \right.$

parameters
for TRANSFER
FUNCTION F1
= $F_1(s)$

$\left\{ \begin{array}{l} K, NZ1, NZ2, ... \text{ etc.} \end{array} \right.$

parameters
for TRANSFER
FUNCTION F2
= $F_2(s)$

$\left\{ \begin{array}{l} K, NZ1, NZ2, ... \text{ etc.} \end{array} \right.$

When the data field is read from paper tape to file in EDITOR, the computer will request "FILE NAME?". The name given by the user will be the name the user must enter when the covariance program, /COV/, is ready to execute.

To use the covariance program, /COV/, it must be called from EXECUTIVE. (e.g. "-GO (LIB)/COV/") The computer will request "FILE NAME?". The user will respond with "/(name of first data file)/".

The computer will then print out the parameters of the three transfer functions in the data field according to the following format.

TRANSFER FUNCTION SHAPE

GAIN =
Z(1) =
...
Z(NZ2) =
ZDR(1) =   ZNF(1) =
...
ZDR(NZ2) =   ,ZNF(NZ2) =
P(1) =
...
P(NP1) =
PDR(1) =   ,PNF(1) =
...
PDR(NP2) =   ,PNF(NZ2) =

And so on for TRANSFER FUNCTION F1 and TRANSFER FUNCTION F2 in that order.

First order poles and zeros are printed one to a line with the root number enclosed in parentheses. Second order poles and zeros are printed with the damping ratio, ζ, first (ZDR and PDR) and the undamped natural frequency, ω, next (ZNF and PNF) with the root number enclosed in parentheses.

Next the computer will print out

COVARIANCE = (value of covariance)

ABSV SQ RT COV = (value of square root of absolute value of covariance)

and then request "FILE NAME?" for the next covariance case to be computed.

2. Program Limitations

(1) All poles of F_0, F_1 and F_2 must be located in the left half of the complex plane.

(2) The order of the denominator of F_0F_k must be greater than the numerator of F_0F_k, $k = 1,2$.

(3) Neither F_0F_1 nor F_0F_2 may have more than 35 poles.

(4) No numerator or denominator of F_0, F_1 or F_2 may have more than

- 15 real zeros or
- 15 pairs of complex zeros.

(5) The program automatically checks to determine that the matrix $[C \mid D]$ is not ill-conditioned for inversion. If this check fails the computer prints the message, "MATRIX IS ILL-CONDITIONED FOR INVERSION".

3. Example

Computation of the covariance of d_e and d_e (the variance of d_e) in response to u_g gusts for the A-7D system is here used as an example.

The input shaping filter for u_g has the following transfer function.

$$F_0 = \frac{8.72}{(0.38)} \qquad \text{(C-24)*}$$

The two system transfer functions are:

$$F_1 = F_2 = \frac{-0.244(0)(0.04354)(1.602)[0.9989, 0.9867]**}{**[0.3844, 2.203]} \frac{}{(0.0368)(0.0428)(0.8954)(0.977)(2.127)**} \qquad \text{(C-25)*}$$
$$**[0.3506, 2.403][0.3656, 0.2841]$$

(F_1 is equal to F_2 in this case because a special case of the covariance, a variance, is here being computed.)

---

* Abbreviated notation is used for polynomial factors in root locus form:

Real factor (λ) means $(s + \lambda)$

Quadratic factor $[\zeta; \omega]$ means $[s^2 + 2\zeta\omega s + \omega^2]$

The input data field for these transfer functions prepared in the proper format is shown below.

```
8.72 0 0 1 0 .38
-.244,3,2,5,2,0,.04354,1.602,.9989,.9867,.3844,2.203
.0368,.0428,.8954,2.127,.977
.3506,2.403,.3656,.2841
-.244,3,2,5,2,0,.04354,1.602,.89989,.9867,.3844,2.203
.0368,.0428,.8954,2.127,.977
.3506,2.403,.3656,.2841
```

This data is entered in EDITOR and given the file name, /K7/, in this example.

Next, the covariance program, /COV/, is loaded. This is shown in the first line of the print out which follows. The covariance program then executes after the user responds to FILE NAME? with /K7/. (See the second and third lines in print out below.)

```
-GO (LIB)/COV/

FILE NAME
? /K7/


  TRANSFER FUNCTION SHAPE

   GAIN =   8.72

P( 1) =   .38


TRANSFER FUNCTION F1

   GAIN = -.244

 Z( 1) =  0

 Z( 2) =  4.354E-02

 Z( 3) =  1.602

 ZDR( 1) = .9989   ZNF( 1) = .9867

 ZDR( 2) = .3844   ZNF( 2) = 2.203
```

P(1) = 3.68E-02

P(2) = 4.28E-02

P(3) = .8954

P(4) = 2.127

P(5) = .977

 PDR(1) = .3506   PNF(1) = 2.403

 PDR(2) = .3656   PNF(2) = .2841

TRANSFER FUNCTION F2

  GAIN = -.244

 Z(1) = 0

 Z(2) = 4.354E-02

 Z(3) = 1.602

 ZDR(1) = .9989 ZNF(1) = .9867

 ZDR(2) = .3844 ZNF(2) = 2.203

P(1) = 3.68E-02

P(2) = 4.28E-02

P(3) = .8954

P(4) = 2.127

P(5) = .977

 PDR(1) = .3506   PNF(1) = 2.403

 PDR(2) = .3656   PNF(2) = .2841

COVARIANCE   = 296.5232

ABSV SQ RT COV = 17.219849

FILE NAME
?

Upon entry of the next file name the covariance program will again execute.

DOCUMENT CONTROL DATA - R&D

(Security classification of title, body of abstract and indexing annotation must be entered when the overall report is classified)

1. ORIGINATING ACTIVITY *(Corporate author)*	2a. REPORT SECURITY CLASSIFICATION
Systems Technology, Inc. 13766 South Hawthorne Blvd. Hawthorne, California 90250	Unclassified
	2b. GROUP NA

3. REPORT TITLE

Investigation of Measuring System Requirements for Instrument Low Visibility Approach

4. DESCRIPTIVE NOTES *(Type of report and inclusive dates)*

Final, July 1969 to June 1970

5. AUTHOR(S) *(Last name, first name, initial)*

Graham, Dunstan
Clement, Warren F.
Hofmann, Lee Gregor

6. REPORT DATE	7a. TOTAL NO. OF PAGES	7b. NO. OF REFS
February 1971	185	42

8a. CONTRACT OR GRANT NO. F33615-69-C-1904	9a. ORIGINATOR'S REPORT NUMBER(S)
b. PROJECT NO. 682C01	
c. Work Unit 002	9b. OTHER REPORT NO(S) *(Any other numbers that may be assigned this report)*
d.	AFFDL-TR-70-102

10. AVAILABILITY/LIMITATION NOTICES

Distribution of this document is unlimited.

11. SUPPLEMENTARY NOTES	12. SPONSORING MILITARY ACTIVITY
NA	Air Force Flight Dynamics Laboratory Aeronautical Systems Division Wright-Patterson Air Force Base, Ohio

13. ABSTRACT

A practical method of determining measuring system requirements for instrument low visibility approach is presented. The method is made to depend on system analysis of the airplane, its control system, and the guidance system, as well as on atmospheric turbulence inputs and radio guidance system fluctuation noise. Requirements on the system are set in terms of a low value of the accident exposure multiplier which is related to the probability of a missed approach in the assumed environment.

The application of the method is demonstrated in connection with two examples: manual-flight director approach in the A-7D attack airplane, and automatically coupled approach with an advanced "windproof" flight control system in the DC-8 transport aircraft. The results, including particularly the implied requirements on scan rate for a scanning beam instrument low visibility approach system, demonstrate the interconnections between scanning rate, flight control, and overall system performance.

DD FORM 1 JAN 64 **1473**

Approved for Public Release

14. KEY WORDS	LINK A		LINK B		LINK C	
	ROLE	WT	ROLE	WT	ROLE	WT
Low-visibility landing approach						
Instrument approach						
Manually controlled approach						
Flight director control						
Automatically controlled approach						
Scanning beam measuring system						
Radio landing guidance						

INSTRUCTIONS

1. ORIGINATING ACTIVITY: Enter the name and address of the contractor, subcontractor, grantee, Department of Defense activity or other organization (corporate author) issuing the report.

2a. REPORT SECURITY CLASSIFICATION: Enter the overall security classification of the report. Indicate whether "Restricted Data" is included. Marking is to be in accordance with appropriate security regulations.

2b. GROUP: Automatic downgrading is specified in DoD Directive 5200.10 and Armed Forces Industrial Manual. Enter the group number. Also, when applicable, show that optional markings have been used for Group 3 and Group 4 as authorized.

3. REPORT TITLE: Enter the complete report title in all capital letters. Titles in all cases should be unclassified. If a meaningful title cannot be selected without classification, show title classification in all capitals in parenthesis immediately following the title.

4. DESCRIPTIVE NOTES: If appropriate, enter the type of report, e.g., interim, progress, summary, annual, or final. Give the inclusive dates when a specific reporting period is covered.

5. AUTHOR(S): Enter the name(s) of author(s) as shown on or in the report. Enter last name, first name, middle initial. If military, show rank and branch of service. The name of the principal author is an absolute minimum requirement.

6. REPORT DATE: Enter the date of the report as day, month, year; or month, year. If more than one date appears on the report, use date of publication.

7a. TOTAL NUMBER OF PAGES: The total page count should follow normal pagination procedures, i.e., enter the number of pages containing information.

7b. NUMBER OF REFERENCES: Enter the total number of references cited in the report.

8a. CONTRACT OR GRANT NUMBER: If appropriate, enter the applicable number of the contract or grant under which the report was written.

8b, 8c, & 8d. PROJECT NUMBER: Enter the appropriate military department identification, such as project number, subproject number, system numbers, task number, etc.

9a. ORIGINATOR'S REPORT NUMBER(S): Enter the official report number by which the document will be identified and controlled by the originating activity. This number must be unique to this report.

9b. OTHER REPORT NUMBER(S): If the report has been assigned any other report numbers (either by the originator or by the sponsor), also enter this number(s).

10. AVAILABILITY/LIMITATION NOTICES: Enter any limitations on further dissemination of the report, other than those imposed by security classification, using standard statements such as:

(1) "Qualified requesters may obtain copies of this report from DDC."

(2) "Foreign announcement and dissemination of this report by DDC is not authorized."

(3) "U. S. Government agencies may obtain copies of this report directly from DDC. Other qualified DDC users shall request through

_____ ."

(4) "U. S. military agencies may obtain copies of this report directly from DDC. Other qualified users shall request through

_____ ."

(5) "All distribution of this report is controlled. Qualified DDC users shall request through

_____ ."

If the report has been furnished to the Office of Technical Services, Department of Commerce, for sale to the public, indicate this fact and enter the price, if known.

11. SUPPLEMENTARY NOTES: Use for additional explanatory notes.

12. SPONSORING MILITARY ACTIVITY: Enter the name of the departmental project office or laboratory sponsoring (paying for) the research and development. Include address.

13. ABSTRACT: Enter an abstract giving a brief and factual summary of the document indicative of the report, even though it may also appear elsewhere in the body of the technical report. If additional space is required, a continuation sheet shall be attached.

It is highly desirable that the abstract of classified reports be unclassified. Each paragraph of the abstract shall end with an indication of the military security classification of the information in the paragraph, represented as (TS), (S), (C), or (U).

There is no limitation on the length of the abstract. However, the suggested length is from 150 to 225 words.

14. KEY WORDS: Key words are technically meaningful terms or short phrases that characterize a report and may be used as index entries for cataloging the report. Key words must be selected so that no security classification is required. Identifiers, such as equipment model designation, trade name, military project code name, geographic location, may be used as key words but will be followed by an indication of technical context. The assignment of links, rules, and weights is optional.